CONTENTS

DESIGN AND APPLICABILITY OF A NEW ARCHITECTURE OF A DOUBLE SCARA ROBOT

Dr. Eng. Iosif TEMPEA, University POLITEHNICA Bucharest ROMANIA
iosiftempea@yahoo.com
Dr. Eng. Adriana LIVADARIU, MATCHTECH Augsburg GERMANIA
adriana.livadariu@gmail.com
Doctoral student Eng. Alexandra-Elza MICU, University POLITEHNICA Bucharest ROMANIA salwaelza@yahoo.com

Abstract: SCARA robot mechanisms can be divided into two categories namely : mechanisms consisting of open kinematic chains and mechanisms consisting of closed kinematic chains. The second category includes Double SCARA robot, which comprises a five bar mechanism. The paper will propose several variants of mechanisms for Double SCARA robots, modeled by CATIA software.

Keywords: SCARA robot, five-bar mechanism, modelling, CATIA software

1. Introduction

The SCARA is acronym for Selective Compliant Assembly Robot Arm or Selective Compliance Articulated Robot Arm [1]. It was first developed in Yamanashi University of Kofu, Japan by Hiroshi Makino. Today this configuration is adopted by companies all over the world like AIBO, COBRA, EPSON, KUKA, STÄUBLI, YAMAHA, for industrial tasks and also in the medical field [2].

This type of robot has been first used as an industrial robot for pick and place tasks, assembly tasks, painting etc. after, entering into the medical field as well. As the name describes, the main function is to simulate an articulated arm, having in its structure an open, articulated kinematic chain, placed in the horizontal plane of the robot [2]. The described mechanism is the serial SCARA Robot.

Further in this paper the design of a Double SCARA Robot is detailed. The configuration is obtained by linking two serial kinematic chains into a closed five-bar-mechanism. This new configuration has the advantage of a wider workspace and a higher capability to carry loads.

2. Modelling of different configurations of planar five-bar mechanism

Planar five-bar mechanism is included in the category of parallel mechanisms [3, 4]. They may present two versions: the general case (Fig. 1a, $d \neq 0$) and the particular case (Fig. 1b, $d = 0$).

To model the five-bar mechanism, kinematic joints and the all system, we utilised CATIA V5, because of advantages offered by this software [5, 6].

For the 3D modelling of the elements, we used CATIA-Part Design product, and for the execution design CATIA-Drafting. The assembling conditions required that the elements must be having different forms. The definition of kinematic joints we achieved with CATIA-DMU Kinematics product, obtaining the mechanism with Assembly Design.

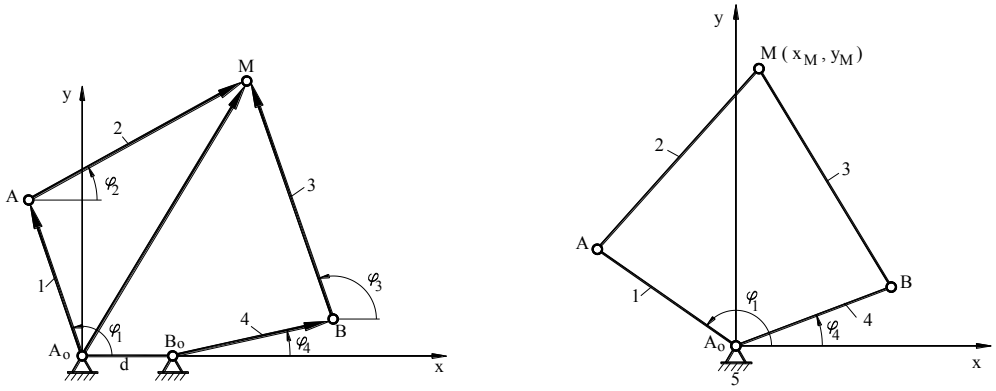

a) b)

Fig. 1 Five-bar mechanisms

To model the five-bar mechanism, kinematic joints and the all system, we utilised CATIA V5, because of advantages offered by this software [5, 6].

For the 3D modelling of the elements, we used CATIA-Part Design product, and for the execution design CATIA-Drafting. The assembling conditions require that the elements must have different forms. The definition of kinematic joints we achieved with CATIA-DMU Kinematics product, obtaining the mechanism with Assembly Design.

The lengths of the elements 1-4, respectively 2-3 are equal (Fig. 1a, b), but the assembling conditions required that the elements must be having different forms. Also, for the 1 and 4 elements we achieved the constructive solution (see Fig. 2a) and the execution design is shown in the Fig. 2 b.

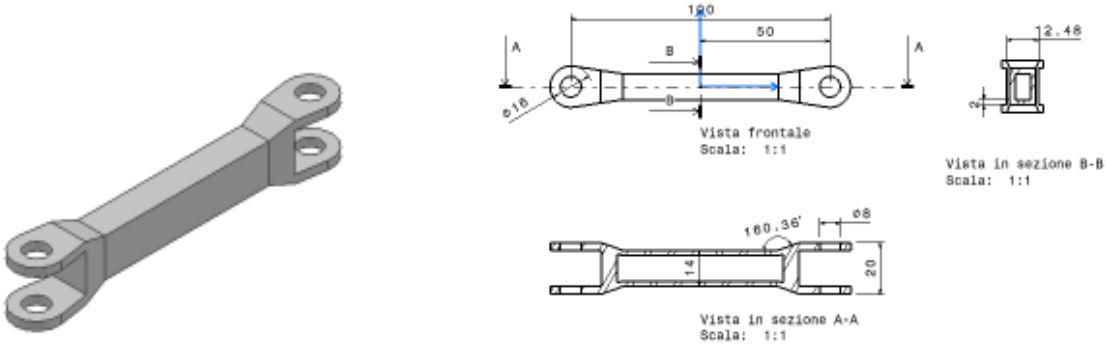

a) b)

Fig. 2 Constructive solution (a) and execution design for 2 and 3 elements (b)

For 2 and 3 elements, the constructive solution is represented in fig. 3a, and the execution design in fig. 3b.

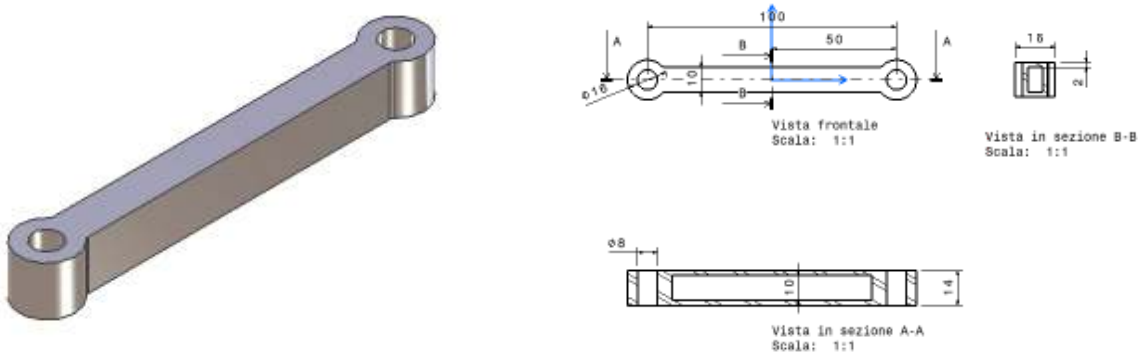

a) b)

Fig. 3 Constructive solution (a) and execution design for 2 and 3 elements (b)

With CATIA Assembly Design we have obtained the models of kinematic chains of five-bar mechanisms from Fig. 1 (a, b).

a) b)

Fig. 4 Kinematic chains generators of five-bar mechanisms

By mounting of kinematic chains on a support we have obtained five-bar appropriate mechanisms (Fig. 5a, b).

a) b)

Fig. 5 Five-bar modelled mechanisms

The second version of the mechanism (Fig. 5b, d=0) has the advantage of compact building, but comparing it to the first version (Fig. 3a, d≠0), the workspace is reduced.

To double the number of operations that this kind of mechanism can perform, starting from the previous configuration, a double five-bar linkage can be built as shown in the Fig. 4.

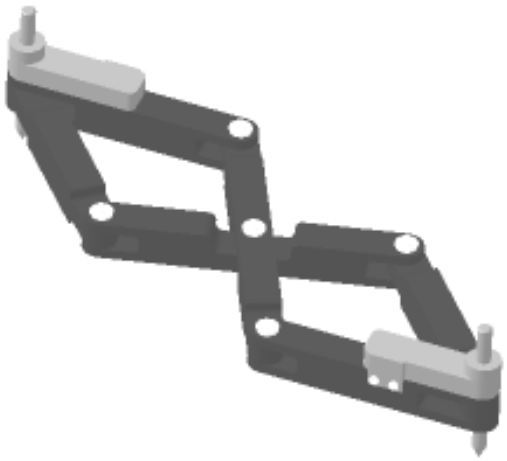

Fig. 6 Double five-bar mechanism

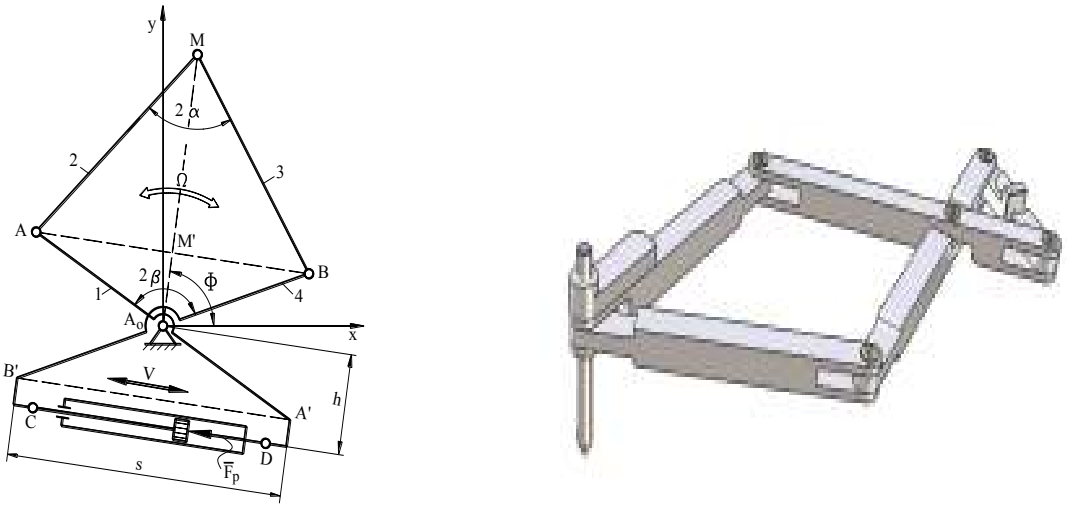

a) b)

Fig. 7 A new acting solution of the mechanism from Fig. 5b and CATIA's design of the five-bar mechanism with translation actuator

For the particular five-bar SCARA mechanism (Fig. 5b) the actuators are located in fix joints, in which case there are some constructive complications. For these reasons, we propose a new acting solution of a five-bar mechanism presented in Fig. 7a.

The design of this mechanism is represented in Fig. 7b.

The mechanism act is performed in this manner:

- - the distance between the joints A-B modifies thanks to the linear motor action, located between joints C-D;
- the mechanism can rotate around the joint A_0, by acting one of element 1, 4.

In this way, the motors overlap from A_0 joint can be eliminated. The command parameters are s and ø.

3. Double SCARA robot models with three degrees of freedom

To obtain three-dimensional workspace of the SCARA robot on attaches of five-bar linkages's base a translational joint, to control the vertical translation of the end-effector. This way a 3D workspace is defined [7]. This configuration can be also presented as two design solutions that can be seen in Fig. 8a (general case d≠0) and in Fig. 8b (particular case $d = 0$).

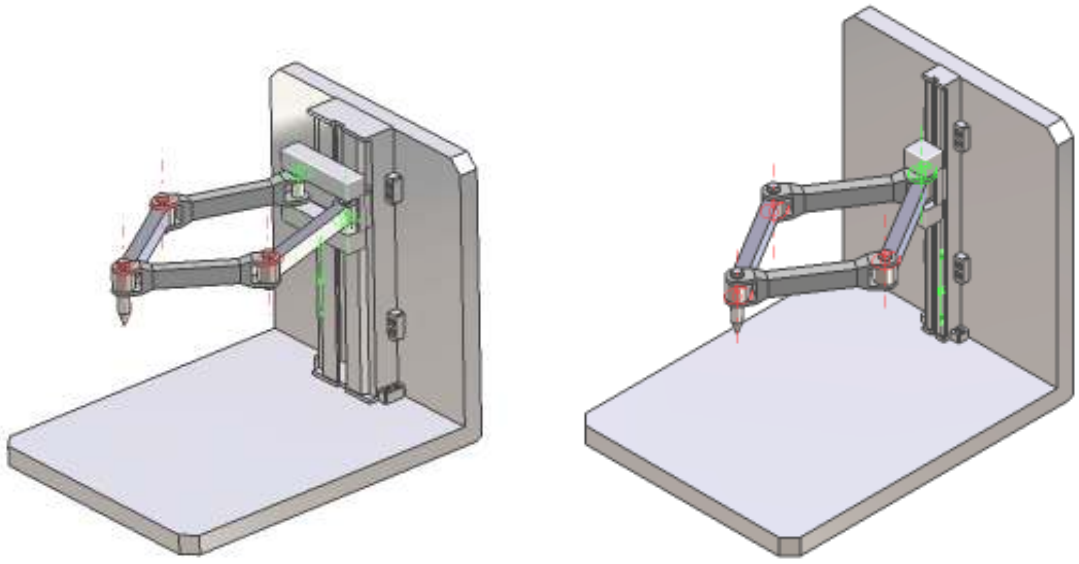

a) b)

Fig. 8 SCARA robots

An application of this type of design is a pick and place robot. In the pictures 5 and 6, various positions of the end-effector's trajectory are presented. The mechanism's trajectory is simulated with the DMU Kinematics Module of the CATIA V5 software [6].

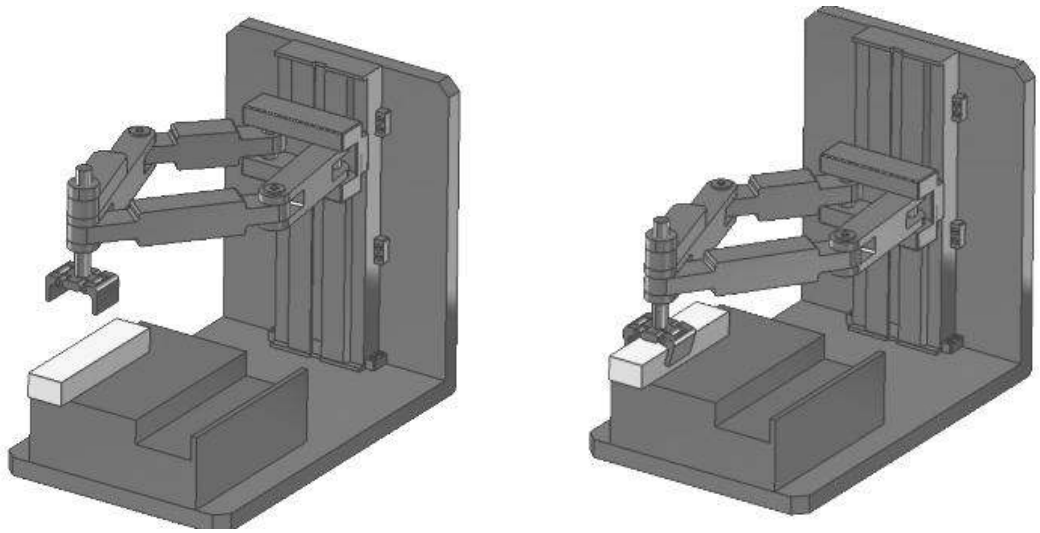

Fig. 9 Positions 1 and 2 of the "pick and place" Double SCARA Robot

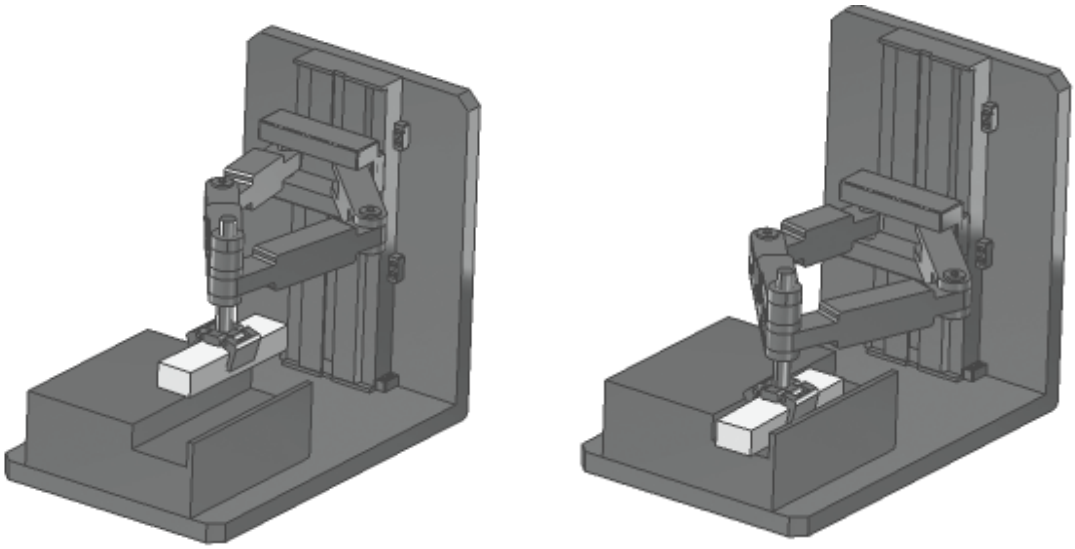

Fig. 10 Positions 3 and 4 of the "pick and place" Double SCARA Robot

4. Conclusions

Double SCARA robots mechanisms can be modularized through two sub-assemblies: a five-bar kinematic chain (five-bar linkage) and a support by which it is linked on a translational joint. The paper presents several variants of five-bar mechanisms, modeled using CATIA software. These constructive solutions differ one from another by configuration and actuation mode. Finally, it shows the constructive model of a SCARA robot for pick-and-place applications. The models were validated, their operation can be watched by an animation program.

REFERENCES

[1] https://en.wikipedia.org/wiki/SCARA
[2] **Tempea, I., Livadariu A. M., Dugaesescu, I.,** Laser Engraving Double Scara Robot Modeling, Proceedings of The third edition of the International Conference "Optimization of the Robots and Manipulators", OPTIROB 2008-Predeal, Romania, May 30th-June 1st, pp 53-58.
[3] **Merlet, J-P**., Les robots parallèles,Hermès, Paris, 2007.
[4] **Tempea, I., Livadariu, A.-M.**, New solutions regarding planar bi-mobile mono-contour parallel mechanisms, Proceedings of the 18th International Workshop on Robotics in Alpe-Adria-Danube Region, May 25-27, 2009, Brasov, Romania, p 41-47.
[5] **STÄUBLI** RX brochure GB.pdf.
[6] **Dassault Systèmes**, CATIA Version 5 User's Documentation.

STATIC AND DYNAMIC ANALYSIS UNDER MECHANICAL AND THERMAL LOADS OF THE DOUBLE SCARA ROBOT

Dr. Eng. Iosif TEMPEA, University POLITEHNICA Bucharest ROMANIA
iosiftempea@yahoo.com
Dr. Eng. Adriana LIVADARIU, MATCHTECH Augsburg GERMANIA
adriana.livadariu@gmail.com
Doctoral student Eng. Alexandra MICU, University POLITEHNICA Bucharest ROMANIA salwaelza@yahoo.com

Abstract: The paper presents a synthesis of the Double SCARA Robot modelling, leading to an optimal solution, from workspace point of view, as well as precision and stability of the end-effector in performing the planned trajectory. For the design of the final mechanism CATIA software has been used, as well as NASTRAN/PATRAN software, for the mechanism analysis under mechanical and thermal loads.

Keywords: CATIA, NASTRAN/PATRAN, modelling, mechanical analysis, Double SCARA Robot

1. Introduction

Due to the fact that the workspace depends directly by the element's geometry and the configuration of the mechanism, a new architecture of the Double SCARA Robot has been developed.

This new architecture of Double SCARA Robot presents a wider workspace, due to the additional translation joints, a lighter structure, due to the configuration of a new kinematic element and a higher capability for higher workload, due to the doubled structure of a serial SCARA robot, was designed. The design is performed using Part and Assembly Module of CATIA V5 software [1].

2. Geometrical configuration of new architecture of Double SCARA Robot

As mentioned, because of the kinematic element's new architecture, the structure is lighter and reduces the risk of bending moments at the active joints.

The new kinematic element used for this manipulator is also a torsion box type, to avoid high torque into the elements.

Two types of design have been used in order to permit assemblage a wide rotation of the joint [1].

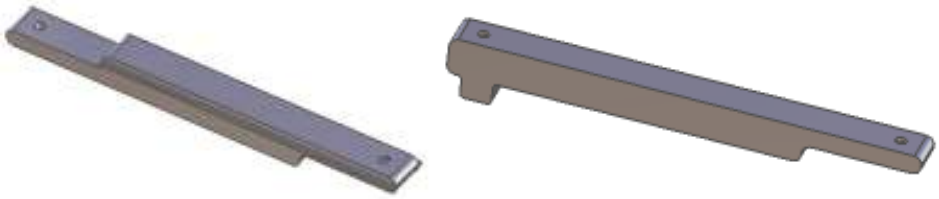

Fig. 1 Three-dimensional modelling in Part Module (CATIA software) of a new kinematic element of the Double SCARA Robot

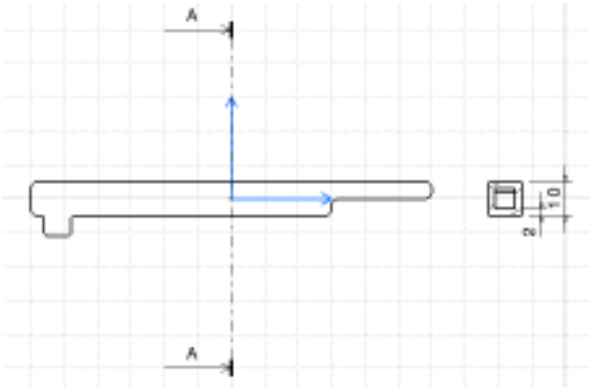

Fig. 2 Bi-dimensional drawing in Drafting Module (CATIA software) of a new kinematic element of the Double SCARA Robot

The mechanism is presented below where all rotational and translational joints can be seen. The definition of the mechanism has been performed with DMU Kinematics Module (CATIA software).

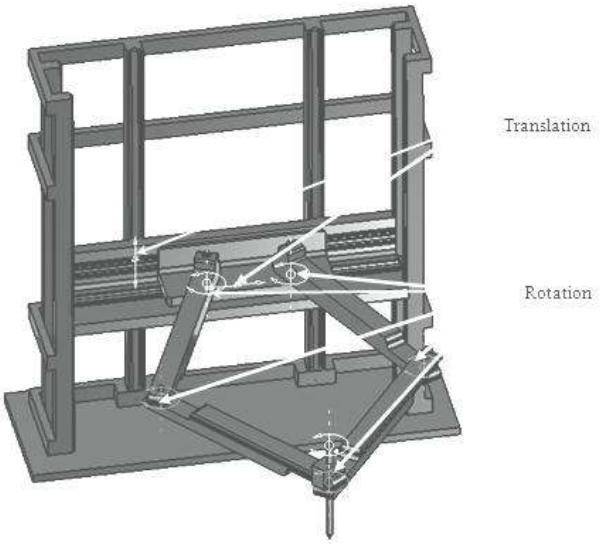

Fig. 3 Rotation and translational joints of the Double SCARA Robot

The translational movements, both in vertical and horizontal are transmitted through 2 rotation-translation links operated by two electric motors

The presented mechanism, only by changing its end-effector, the use can be changed as well as follows:

- Double SCARA Robot for laser engraving tasks.
- Double SCARA Robot for pick and place tasks.

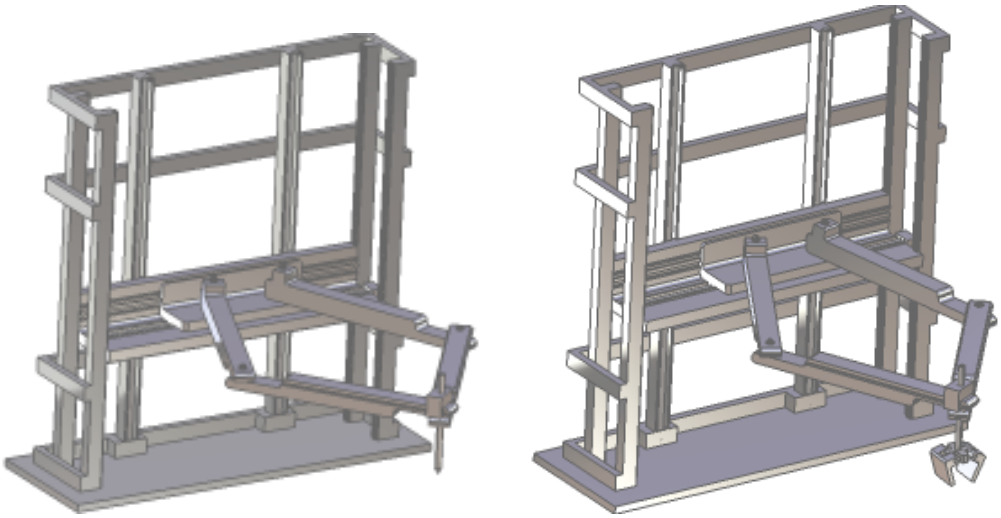

Fig. 4 Double SCARA Robot for laser engraving tasks and pick and place tasks

2. Static and dynamic analysis under mechanical and thermal loads

In order to see the limitations of this kind of manipulator, a study with NASTRAN/PATRAN has been performed. The mechanism has been analyzed under mechanical and thermal loading to determine its capability [2].

2.1. Finite element model

For the study, a finite element model of the mechanism has been performed. The materials taken into account for this configuration are aluminum 2024T6 for the kinematic elements, for its lighter but resistant properties, and steel AISI316L for the support, to add mass for balance, due to the fact that the mechanism behaves like a cantilever.

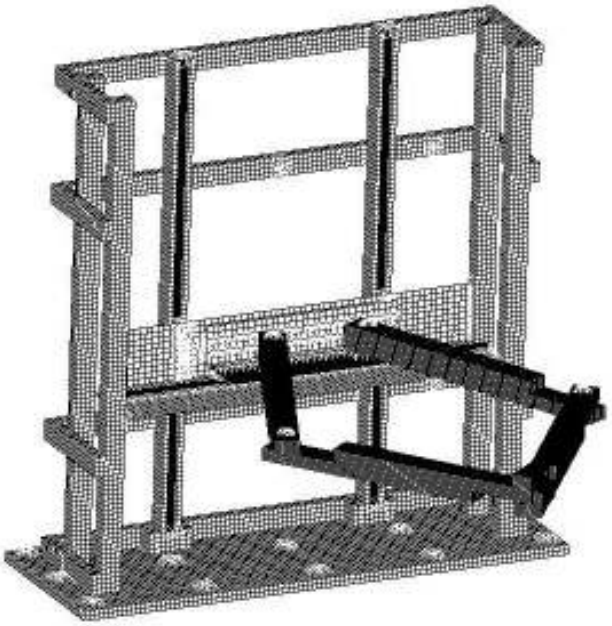

Fig. 5 Finite element Model of the Double SCARA Robot

The hypotheses used for the finite element model are [3, 4, 5]:

- The analyzed position is a stationary one;
- The kinematic joints cannot transmit rotational movements around their own axis of symmetry;
- 2D elements are used, for the representation of the kinematic elements;
- 3D elements are used for the support;
- 1D elements are used for screws and bolts representation.
- The structure is clamped, through MPC elements and SPC1 boundary conditions, at all its interface points.

2.2. Static analysis

The structure is loaded with a 100N force in the end-effector, to determine the capability of the mechanism for the material used and given geometry.

The maximum stress in the structure is 213Mpa.

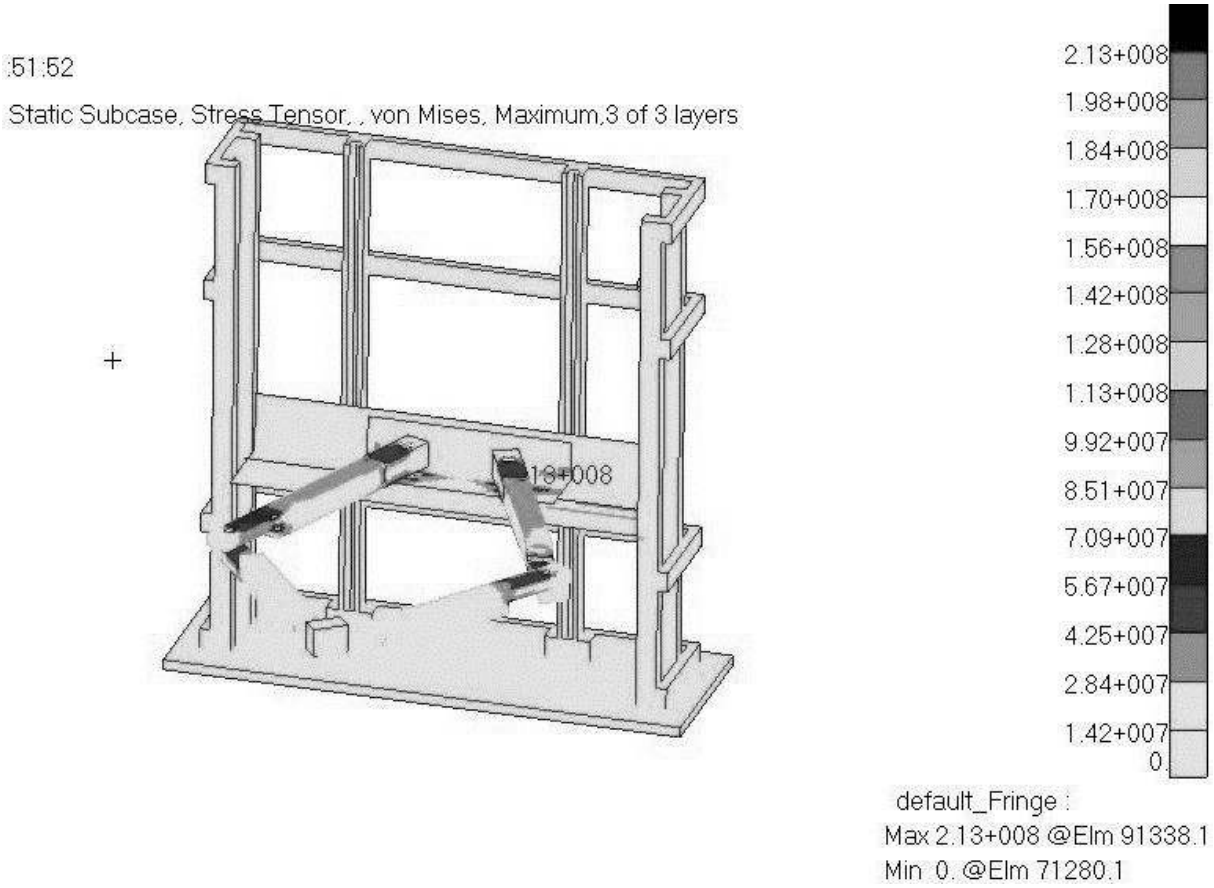

Fig. 6 Maximum tension of 213MPa under mechanical loads

The bonding elements are the dimensioning ones for the mechanism, with a maximum tension of 261MPa and the tension yield allowable of 290Mpa [6].

The reserve factor is determined by the formula:

$$RF = \frac{\sigma_{\text{yield allowable}}}{\sigma_{VM}} = 1.11 \geq 1 \quad (1)$$

Therefore, for a RF of 1, is determined the maximum load that the structure can sustain, this load being 110 N.

2.3 Thermo elastic analysis

These kinds of manipulators can work in quite rough environments with high temperatures. In order to determine the maximum temperature at which the robot can work, a thermo-elastic analysis has been made.

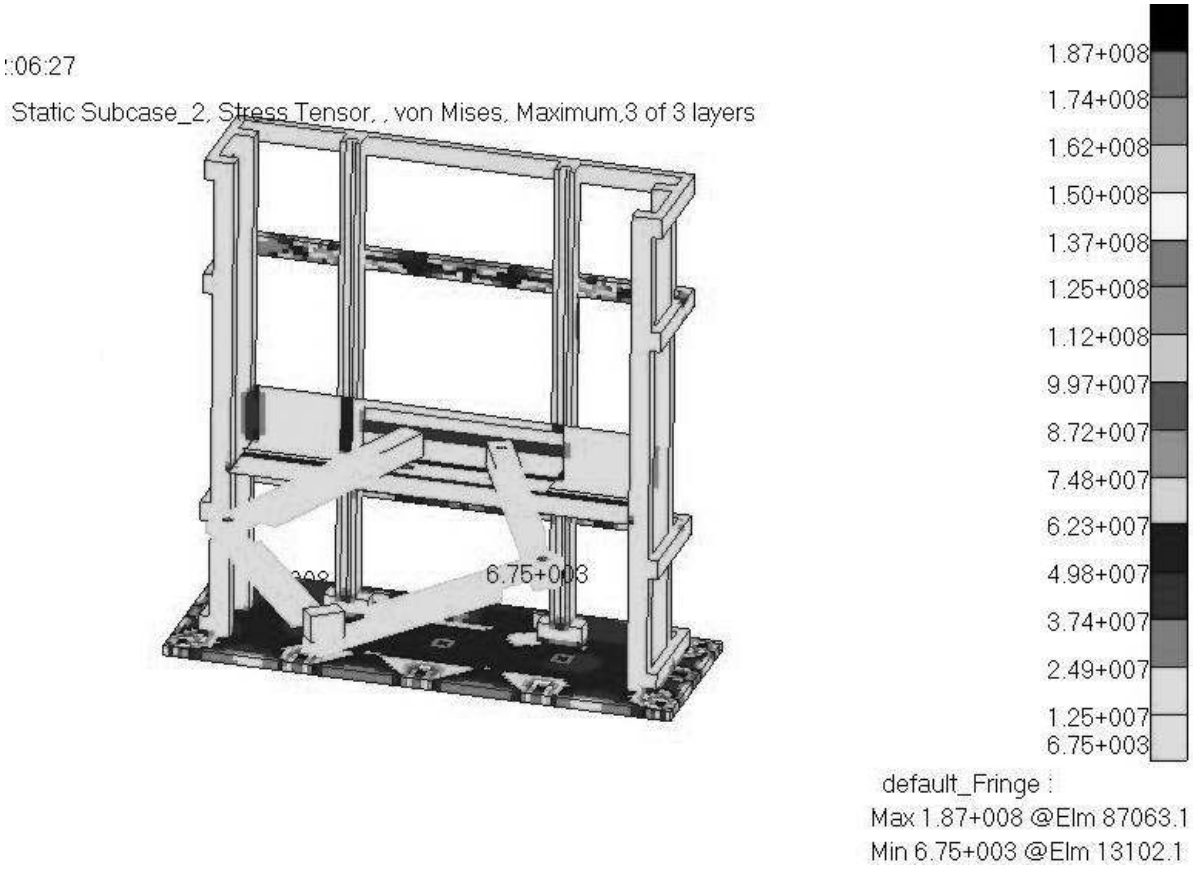

Fig. 7 Maximum Tension at 30ºC temperature gradient

The most loaded part is the structure with 187Mpa, the allowable at yield tension being 315MPa [6].

$$RF = \frac{\sigma_{\text{yield allowable}}}{\sigma_{VM}} = 1.68 \geq 1 \quad (2)$$

Therefore, for a RF of 1, the maximum temperature that the manipulator can sustain is 50°C

4. Conclusions

Studying various designs for the five bar-linkage mechanisms, an optimization of the design has been performed, in order to obtain a balance between the workspace, the precision of the mechanism and the stability in performing the planned trajectory.

The geometric shape of the kinematic elements has been optimized in order to reduce the torque that can appear during the functionality of the mechanism, as well as the weight in order to reduce the bending moments.

For a detailed capacity of the mechanism, a study under mechanical and thermal loads has been performed. It has been studied the maximum load that the end-effector can sustain and the thermal environment in which the mechanism can work.

REFERENCES

[1] **Dassault Systèmes**, *CATIA Version 5 User's Documentation*
[2] **MSC Software, Nastran/Patran**, 2008 Reference Manual
[3] **Zienkiewicz**, **O. C**., The Finite Element Method, 2000, 5th ed.
[4] **Dumitru, N., Ungureanu, A**., Bazele modelarii sistemelor mecanice. Elemente finite, Ed. Universitaria Craiova 2000
[5] **Dumitru, N., s.a.,** Mecanisme si transmisii mecanice. Tehnici de modelare clasice si modern, E.D.P. R.A., Bucuresti, 2008
[6] **www.matweb.com**, Materials mechanical properties

CONSIDERATIONS CONCERNING THE MECHANISM CALLED THE CHEBYSHEV'S PARADOX

Prof.PhD. Iulian POPESCU, University of Craiova, rodicaipopescu@yahoo.com
Prof.PhD. Liliana LUCA, University Constantin Brancusi of Targu-Jiu, lylyanaluca@yahoo.com

Abstract. *We study the kinetics of the mechanism called the Chebyshev's paradox. We show the mechanism* consecutive positions, than detailed according to the trigonometrical dials. We notice complex movements, the conducted final part has an irregular movement, with returns. The whole is explained by the appearing of 6 positions where the last conducted part and the anterior crank superpose or prolong each other, the dead point positions where the movements may change the direction. We give the diagrams explaining this ingenuous system.

Key-words: Chebyshev's paradox, mechanism dead point.

1.**Introduction**

The Russian mathematician P.L. Chebyshev worked too in the mechanism theory field, focusing on the analytical synthesis methods, on generating segments (linearization mechanisms), useful in locomotives, on the centrifugal regulator and on other mechanisms. An interesting mechanism created by Chebyshev is a mechanical paradox. The mechanism given in figure 1 [3, 2] contains the ABCM Chebyshev dyad with equal sides.

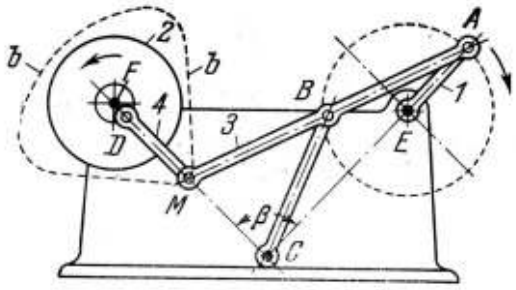

Fig. 1

Chebyshev calculated the mechanism sizes obtaining the values:
AB=CB=MB=1; EA=0,557; CE=1,324; FC=1,387; DM==0,584; FD=0,123; $\beta=90^0$

If the EA rod does a complete rotation clockwise, then the ED rod does two rotations clockwise or four rotations anticlockwise.

In [1] we proceed from the Chebyshev dyad to generate a symmetrical curve, one point following another given symmetrical curve. Furthermore the given curve is a circle, and for the prescribed part sizes we obtain a equilateral triangle-type crank curve with large ray-round tips. We reach the Chebyshev paradox and realize its animation, noticing that there are 6 points where the last rod and the connected crank are prolonging each other or superposed (figure 2). We check the observations of Chebyshev and we confirm them.

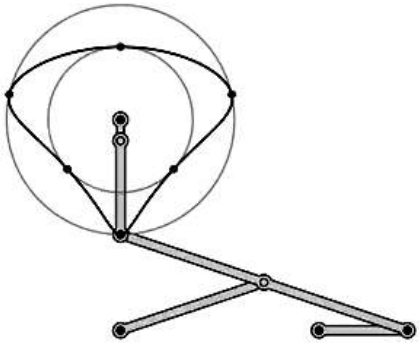

Fig. 2

In [5] we present the Chebyshev's paradox and we give various mechanism positions, confirming its functioning. In [6] we realize the mechanism animation, following in details the movement of the last conducted part. In [7] we give the Chebyshev's mechanism, pointing out its geometrical sizes. In [4] we studied the mechanism kinetics, obtaining the diagram ψ' (φ'), with some difficulties caused by the arctangent function.

2. Research on this mechanism

We realized the mechanism scheme in figure 3 and we detailed the CFE triangle in figure 4.

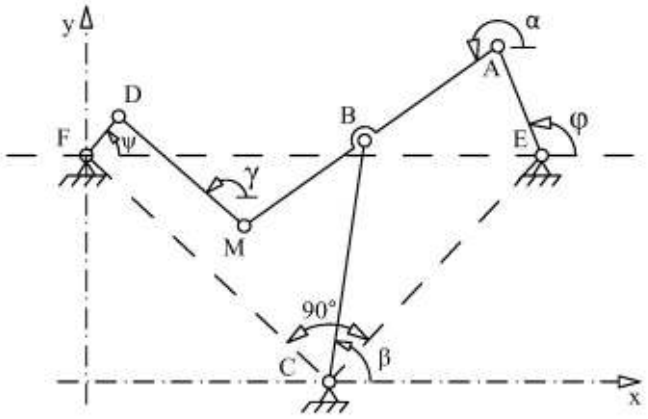

Fig. 3

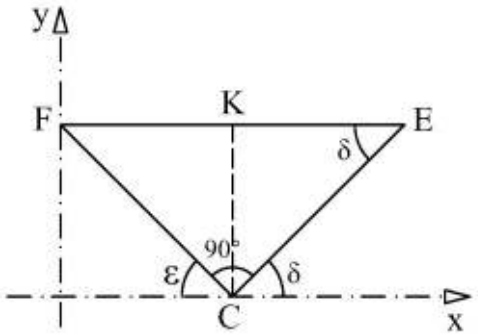

Fig. 4

We write the following equations for the positions:

$X_E^2=EF^2=FC^2+CE^2$ (1)

$FE/\sin 90=FC/\sin\delta=FC/(KC/CE)$ (2)

$Y_E=Y_F=K_C$ (3)

$\varepsilon = \pi-\delta-90=90-\delta$ (4)

$X_C=FC\cos\varepsilon$ (5)

$$X_E + EA\cos\varphi + AB\cos\alpha = X_C + CB\cos\beta \quad (6)$$

$$Y_E + EA\sin\varphi + AB\sin\alpha = CB\sin\beta \quad (7)$$

$$X_M = X_A + AM\cos\alpha \quad (8)$$

$$Y_M = Y_A + AM\sin\alpha \quad (9)$$

$$X_D = X_M + DM\cos\gamma = X_F + FD\cos\psi \quad (10)$$

$$Y_D = Y_M + DM\sin\gamma = Y_F + FD\sin\psi \quad (11)$$

By their derivation related to time we obtain the equations for speeds:

$$-EA\sin\varphi\cdot\dot{\varphi} - AB\sin\alpha\cdot\dot{\alpha} = -CB\sin\beta\cdot\dot{\beta} \quad (12)$$

$$EA\cos\varphi\cdot\dot{\varphi} + AB\cos\alpha\cdot\dot{\alpha} = CB\cos\beta\cdot\dot{\beta} \quad (13)$$

$$\dot{X}_M = -EA\sin\varphi\cdot\dot{\varphi} - AM\sin\alpha\cdot\dot{\alpha} \quad (14)$$

$$\dot{Y}_M = EA\cos\varphi\cdot\dot{\varphi} + AM\cos\alpha\cdot\dot{\alpha} \quad (15)$$

$$\dot{X}_M - DM\sin\gamma\cdot\dot{\gamma} = -FD\sin\psi\cdot\dot{\psi} \quad (16)$$

$$\dot{Y}_M + DM\cos\gamma\cdot\dot{\gamma} = FD\cos\psi\cdot\dot{\psi} \quad (17)$$

It results:

$$\dot{\beta} = \frac{EA\sin\varphi\cdot\dot{\varphi} + AB\sin\alpha\cdot\dot{\alpha}}{+CB\sin\beta} \quad (18)$$

$$\dot{\alpha} = \frac{EA\sin\varphi\cdot\dot{\varphi} - EA\cos\varphi\cdot\dot{\varphi}\cdot\tan\beta}{AB\cos\alpha\tan\beta - AB\sin\alpha} \quad (19)$$

$$\dot{\psi} = \frac{\dot{X}_M + \dot{Y}_M\cdot\tan\gamma}{FD\cos\psi\cdot\tan\gamma - FD\sin\psi} \quad (20)$$

3. Obtained results

Based on the equations above we realized a program obtaining the results above. We used the following data, calculated based on Chebyshev's data:
XC=200:XB=XC+132.4*COS(55):YB=132.4*SIN(55):XF=XC-138.7*COS(35)
YF=138.7*SIN(35):EA=55.7:AB=100:CD=100:BM=100:MD=58.4:FD=12.42.
In figure 5 we show the kinetic chain to M, obtained on display. In figure 6 we see the crank curve realized by the point M, a symmetrical curve.

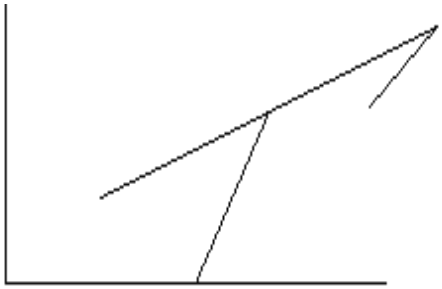

Fig. 5

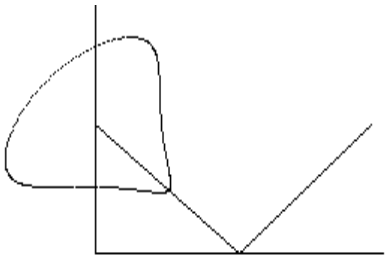

Fig. 6

The successive positions of this kinetic chain are shown in figure 7.

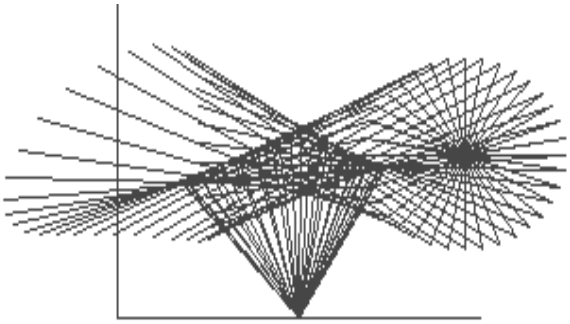

Fig. 7

The coordinate variation of the point M is given in figure 8.

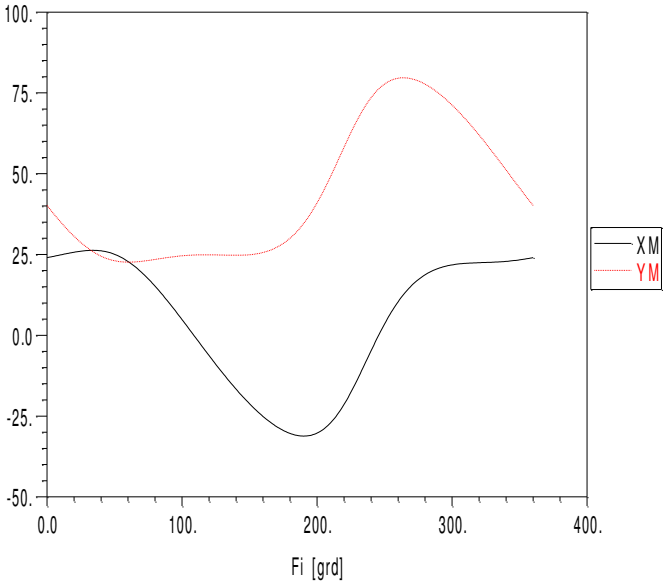

Fig. 8

The calculated trajectory of M is seen in figure 9.

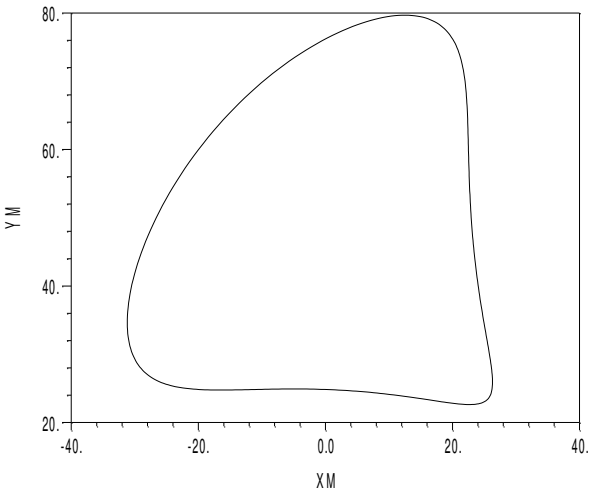

Fig. 9

We are interested especially in the movement of the dyad MDF; the small length of EF makes invisible the movement of DF with all the mechanism, so it was shown separately. So, in figure 10 we show the successive positions of the part MD, noticing positions with many superpositions.

In figure 11 we show the successive positions of part FD and the trajectory of M, noticing irregular movements of FD.

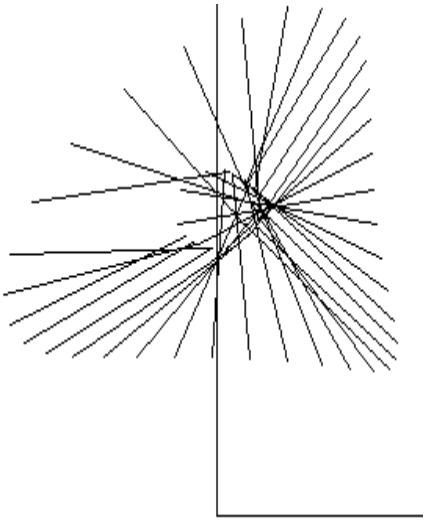

Fig. 10

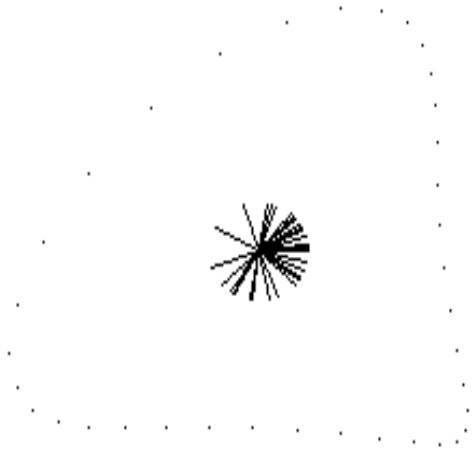

Fig. 11

The positions of FD on a larger scale are given in figure 12.
We give the more detailed positions of FD for the trigonometrical dials of φ, so: figure 13 (dial I), figure 14 (dial II), figure 15 (dial III) and figure 16 (dial IV).

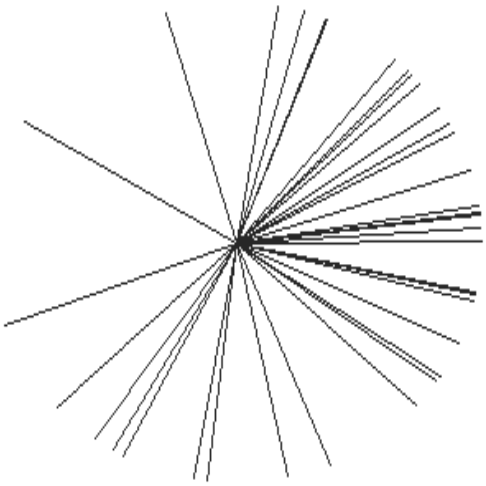

Fig. 12

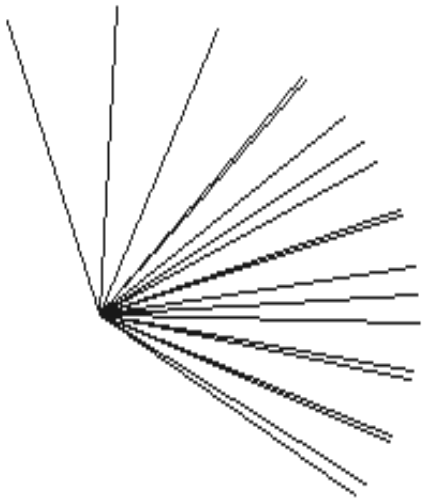

Fig. 13

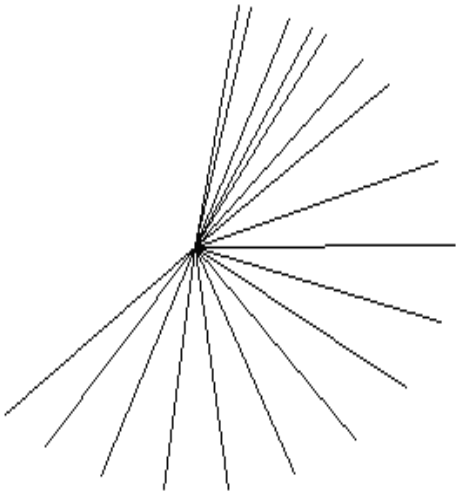

Fig. 14

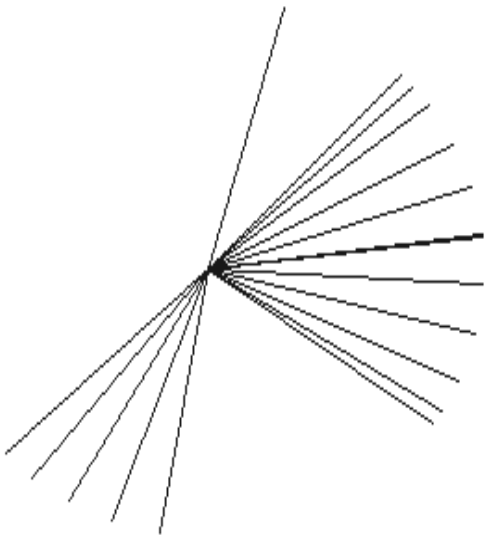

Fig. 15

We notify a great irregularity of the positions of the part FD depending on the rod movement, there appear returns, according to the Chebyshev's affirmations. The coordinate variation of D is given in figure 17.

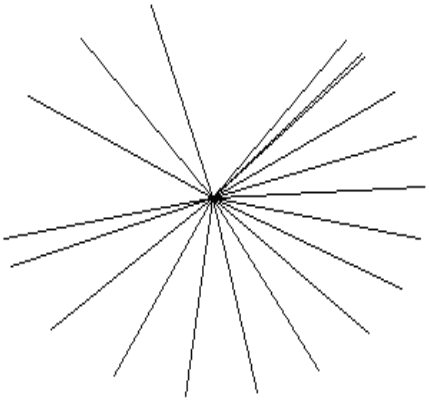

Fig. 16

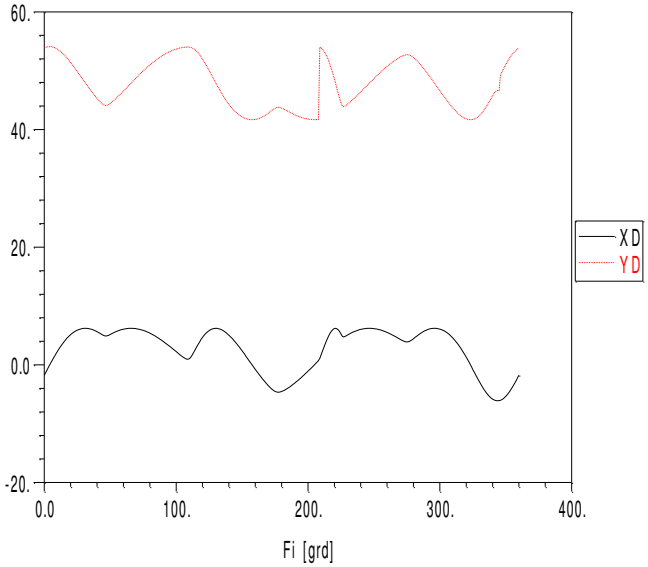

Fig. 17

In figure 18 we see the variations of the angle ψ realized by the final conducted part FD by the abscissa; we notice six subintervals where there appear skips, caused by the superposed positions or by the prolongation of the parts MD and FD, corresponding to the points noted on figure 2.

Considering the angular speed of EA equal to 1 (φ'=1), we obtain the angular speed variation of FD (ψ') in figure 19; on the same diagram there appears also the situation where φ'=-1. The curves are symmetrical related to the axis x.

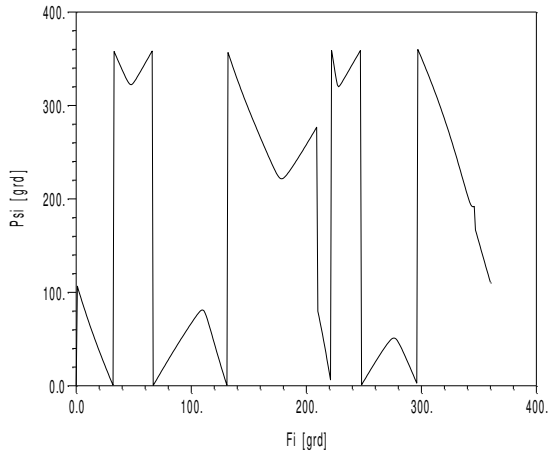

Fig. 18

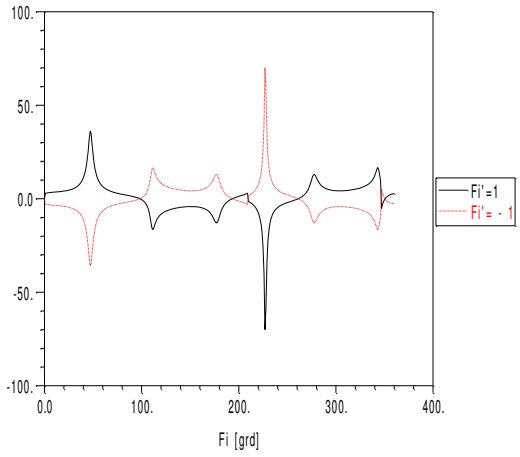

Fig. 19

This diagram explains the mechanism functioning. In fact all is due to the dead point positions, of which the movement may be in any direction. We realized an experimental model but it did not work out, needing large sizes of the parts and very tight tolerances, so the movement in joins change the law of movement of the last conducted part. On launching on the computer we noticed that in order for the mechanism to function, the length must be $FD=12.4^{+0.02}$.

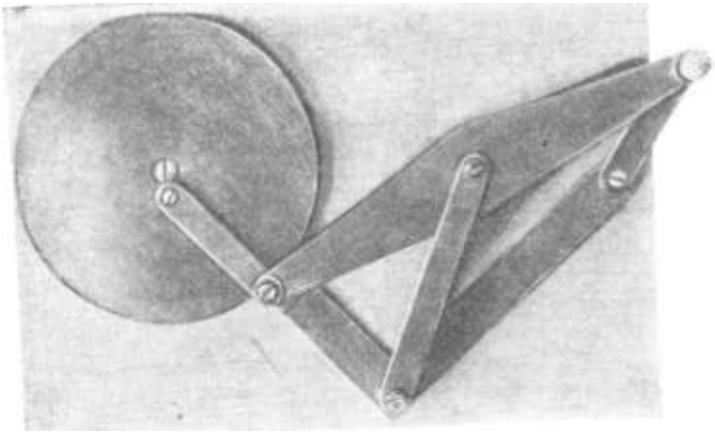

Fig. 20

A dynamic study will simplify the problem, the part inertias help the passage through the dead points, in the antecedent direction. Chebyshev used a wooden model (figure 20), manually operated, subsequently for neglected inertia forces, following the movement and the influence of the dead point positions on the mechanism kinetics. However, the mechanism is very ingenuous.

4. Conclusions

We studied the kinetics of the mechanism called the Chebyshev's paradox, following the successive positions, including for dials, noticing the existence of the dead point positions from which the movement may go on in any direction. We give many examples of mechanism position, explaining the situations obtained. We give diagrams explaining the functioning of the mechanism. We establish the accurate value of the final conducted part length, with tolerance. We conclude that the mechanism is a geometrical curiosity, a dynamic study showing that it passes through the dead point positions due to inertia. We notice the Chebyshev's ingenuity who conceived such a mechanism.

References

1. Andreev N., Kokşarovu, R., Kalinicenko, M. – Paradoxalnâi mehanizm P. L. Cebâşeva.
2. Artobolevskii, I.I, Leviţki, N. I., Cerkudinov, S.A. – Sintez ploskih mehanizmov. Izd. GIFML, Moskva, 1959.
3. Cebâşev, P.L. – Izbrannâe trudî. Izdatelstvo Akademii Nauk SSSR, Moskva, 1955.
4. Popescu, I. – *Mecanisme. Noi algoritmi şi programe*. Universitatea din Craiova, 1997.
5. http://www.etudes.ru/ru/etudes/paradox/]
6. http://www.futilitycloset.com/2015/01/03/chebyshevs-paradoxical-mechanism/
7. http://www.europeana.eu/portal/record/2020801/dmglib_handler_image_16283023.html
8. https://www.youtube.com/watch?v=Qi2Yk4OHU3I]

TRAJECTORIES GENERATED BY MECHANISMS CONTAINING THE CHEBYSHEV DYAD

Prof.PhD. Liliana LUCA, University Constantin Brancusi of Targu-Jiu,
lylyanaluca@yahoo.com
Prof.PhD. Iulian POPESCU, University of Craiova, rodicaipopescu@yahoo.com

Abstract. We study the trajectories generated by the articulated quadrangle, crank-rod and articulated pentagon mechanisms, each containing the Chebyshev dyad, characterized by the equality of three segments (two welded together), forming a RRR-type dyad. We chose mechanism sizes not mentioned by Chebyshev. We obtain symmetrical trajectories for the articulated quadrangle, trajectories formed of lines and circle arcs for the crank-rod mechanism and incomplete trajectories for the articulated pentagon because of not observing the geometrical conditions for a full rotation of the cranks.

Key-words: Chebyshev dyad, trajectories, fourbar, crank-rod, pentagon.

1.Introduction

The Chebyshev dyad consists of a bent rod, with the angle γ among the two bars and another part (figure 1), all these segments of length "a". It is given in [3], and in [2] it is shown how with this dyad, connected to a mechanism, we may create symmetrical curves. This dyad was studied thoroughly by Prof. Dijskman within various papers, connecting it to other observations on the mechanism geometry. So, in [4] the author connects it to a symmetrical Watt mechanism, with 6 bars, we may generate an 8-degree curve. In [1] it is synthesized a spherical quadrangle mechanism using functions and the superposition method, and finally reaching Chebyshev-type approximation functions. In [6] it is shown how the Chebyshev dyad is used for aeolian turbines. The Chebyshev dyad mechanism insures the regularization of the turbine paddle position depending on the wind force and direction. In [5] it is shown how to generate a symmetrical curve using the Chebyshev dyad (figure 2), with the side sizes calculated by Chebyshev and given in [2].

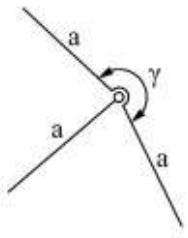

Fig. 1

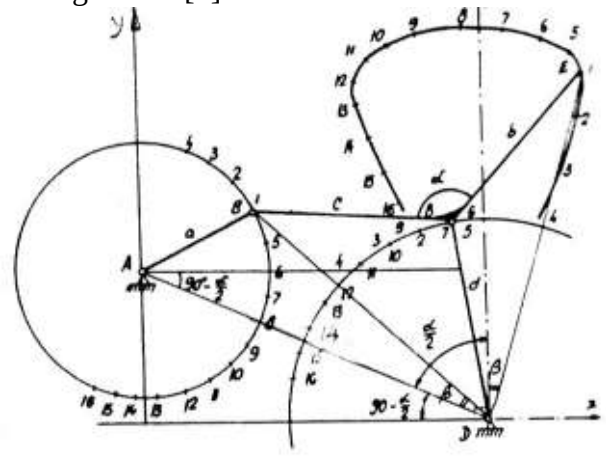

Fig. 2

2. Chebyshev dyad within the articulated quadrangle mechanism

This time we did not use mechanism sizes given by Chebyshev. We considered the mechanism in figure 3 where we see the BCDE Chebyshev dyad, have sides equal to "a". We look for the trajectories generated by the point E.

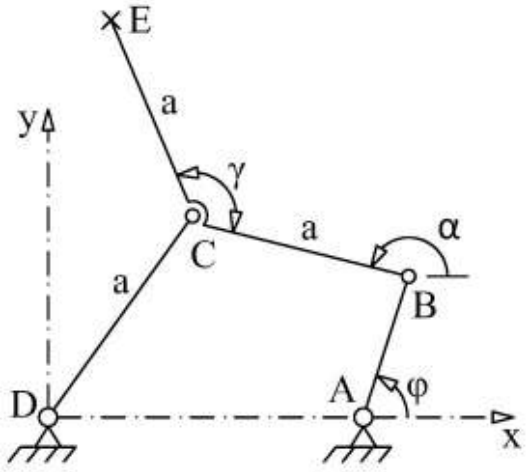

Fig. 3

We write the following equations:

$X_B=X_A + AB\cos\varphi;\ Y_B=Y_A + AB\sin\varphi;$ (1)

$X_E=X_C + a\cos(\gamma-\pi+\alpha);\ Y_E=Y_C + a\sin(\gamma-\pi+\alpha).$ (2)

We created a computer program where we used these equations and the RRR dyad subroutine. We used the following values, determined by attempts: XA=163, AB=25, a=48, γ=variable. We give beneath curves obtained for various values of γ, mentioned under the images.

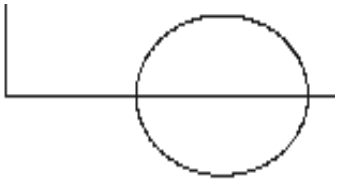

Fig. 4 (γ =0)

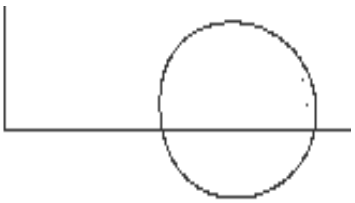

Fig. 5 (γ =10)

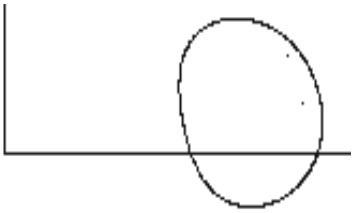

Fig. 6 (γ =20)

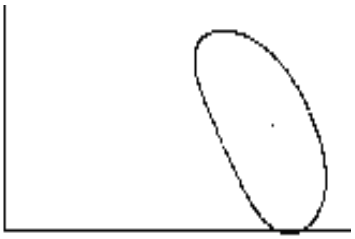

Fig. 7 (γ =45)

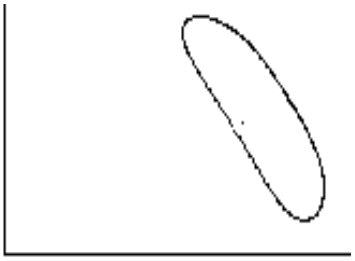

Fig. 8 (γ =60)

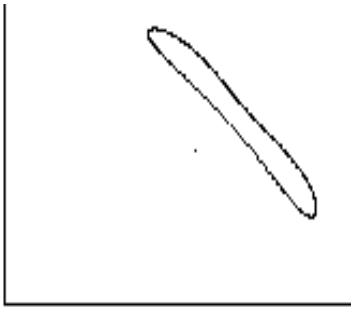

Fig. 9 (γ =80)

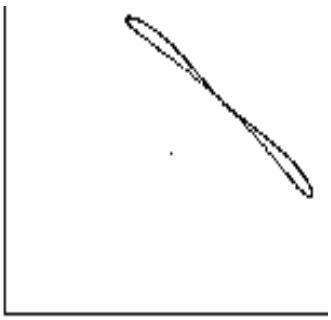

Fig. 10 (γ =90)

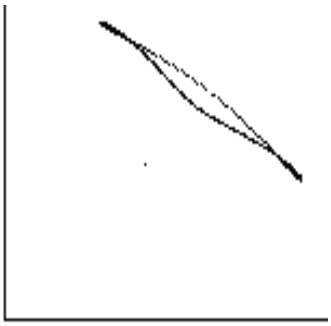

Fig. 11 (γ =100)

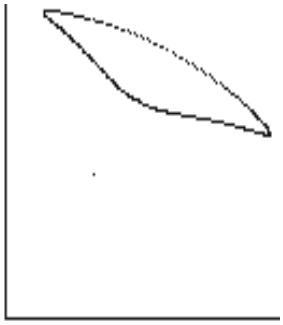

Fig. 12 (γ =120)

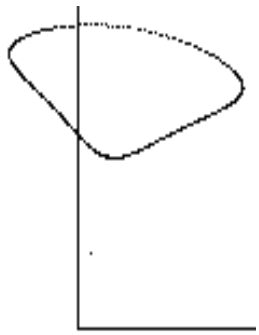

Fig. 13 (γ =160)

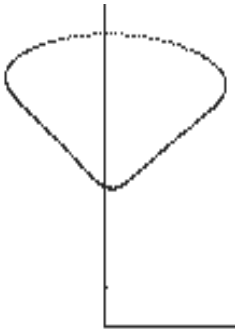

Fig. 14 (γ =175)

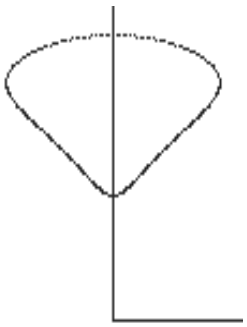

Fig. 15 (γ =180)

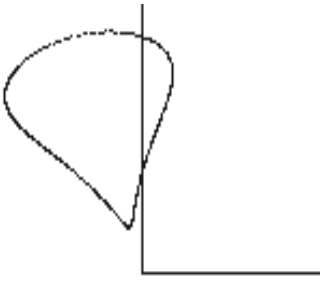

Fig. 16 (γ =210)

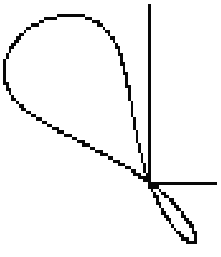

Fig. 17 (γ =250)

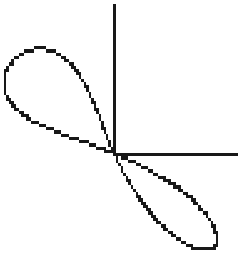

Fig. 18 (γ =270)

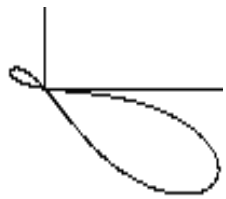

Fig. 19 (γ =300)

Fig. 20 (γ =330)

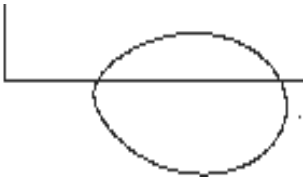

Fig. 21 (γ =345)

We notice that all curves generated are symmetrical, the symmetry axis varying from an angle to another.

3. Chebyshev dyad within the crank-rod mechanism

For the mechanism in figure 22, where AB=BC=BD=a, we write the equations:

$X_B = X_A + a\cos\varphi$; $Y_B = Y_A + a\sin\varphi$; (3)

$X_B = S + a\cos\alpha$; $Y_B = a\sin\alpha$; (4)

$X_D = X_B + a\cos(\gamma-\pi+\alpha)$; $Y_D = Y_B + a\sin(\gamma-\pi+\alpha)$. (5)

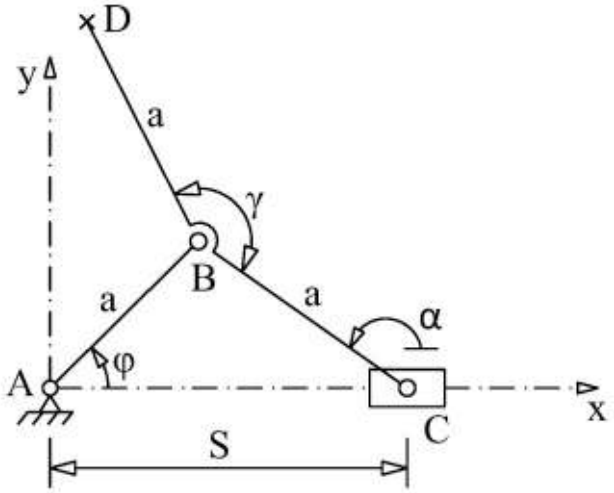

Fig. 22

Here we also look for the trajectories generated by a point, D. In figure 23 we show the mechanism generated for a position with the sizes: AB=a=60, γ=220.

Furthermore we worked with γ=120. In figure 24 we show the consecutive positions of the mechanism.

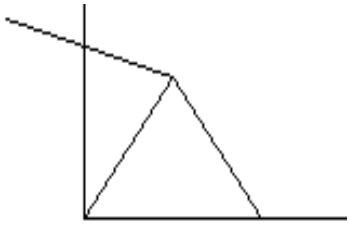

Fig. 23

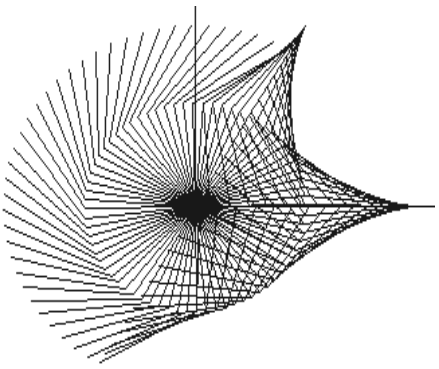

Fig. 24

We notice the generation of segments and of a circle arc; in figure 25 we may see this trajectory.

Because from an equation already mentioned we calculate sin α, and furthermore we need too the value of cos α, we use the sign in front of the radical, which may change. The trajectory in figure 25 connects to Se=-1, and the one in figure 26 to Se=+1, the same, but displaced in the base part of the image.

In order to explain the way to obtain this trajectory, we checked the movement in the trigonometrical dials: figure 27 – dial I, figure 28 – dial II, figure 20 – dial III, figure 30 – dial IV. For dial I we notice that the trajectory is a segment.

Fig. 25

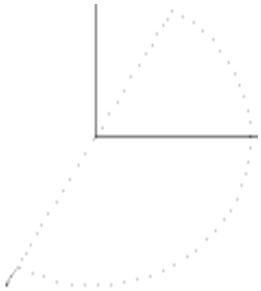

Fig. 26

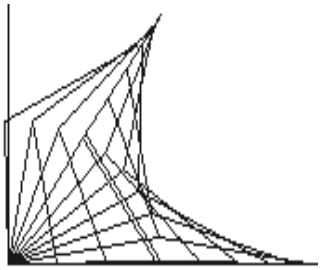

Fig. 27

For dial II the trajectory is a circle arc. The cause consists of that φ=90 CB segment is superposed on AB segment, furthermore acting as AB rod, meaning S=0, and point C remains in the center of the axes system. The same applies to dial III.

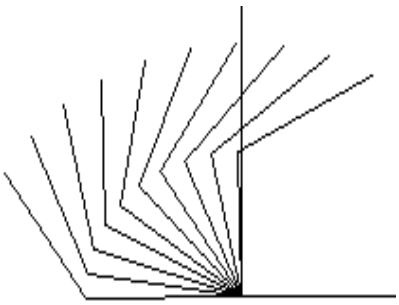

Fig. 28

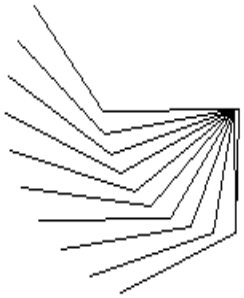

Fig. 29

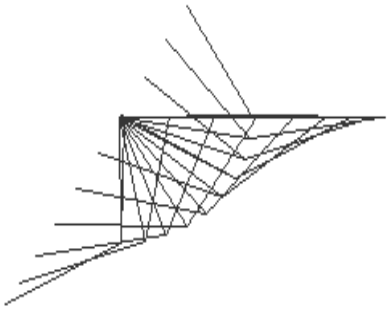

Fig. 30

In dial IV, after the rod passed φ=270 degrees, we come back to the trajectory after a segment, with S not zero and larger than zero.

In conclusion, for the crank-rod mechanism we do not obtain spectular trajectories.

4. Chebyshev dyad within the articulated pentagon mechanism

We consider the articulated pentagon mechanism in figure 31, similar to the quadrangle in figure 3, with the GD part besides. The Chebyshev dyad is BCDE. The new conductor part GD may rotate independently of the AB conductor, or dependently by a linear equation $\psi = c.\varphi$, modifying "c" from a case to another.

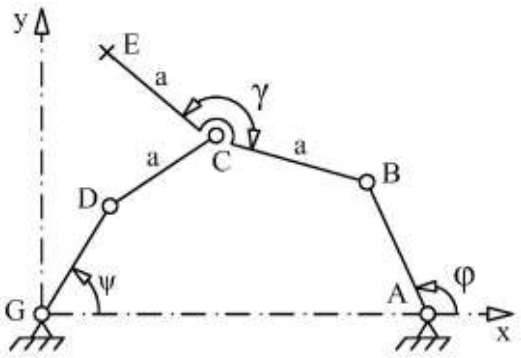

Fig. 31

We used the following input: XA=63, AB=25, a=48, GD=30, γ=156. Beneath we give the trajectories generated for various values of "c", values mentioned under the images.

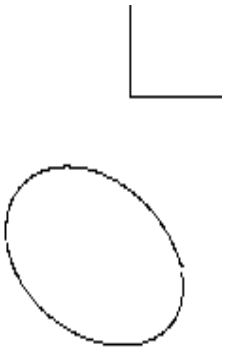

Fig. 32 (c=1)

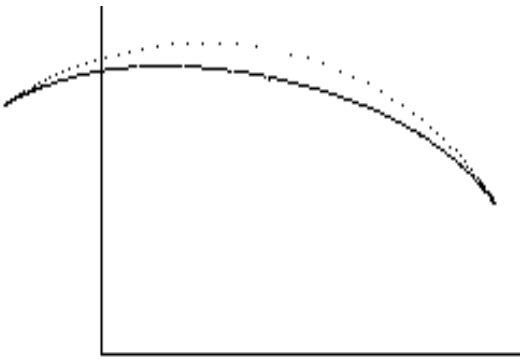

Fig. 33 (c=0)

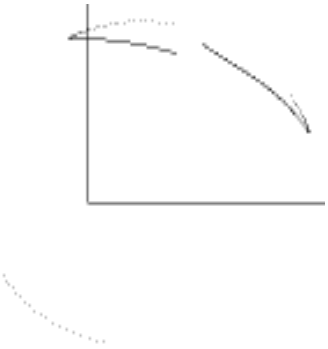

Fig. 34 (c=0,1)

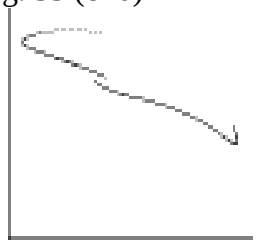

Fig. 35 (c=0,2)

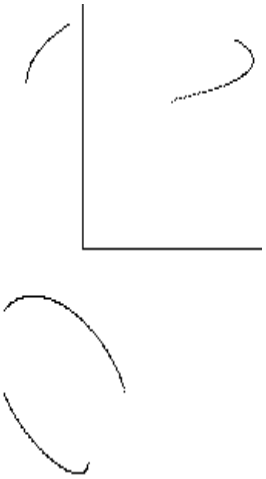

Fig. 36 (c=1,1)

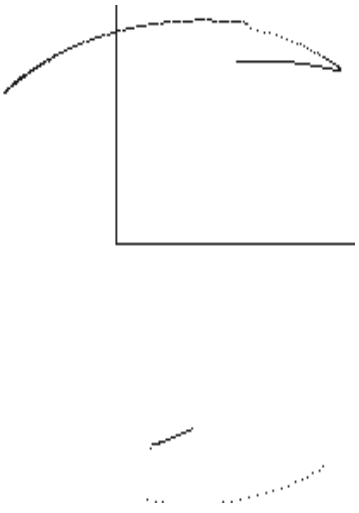

Fig. 37 (c= – 0,1)

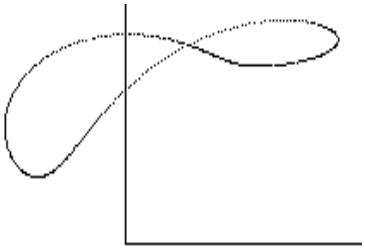

Fig. 38 (c= –1)

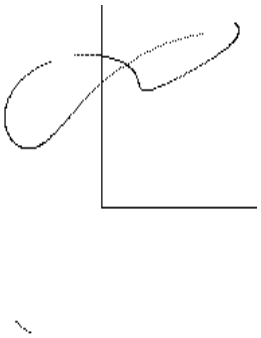

Fig. 39 (c= – 0,9)

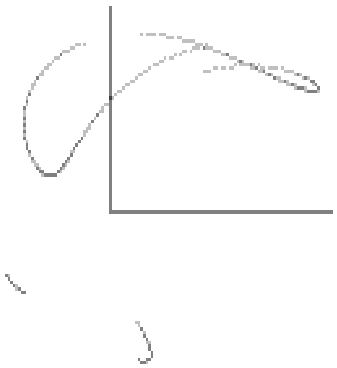

Fig. 40 (c= – 1,2)

We notice that some curves are symmetrical, and others are asymmetrical, some being incomplete, with different branches.

Furthermore we worked with GD=50, obtaining the images beneath.

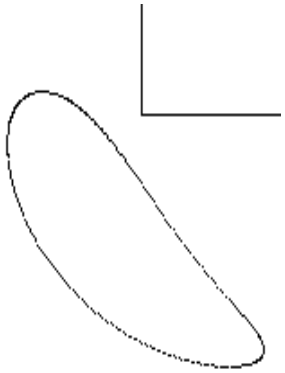

Fig. 41 (c=1)

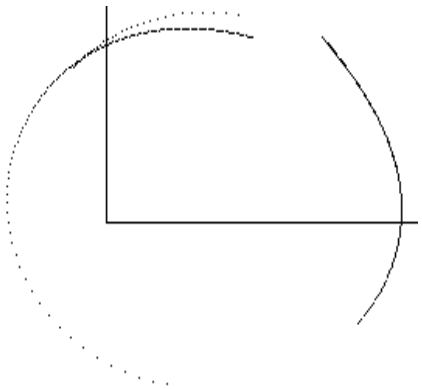

Fig. 42 (c=0,1)

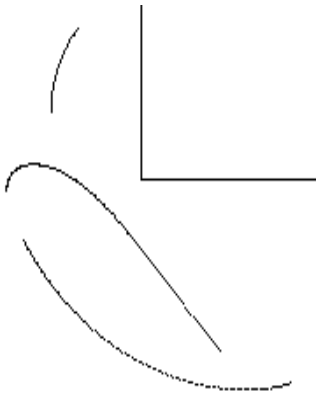

Fig. 43 (c=0,9)

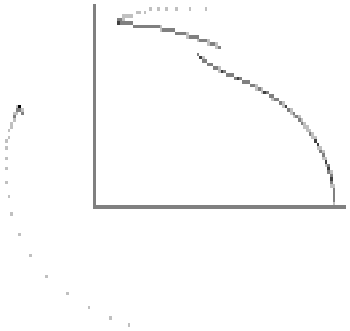

Fig. 44 (c=0,2)

We notice that other curves are generated, consequently the GD rod length influence the generated curves. And here, as in the examples above (still for the pentagon), there appear incomplete curves and more branches, caused by the Grashof-type conditions avoiding the complete rotation of both rods, for the adopted sizes. Furthermore the "c" value influences the position of the point D and of the rod GD related to AB, which modifies the conditions concerning the complete rotations.

5. Conclusions

It checked by many examples what trajectories are obtained for three types of mechanisms using the Chebyshev dyad, but with sizes not calculated by him. For the articulated pentagon mechanism we obtained symmetrical curves, but not spectacular. For the crank-rod mechanism the trajectories are not interesting because the rod and the crank are equal, they superpose within dials II and III, acting as a unique rod. For the articulated pentagon the curves are not special, generating many incomplete curves, or more different branches, caused by the values of "c" and by the part lengths, so they do not observe the complete rotation conditions of both rods.

References

1. Alizade, R., Can, F.C, Kilit, O. – Least square approximate motion generation synthesis of spherical linkages by using Chebyshev an equal spacing. Mechanism and Machine Theory. 61, 2013, pg. 123-135.
2. Artobolevskii, I.I, Leviţki, N. I., Cerkudinov, S.A. – Sintez ploskih mehanizmov. Izd. GIFML, Moskva, 1959.
3. Cebâşev, P.L. – Izbrannâe trudî. Izdatelstvo Akademii Nauk SSSR, Moskva, 1955.
4. Dijksman, E.A. – Watt-1 linkages with shunted chebyshev-dyads, producing symetrical 6-bar curves. Mechanism and Machine Theory, Volume 16, Issue 2, 1981, pag. 153-165.
5. Popescu Iulian -Sinteza mecanismului patrulater articulat pentru trasarea unor curbe simetrice In: "Lucrarile simpozionului de mecanisme si transmisii mecanice", Reşiţa, 1976, vol. I, pg. 291-298.
6. Shrestha, K. – Development of vertical axis flap type wind turbine with Chebyshev-Dyad link Mechanism. Nepal Engineers`Association Japan Center (NEA-JC). Research Digest, aprilie 2013, pg. 7.

SYNTHESIS OF CERTAIN MECHANISMS WHICH GENERATE LUNULES OVER POLYGONS WITH 5 SIDES

Professor Iulian POPESCU,
University of Craiova, rodicaipopescu@yahoo.com
Associate Professor PhD Ludmila SASS,
University of Craiova, Faculty of Mechanics, ludmila_sass@yahoo.com

Abstract. A synthesis for a mechanism relying on a sequence of articulated quadrilaterals which plot lunules along a penthagon is made. The plotting is successful. The speeds of plotting points are neither equal, nor constant. Afterward the synthesis of another mechanism, relying on a *sequence or articulated parallelograms is performed. In this case the lunules' plotting was made* at constant speed.

Keywords: Hyppocrates's lunules, mechanism to plot lunules

1. Introduction

The lunule, similar to a half-moon, represents a surface between two arcs of circle: one belongs to a circle on which a chord AB is placed, the second one is built along that chord, with the radius AB/2 and the centre in the middle of the chord. Hyppocrates from Chios (430-380 B.C.) has tried to solve the squaring of a circle – that is to built (by using only a only the ruler and compass) a squre with aria equal to that of a circle [2]. Ferdinand von Lindemannn has proven in 1882 that this technique cannot be successful, because of the irrational character of the constant π.

[3] presents an analysis of lunules and surfaces at isosceles triangles. Other demonstrations are provided by [4]. The case of a rectangular triangle is also approached in [5]. Detailed calculations are given in [6] with respect to the values of some surfaces for lunules when dealing with rectangular, isosceles and equilateral triangles. The correlation between the surfaces of lunules and that of a triangle, by using the Pitagora's Theorem, is demonstrated in [7]. Lunules are also plotted for a hexagon, by computing the lunules' arias.

A synthesis of two mechanisms plotting lunules is made in [1]. One is plotting lunules along the sides of a rectangular triangle, the other is plotting lunules along the sides of a square. To our knowledge, no other information on mechanisms generating lunules could be found in the specialty literature.

2. Synthesis of a mechanism for plotting lunules

Fig. 1 represents the starting point. It depicts a pentagon with notations on the angles presenting interest. The point B from the crank AB is plotting the arc HBF. The lunule for this side is obtained as the surface between the traced arc of circle and the arc with the radius OF, generated by a leading crank, as independent leading element. In order to avoid useless elements on the drawing, only the lunules corresponding to two sides are studied. The mechanism for the other sides is conceived in a similar manner.

The solving was made by using an articulated quadrilateral mechanism (ABCD), where CD=AB=a/2, BC=a. The sides AB and CD are not parallel and „a" represents the length of the pentagon's side.

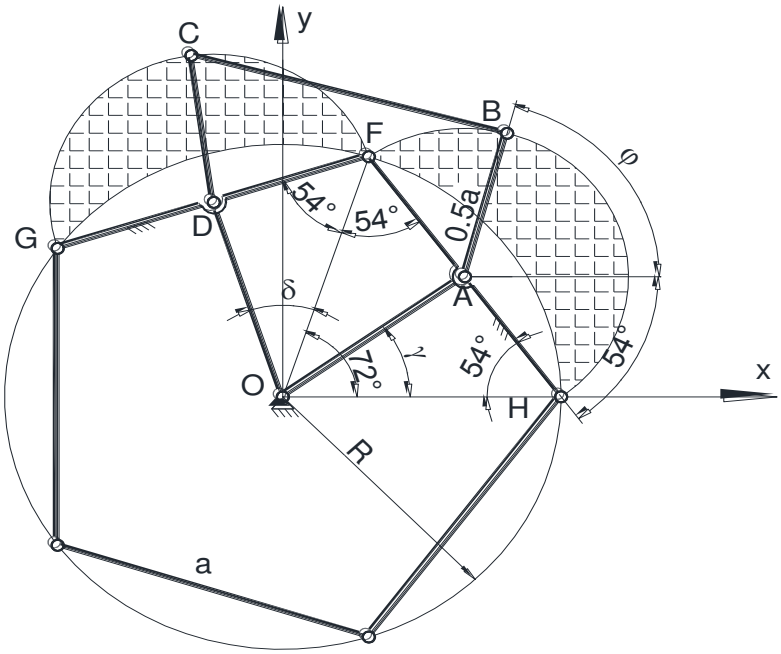

Fig. 1. Articulated quadrilateral mechanism used to plot lunules

The following equations can be written by using Fig. 1:

$$\frac{a}{\sin 72^o} = \frac{R}{\sin 54^o} \tag{1}$$

$$OA^2 = R^2 + \frac{a^2}{4} - 2R\frac{a}{2}\cos 54^0 \tag{2}$$

$$\begin{cases} x_A = R\cos\gamma \\ y_A = R\sin\gamma \end{cases} \tag{3}$$

$$OD^2 = \frac{a^2}{4} + R^2 - 2R\frac{a}{2}\cos 54^o \tag{4}$$

$$\begin{cases} x_D = OD\cos\left(72^o + \delta\right) \\ y_D = OD\sin\left(72^o + \delta\right) \end{cases} \tag{5}$$

$$\delta = \frac{\pi}{2} - 54^o \tag{6}$$

Calculations with respect to ABCD are made from this point on.

Fig. 2 depicts the pentagon and the quadrilateral mechanism for a certain position, generated by a program relying on the above equations, which call a procedure dedicated to the quadrilateral mechanism.

The point B is running from H up to F whilst C is running from F up to G. It means that the crank AB will cover an angle equal to 180^o.

Fig. 3 depicts the successive positions of the mechanism for this range, corresponding to the plotting of two lunules.

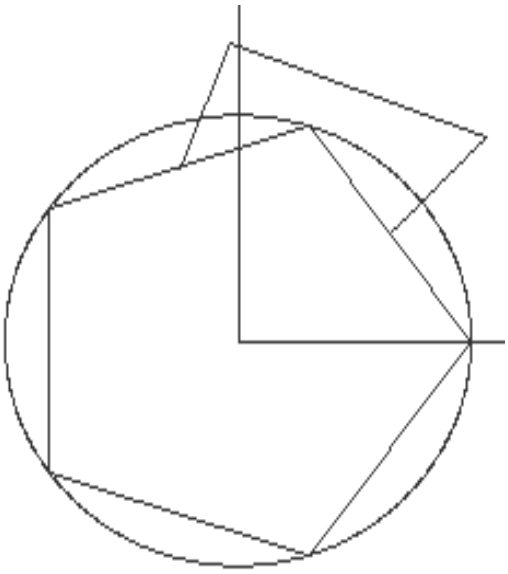

Fig. 2. The articulated quadrilateral mechanism in a certain position

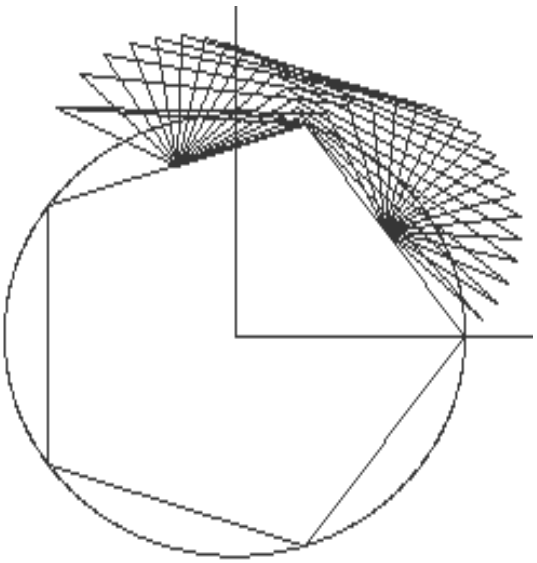

Fig. 3. Successive positions of the mechanism

It is easy to see that the rod BC is not parallel to previous positions of itself and the point C moves with a variable speed across the arc FCG. The angles FDC are variable (feature specific to an articulated quadrilateral). The point C reaches the position D. The figure represents a sub-range out of the rod's route – the explanation residing in the high value of the step φ chosen for cycling.

Fig. 4, representing the lunules plotted for both analyzed sides, reveals that C reaches the position G. Fig. 5 depicts the successive positions of the cranks plotting both lunules.

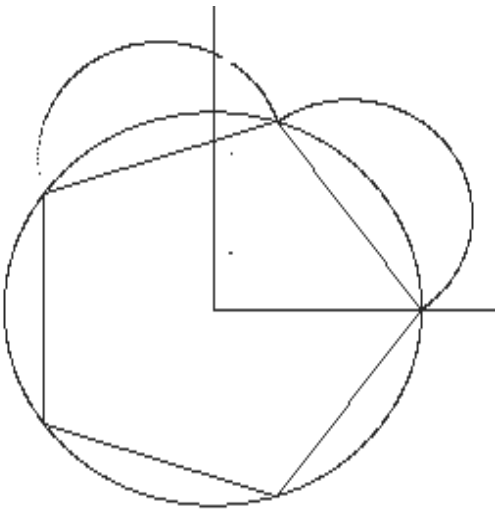

Fig. 4. Lunules plotted across both analyzed sides of the pentagon

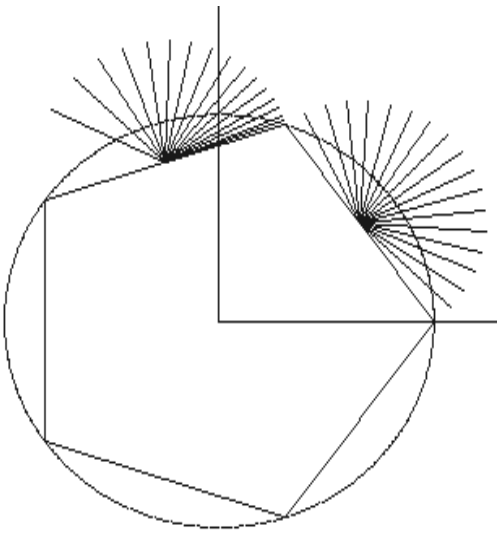

Fig. 5. Successive positions of the cranks AB and CD which plot both lunules

Providing that an articulated parallelogram mechanism is used (Fig. 6), the deficiencies occurred when using an articulated quadrangle are avoided. In this case the lunule from the side HF, instead of being plotted by the point B, is plotted by the crank AP, made rigidly secured with AB, but shifted to it by the angle between the pentagon's sides.

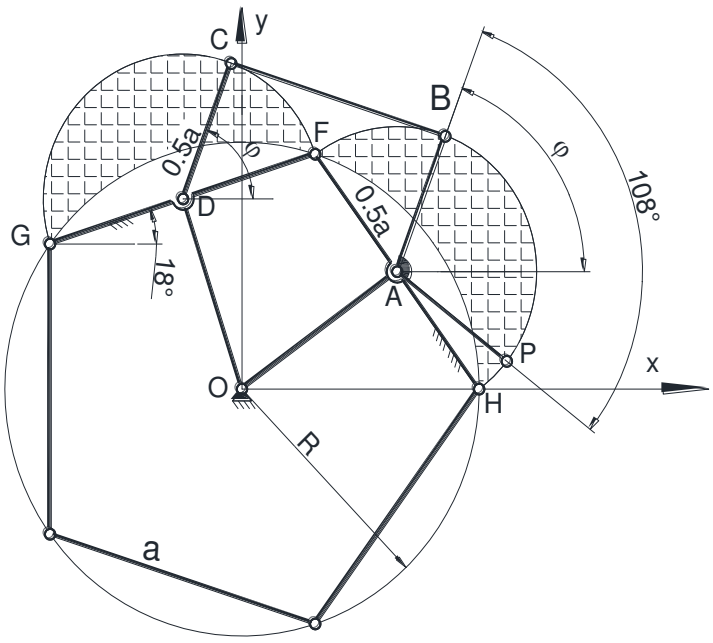

Fig. 6. Plotting lunules with the articulated parallelogram mechanism

The following equations can be written:

$$AB = CD = AP = \frac{a}{2} \tag{7}$$

$$\begin{cases} x_B = x_A + AB\cos\varphi \\ y_B = y_A + AB\sin\varphi \end{cases} \tag{8}$$

$$\begin{cases} x_C = x_D + CD\cos\varphi \\ y_C = y_D + CD\sin\varphi \end{cases} \tag{9}$$

$$\begin{cases} x_P = x_A + AP\cos\varepsilon \\ y_P = y_A + AP\sin\varepsilon \end{cases} \tag{10}$$

$$\varepsilon = 2\pi - \left(108^o - \varphi\right) \tag{11}$$

A program was conceived and used to plot the mechanism for a certain position (Fig. 7).

The successive positions of the mechanism are depicted by Fig. 8. One can see that the point B, which does not plot lunules, overcomes the point F. The crank AP stops in F – at the end of race. This represents a drawback for this mechanism.

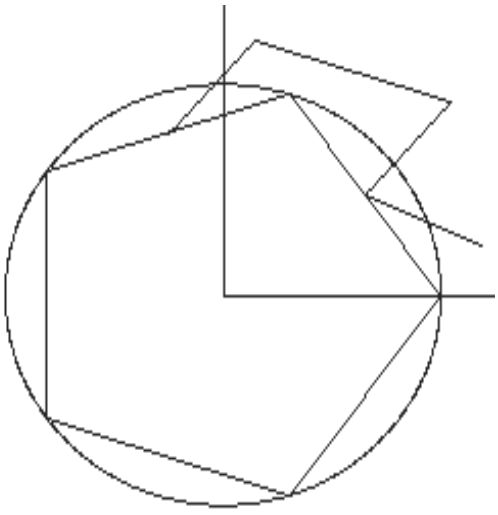

Fig. 7. Articulated parallelogram mechanism

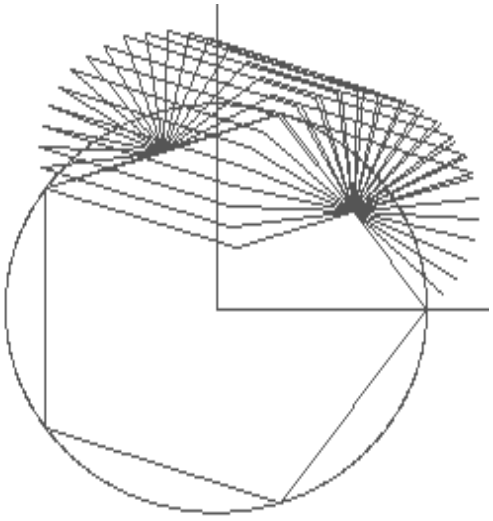

Fig. 8. Successive positions of the mechanism

Fig. 9 depicts the cranks AP and DC which plot lunules. The yielded lunules are given in Fig. 10.

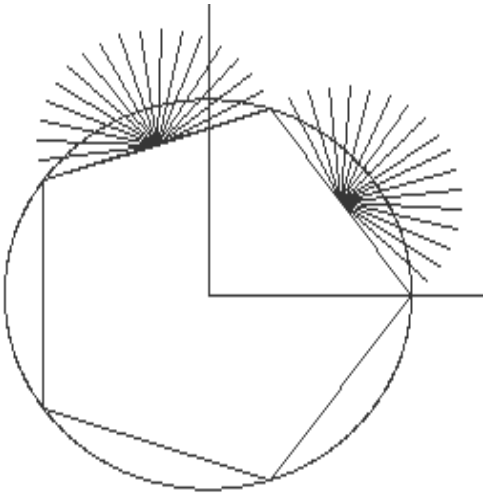

Fig. 9. The positions of the cranks AP and DC which plot lunules

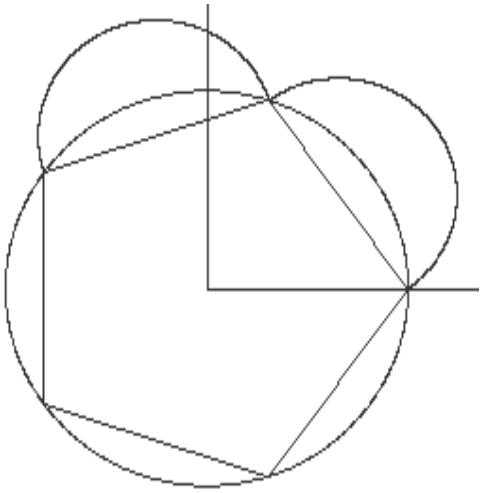

Fig. 10. Two lunules plotted along the sides HF and FG of the polygon

For the rest of the polygon's sides, shifted cranks (by an angle of 108^{o}) cranks and parallelogram are built, in a manner similar to that described above.

Conclusions

- Two mechanisms were conceived in order to generate lunules along the sides of a polygon with 5 sides.
- The first mechanism used to plot lunules was built by using a sequence of articulated quadrangles.
- The speeds of plotting points are not equal to each other.
- A second mechanism was built afterward. It relies on a sequence of some articulated parallelogram mechanisms. The cranks are shifter relative to the leading ones.
- The lunules are plotted with constant and equal speeds.

References

1. **Popescu Iulian, Sass, L**. - *Figuri geometrice ale antichităţii, generate cu mecanisme*. În: Vol. The VII-th Edition of the National Conference with International Participation, GRAFICA-2000, Craiova, oct. 2000, pg. 341-346.
2. https://en.wikipedia.org/wiki/Lune_of_Hippocrates] [Accessed: 15 th November 2015].
3. http://pro-didactica.ro/forum/index.php?forumID=8&ID=9435 [Accessed: 11 th November 2015].
4. https://tube.geogebra.org/material/simple/id/39636 [Accessed: 11 th November 2015].
5. https://tube.geogebra.org/m/45575 [Accessed: 12 th November 2015].
6. http://mathworld.wolfram.com/Lune.html] [Accessed: 16 th December 2015].
7. http://jwilson.coe.uga.edu/emt668/EMAT6680.F99/Williford/Lunes/lunes.html [Accessed: 15 th December 2015].

SYNTHESIS OF TWO MECHANISMS WHICH GENERATE LUNULES OVER AN EQUILATERAL TRIANGLE'S SIDES

Associate Professor PhD Ludmila SASS,
University of Craiova, Faculty of Mechanics, ludmila_sass@yahoo.com
Professor Iulian POPESCU,
University of Craiova, rodicaipopescu@yahoo.com

Abstract. A synthesis for a mechanism generating lunules across the sides of an equilateral triangle is performed. The mechanism consists of an articulated quadrilateral, prolonged with a RRR dyad. It is proved that lunules can be generate, but the speeds of plotting points are neither equal, nor constant. The synthesis of another mechanism, composed of two articulated parallelograms is afterward performed. Delayed cranks are used this time and consequently equal speeds are obtained.

Keywords: Hyppocrates's lunules, mechanism to plot lunules

1. Introduction

A lunule represents a plane geometric surface with a half-moon shape. It is built across a chord on a circle and it is delimited by the arc from a circle and another arc of circle, built across that chord, now representing the diameter for the new arc.

Hyppocrates from Chios (430-380 B.C.) has built lunules across the sides of a rectangular triangle. The small surfaces from the basis of people fingers' nails are also called lunules.

[3] presents an analysis of lunules and surfaces at isosceles triangles. Lunules generated along the sides of a trapezoid are studied in [4]. A history of Hyppocrates's lunules is presented in [5], along with their analysis when considering a isoscel rectangular triangle and a trapezoid. The lunules' aria is computed in [6] for a regular triangle. Geometrical aspects of lunules are approached in [1], along with details on the modality to construct. A synthesis of a mechanism used to trace lunules for a rectangular triangle can be found in [1]. Here is also provided a description for a mechanism used to plot lunules along the sides of a square. No other similar information was found with respect to lunules' plotting in the specialty literature.

2. Synthesis of the first mechanism

An equilateral triangle GHK was firstly built (Fig. 1). The angles which present interest for our paper are emphasized. The generated lunules are between the circle of radius OH and centre in O - described by the road OH, and arcs of circle whose diameters are the sides of the equilateral triangle. OH is a separate leading element, not related to the mechanism which generates the other arcs of lunules.

The mechanism's synthesis is made by noticing the following particular movements. If the road AB is rotating and the point B is plotting the arc corresponding to the lunule from the side GH, starting from G, then the point C, starting from H is plotting the arc corresponding to the lunule of the side HK. The articulated quadrilateral mechanism ABCD is built as described above.

For the lunule corresponding to the side KGM, a tracing point F is used. F belongs to the element EF which belongs to the dyad BFE of type RRR, added to the quadrangle.

In this way a mechanism DCBAFE was obtained. It consists of a leading element and two dyads.

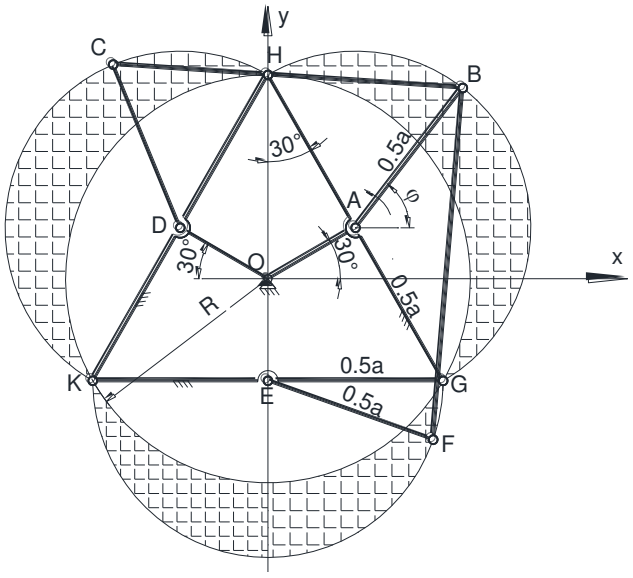

Fig. 1. Mechanism with two dyads tracing lunules

The following equations can be written:

$$KH = KG = GH = BC = BF = a \tag{1}$$

$$EH = GH\cos 30^{o} = a\cos 30^{o} \tag{2}$$

$$EG = a\sin 30^{O} \tag{3}$$

$$R = \frac{0{,}5a}{\cos 30^{o}} \tag{4}$$

$$OA = OD = OE = R\sin 30^{o} \tag{5}$$

$$\begin{cases} x_A = OA\cos 30^{o} \\ y_A = OA\sin 30^{o} \end{cases} \tag{6}$$

$$\begin{cases} x_D = -x_A \\ y_D = y_A \end{cases} \tag{7}$$

$$\begin{cases} x_E = 0 \\ y_E = -OE \end{cases} \tag{8}$$

$$AB = CD = EF = 0{,}5a \tag{9}$$

$$\begin{cases} x_B = x_A + \frac{a}{2}\cos(\varphi) \\ y_B = y_A + \frac{a}{2}\sin(\varphi) \end{cases} \quad (10)$$

$$\begin{cases} x_G = \frac{a}{2} \\ y_G = -OA \end{cases} \quad (11)$$

$$\begin{cases} x_H = 0 \\ y_H = a\cos 30^o - OE \end{cases} \quad (12)$$

$$\begin{cases} x_K = -\frac{a}{2} \\ y_K = y_G \end{cases} \quad (13)$$

A program was built to trace the mechanism for $\varphi = 55^o$ (Fig. 2).

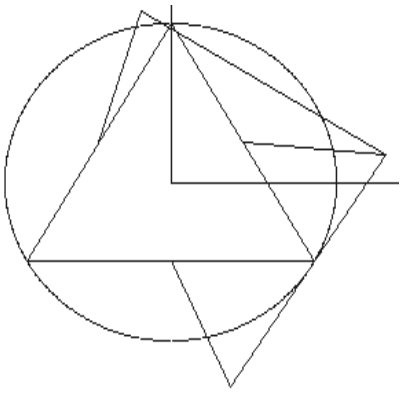

Fig. 2. The mechanism in a certain position

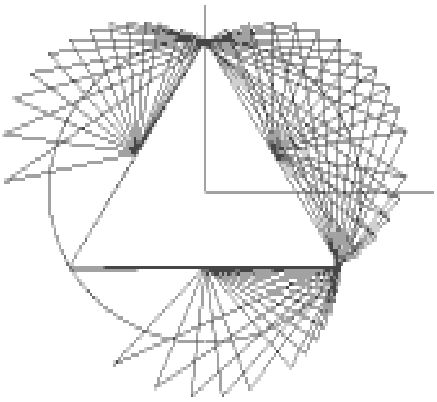

Fig. 3. Successive positions

Certain successive positions of the mechanism are depicted by Fig. 3. As long as the quadrilateral mechanism does not provide constant angles of the rocker CD, when rotating the road AB at constant angles one can notice crescent values for the angle CDH toward the zone neighboring K. When the cycling step is adopted to get more clarity for the drawing, a higher angle is obtained toward extremity. The same phenomenon is noticed in the zone EK.

One can see that for small cycling steps, these areas are swept too. Fig. 4 depicts the lunules traced with this mechanism across the three sides of the triangle.

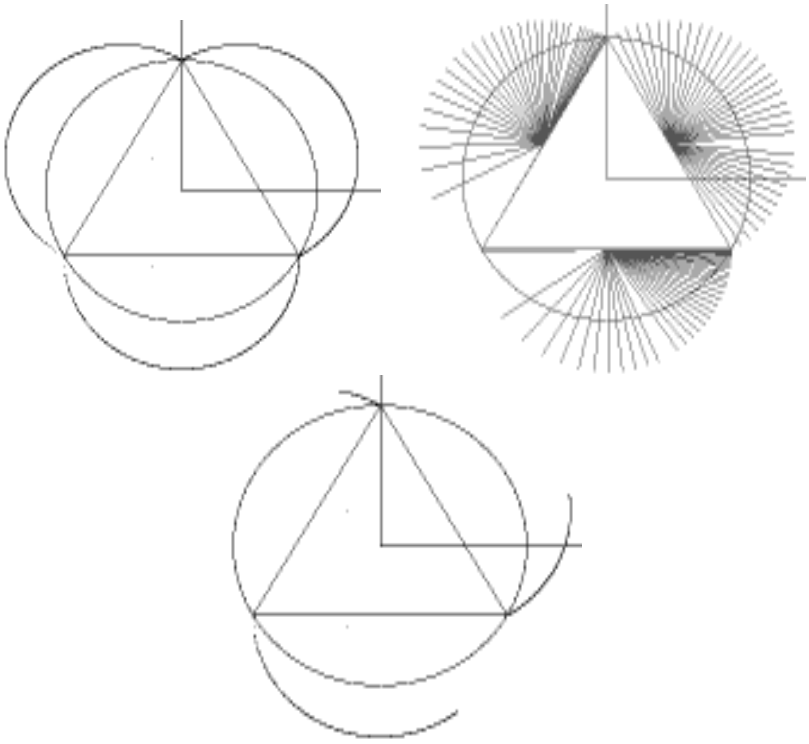

Fig. 4. Traced lunules Fig. 5. Successive positions of radii Fig. 6. Arcs at a certain moment

Fig. 5 depicts the successive positions of the elements AB, CD and EF for an operational cycle.

Variable angles can also be noticed at the road CD. The different speeds of the tracing point are emphasized by Fig. 6. Here, for the same range of variation of the generalized coordinate, the traced curves have different lengths. Only at the end they get fulfilled. The arcs traced at a given moment are presented here.

3. Synthesis of the second mechanism

The second step was to realize the synthesis of another mechanism, relying on a sequence of articulated parallelograms, each having two welded cranks (Fig. 7). The mechanism is represented by dashed lines. The lunule across the side GH is plotted by the point P belonging to the crank AB, welded to AB_1. The lunule across the side KH is traced by the point P_1 from the crank DP_1, welded to the crank DC, and the lunule across the side KG is traced by the point C_2 from the crank EC_2.

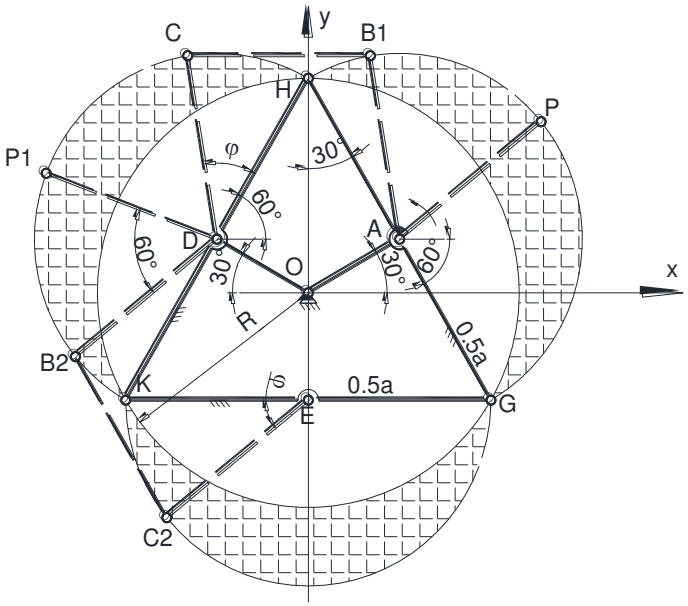

Fig. 7. The second mechanism, built across a sequence of parallelograms

Based on the angle φ between the crank AB_1 and the abscissa, on the coordinates of the points A, D, E (provided by the corresponding equations) and on the equations (6), (7) and (8), we get:

$$B_1C = AD \tag{14}$$

$$\begin{cases} x_C = x_D + 0{,}5a\cos\left(60^o + \varphi\right) \\ y_C = y_D + 0{,}5a\sin\left(60^0 + \varphi\right) \end{cases} \tag{15}$$

$$\begin{cases} x_{B1} = x_A + 0{,}5a\cos\left(\varphi + 60^0\right) \\ y_{B1} = y_A + 0{,}5a\sin\left(\varphi + 60^o\right) \end{cases} \tag{16}$$

$$\begin{cases} x_P = x_A + 0{,}5a\cos\left(\varphi - 60^o\right) \\ y_P = y_A + 0{,}5a\sin\left(\varphi - 60^o\right) \end{cases} \tag{17}$$

$$\begin{cases} x_{P1} = x_D + 0{,}5a\cos\left(120 + \varphi\right) \\ y_{P1} = y_D + 0{,}5a\sin\left(120 + \varphi\right) \end{cases} \tag{18}$$

$$\begin{cases} x_{C2} = x_E + 0{,}5a\cos\left(\pi + 2\varphi\right) \\ y_{C2} = y_E + 0{,}5a\sin\left(\pi + 2\varphi\right) \end{cases} \tag{19}$$

$$\begin{cases} x_{B2} = x_D + 0{,}5a\cos\left(\pi + \varphi\right) \\ y = y_D + 0{,}5a\sin\left(\pi + \varphi\right) \end{cases} \tag{20}$$

The resulting mechanism is given by Fig. 8, which also presents both shifted cranks. Fig. 9 depicts the successive positions of the mechanism.

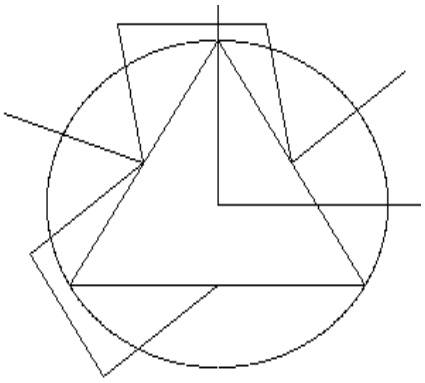

Fig. 8. The mechanism in a certain position

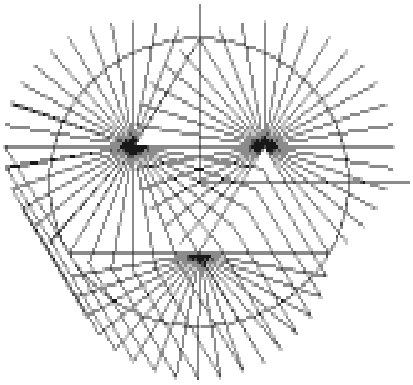

Fig. 9. Successive positions

The successive positions of the plotting cranks are presented by Fig. 10.

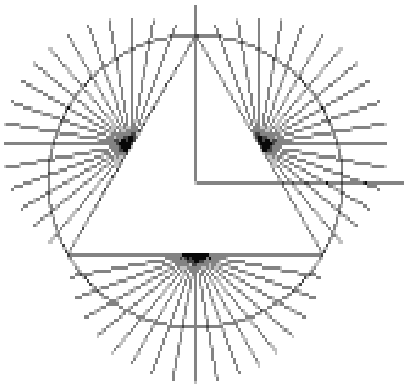

Fig. 10. Positions of plotting cranks

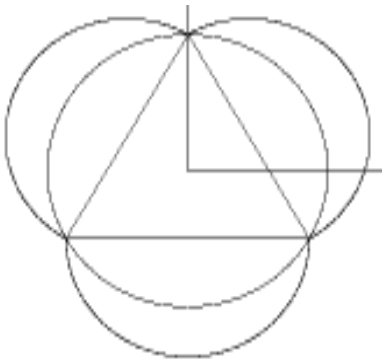

Fig. 11. Lunules

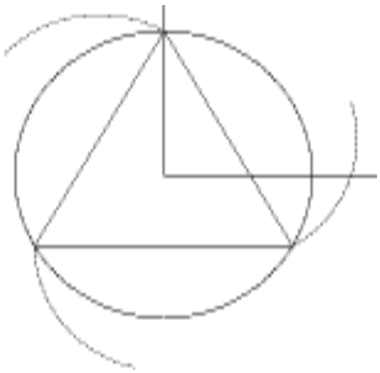

Fig. 12. Curves at a certain moment

Fig. 11 presents the lunules traced by this mechanism across the three sides of the equilateral triangle. This time the curves' plotting is performed at constant speeds (Fig. 12), unlike the case of articulated quadrilaterals. The curves plotted at a certain moment are also plotted and one can see that they are equal.

Conclusions

- The synthesis of two original mechanisms was performed. They plot lunules across the sides of an equilateral triangle.
- The first mechanism relies on an articulated quadrilateral, prolonged with a dyad of type RRR.
- The checking of the mechanism's successive positions demonstrated its correct operation.

- Because at this mechanism the last driven element has angles which are variable from one position to another (and therefore exhibits a non-uniform movement), the lunules, although correct, are plotted with variable speeds.

- The second mechanism relies on two articulated parallelograms, with shifted cranks, welded to real cranks from mechanism.
- In this last case the lunules' plotting speeds are equal and constant**.**

References

1. **Popescu Iulian, Sass, L**. - Lunulele lui Hipocrate. Vol. "The VII-th Edition of the National Conference with International Participation, GRAFICA-2000, Craiova, oct. 2000", pp. 337-340.
2. **Popescu Iulian, Sass, L**. - *Figuri geometrice ale antichităţii, generate cu mecanisme*. Vol. The VII-th Edition of the National Conference with International Participation, GRAFICA-2000, Craiova, oct. 2000, pp. 341-346.
3. http://web.calstatela.edu/faculty/hmendel/Ancient%20Mathematics/HippocratesOfChios/Lunules/IntroductionToLunules.htm [Accessed: 11 th November 2015].
4. http://isites.harvard.edu/fs/docs/icb.topic1055167.files/Knorr_ch_2.pdf [Accessed: 11 th November 2015].
5. http://areeweb.polito.it/didattica/polymath/htmlS/argoment/ParoleMate/Ott_06/LunuleIppocrate.htm [Accessed: 1 st December 2015].
6. http://calculis.net/q/lunules-d-Hippocrate-30 [Accessed: 11 th November 2015].

DETERMINATION OF THE TECHNICAL (GEOMATRICAL) DEVIATIONS EXPRESING IN PLÜCKER COORDINATES FOR 4R ASYMMETRICAL QUADRILATERAL MECHANISM

Ion BULAC
Doctor, University of Pitești, email: ionbulac57@yahoo.com

Abstract-The technological (geometrical) deviations which inevitable appear during the manufacturing and montage process at the component elements of the mechanism lead to supplementary efforts in the kinematic pairs.Being statically undetermined, for calculating the reactions it is using the elastic linear calculation For this is necessary the knowledge the forms of the technical (geometrical) deviations in the general system of reference for writing the the equations of elastic balanced.This paper presents the calculation modality of these deviations .

Keywords: cardan joint, kinematic pair, quadrilateral mechanism, cardan transmission .

1. INTRODUCTION

The technical (geometrical) deviations lead to supplementary efforts in the kinematic pairs and changes the kinematic parameters of the mechanism.This deviations are defined in the local systems of reference of the elements.Mechanism elements are found in different systems of reference [1,2].The equations of elastic balanced for calculating the reaction from kinematic pairs are written in the chosen general system of reference.In this paper is presented the mathematic model for passing the geometrical deviations from the local systems of reference in the general system of reference of the mechanism.

2. GENERAL ASPECTS

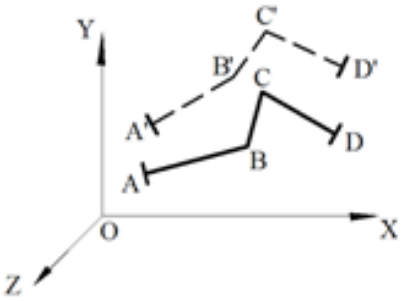

Fig.1 Angle bar

It is considered the angle bar ABCD [3] (see Fig. 1) made of the sections AB, BC, CD. Because of the geometrical deviations the bar is distorted and the normal sections from A and D reach the position A', D'.These displacements are small and defined by the low rotation vectors $\bar{\theta}_A, \bar{\theta}_D$ and by the small displacements

$\bar{\delta}_A = A\bar{A}'$; $\bar{\delta}_D = DD'$ of points A and D. In the local reference systems with the abscise along the bars AB, CD and with the other axes along the other main central inertia axes of the sections, the displacements are assigned the column matrixes of the plücker coordinates

$$\{\delta_A\} = [\theta_{Ax}, \theta_{Ay}, \theta_{Az}, \delta_{Ax}, \delta_{Ay}, \delta_{Az}]^T \quad ; \quad \{\delta_D\} = [\theta_{Dx}, \theta_{Dy}, \theta_{Dz}, \delta_{Dx}, \delta_{Dy}, \delta_{Dz}]^T \tag{1}$$

then the displacements of the sections from A, D expressed in the OXYZ system, are [3,4]:

$$\{\Delta_A\} = [T_{AB}]\{\delta_A\} \; ; \; \{\Delta_D\} = [T_{CD}]\{\delta_D\} \tag{2}$$

where $[T_{AB}]$, $[T_{CD}]$, are the position matrixes of the local reference system towards the system OXYZ

3. GEOMETRICAL DEVIATIONS AT 4R ASYMMETRICAL SPHERICAL QUADRILATERAL MECHANISM

It is considered the 4R asymmetrical spherical quadrilateral mechanism [1,2], (see Fig. 2) with the axes OA, OB, OC, OD concurrent in O and also considered that the parts AB, BC, CD have geometrical deviations $\{\tilde{\Delta}_A, \tilde{\Delta}_B, \tilde{\Delta}_C\}$., deviations considered in general system of reference.

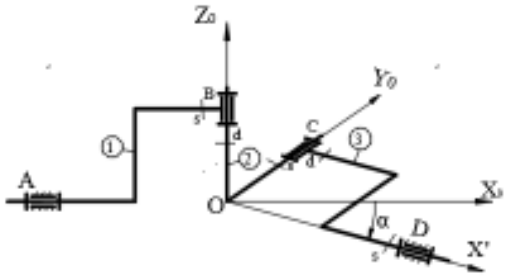

Fig. 2. The 4R Asymmetrical spherical quadrilateral mechanism

The deformation of part AB, indexed with the number 1 is defined by the displacement of the section noted with $\{\tilde{\Delta}_{Bs}\}$ and then:

$$\{\tilde{\Delta}_{AB}\} = \{\tilde{\Delta}_A\} - \{\tilde{\Delta}_{B1s}\} \tag{3}$$

The deformation of part BC, indexed with number 2 is $\{\tilde{\Delta}_{B2d}\}$ and the deformation of part CD, indexed with 3 is $\{\tilde{\Delta}_{D3s}\}$ and to that is added the displacement $\{\tilde{\Delta}_D\}$ of the bearing, so results:

$$\{\tilde{\Delta}_{BC}\} = -\{\tilde{\Delta}_{C2s}\} \; ; \; \{\tilde{\Delta}_{CD}\} = -\{\tilde{\Delta}_{D3s}\} - \{\tilde{\Delta}_D\} \tag{4}$$

In the elastically linear calculation it is considered that the kinematic pair from A is fixed and the technical deviation of the AB element, represented in Fig. 3, is given in the local reference system $Bxyz$, by the small rotation angle $\overline{\theta}_B^l$ and by the small displacement $\overline{\delta}_B^l = B\overline{B}'$.

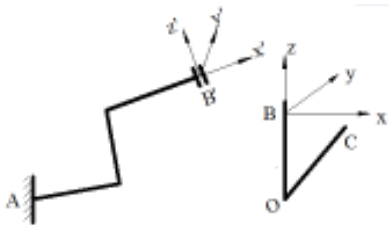

Fig. 3. The technical deviation of element AB

In plücker coordinates [3,5], the deviations $\left\{\Delta_B^l\right\}$, in the local system of reference $Bxyz$ is written under the form:

$$\left\{\Delta_B^l\right\} = \left[\theta_{Bx}^l, \theta_{By}^l, \theta_{Bz}^l, \delta_{Bx}^l, \delta_{By}^l, \delta_{Bz}^l\right]^T \tag{5}$$

where $\left[\theta_{Bx}^l, \theta_{By}^l, \theta_{Bz}^l, \delta_{Bx}^l, \delta_{By}^l, \delta_{Bz}^l\right]^T$ are the projections on the local axis of the vectors $\overline{\theta}_B^l, \overline{\delta}_B^l$.
It is considered the reference systems [4]:

- $OX_0Y_0Z_0$, fixed system;
- $OX'Y_0Z_0'$, obtained by rotating the reference system $OX_0Y_0Z_0$,around the axis OY_0 with the angle α, that contain the elements of exit fork (see Fig. 4,a);
- OX_0Y^*Z, obtained by rotating the system $OX_0Y_0Z_0$ around the axis OX_0 with the angel θ_1, that contain the elements of entry fork (see Fig. 4, b);
- $OX'YZ_0^{\bullet}$, obtained by rotating the system $OX'Y_0Z_0'$ around the axis OX' with the angle θ_2, that contain the elements of cardan cross (see Fig. 4,c);
- $ix_iy_iz_i$, $i = A,B,C,D$ the local systems of reference.

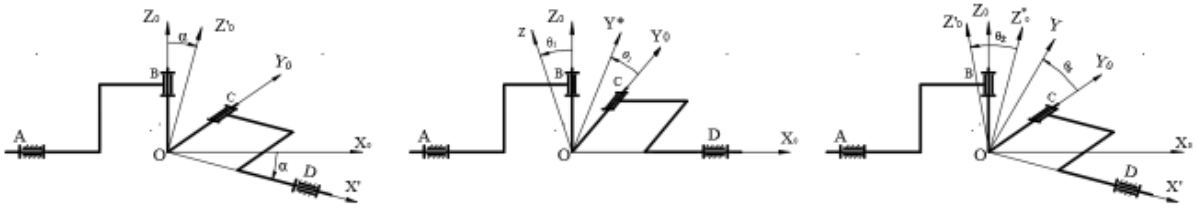

a b c

Fig. 4. The mobile reference systems
(a – $OX'Y_0Z_0'$; b – OX_0Y^*Z; c – $OX'YZ_0^{\bullet}$)

Notating next with

- $\{\Delta_i^l\}=[\theta_{ix}^l,\theta_{iy}^l,\theta_{iz}^l,\delta_{ix}^l,\delta_{iy}^l,\delta_{iz}^l]^T$, $i=A,B,C,D$-geometrical deviations in local systems of reference
- $\{\Delta_i\}=[\theta_{ix},\theta_{iy},\theta_{iz},\delta_{ix},\delta_{iy},\delta_{iz}]^T$, $i=A,B,C,D$-geometrical deviations in systems of reference, $OX'Y_0Z_0'$, OX_0Y^*Z, $OX'YZ_0^*$.
- $\{\tilde{\Delta}_i\}=[\tilde{\theta}_{ix},\tilde{\theta}_{iy},\tilde{\theta}_{iz},\tilde{\delta}_{ix},\tilde{\delta}_{iy},\tilde{\delta}_{iz}]^T$, $i=A,B,C,D$-geometrical deviations in general system of reference .

Solving the equations system of elastic balanced [3] , written for this mechanism who is multiple statically undeterminate are obtained the relations for the relativ rotations $[\xi]$ and for the rection forces from kinematic pair A under form [3] , where appears $\{\tilde{\Delta}\}$ which to be calculated:

$$\{\xi\}=-[[\tilde{U}][K_{AD}][U]]^{-1}[U][K_{AD}]\{\tilde{\Delta}\}\ ;\ \{R_A\}=[K_{AD}]\{[U]\{\xi\}+\{\tilde{\Delta}\}\} \tag{7}$$

The deviations are first locally defined and then in one of the three reference systems OX_0Y^*Z, OX^*YZ, $OX'YZ_0^*$ that do not depend on θ_1,θ_2 and then in the system $OX_0Y_0Z_0$ and under this form by summing:

$$\{\Delta\}=\{\tilde{\Delta}_{AB}\}+\{\tilde{\Delta}_{BC}\}+\{\tilde{\Delta}_{CD}\} \tag{8}$$

the relation (7) are involved.

4. THE GEOMETRICAL DEVIATIONS IN THE MOBILE REFERENCES SYSTEMS

$OX'Y_0Z_0'$, OX_0Y^*Z, $OX'YZ_0^*$.

The calculation of $\{\Delta_{AB}\}$. (see Fig. 5)

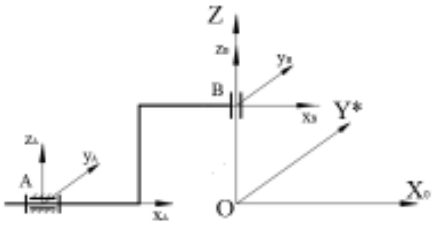

Fig.5. Entry fork

The deviation from A, in local reference system $Ax_Ay_Az_A$ is writed under the form

$$\{\Delta_A^l\}=[\theta_{Ax}^l,\theta_{Ay}^l,\theta_{Az}^l,\delta_{Ax}^l,\delta_{Ay}^l,\delta_{Az}^l]^T \tag{9}$$

$$X_A=-OA,\quad Y_A=0,\quad Z_A=0 \tag{10}$$

$$[G_A]=\begin{bmatrix}0&0&0\\0&0&-X_A\\0&X_A&0\end{bmatrix}\ ;\ [R_A]=[I]=\begin{bmatrix}1&0&0\\0&1&0\\0&0&1\end{bmatrix}\ ;\ [T_A]=\begin{bmatrix}[R_A]&[0]\\[G_A][R_A]&[R_A]\end{bmatrix} \tag{11}$$

$$\{\Delta_A\}=[T_A]\{\Delta_A^l\} \tag{12}$$

The deviation from B, in local reference system $Bx_B y_B z_B$ is writed under the form (5)

$\{\Delta_B^1\} = [\theta_{Bx}^1, \theta_{By}^1, \theta_{Bz}^1, \delta_{Bx}^1, \delta_{By}^1, \delta_{Bz}^1]^T$

$$X_B = 0, \quad Y_B = 0, \quad Z_B = OB; \tag{13}$$

$$[G_B] = \begin{bmatrix} 0 & 0 & Y_B \\ 0 & 0 & 0 \\ -Y_B & 0 & 0 \end{bmatrix}; \quad [R_B] = [I] = \begin{bmatrix} 1 & 0 & 0 \\ 0 & 1 & 0 \\ 0 & 0 & 1 \end{bmatrix}; \quad [T_B] = \begin{bmatrix} [R_B] & [0] \\ [G_B][R_B] & [R_B] \end{bmatrix} \tag{14}$$

$$\{\Delta_B\} = [T_B][\Delta_B^1] \tag{15}$$

The calculation of $\{\Delta_{BC}\}$. (see Fig. 6)

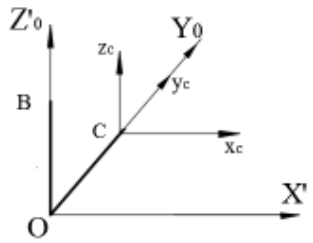

Fig. 6. Cross

The deviation from C, in local reference system $Cx_C y_C z_C$ is writed under the form

$$\{\Delta_C^1\} = [\theta_{Cx}^1, \theta_{Cy}^1, \theta_{Cz}^1, \delta_{Cx}^1, \delta_{Cy}^1, \delta_{Cz}^1]^T \tag{16}$$

$$X_C = 0, Y_C = OC, \; Z_C = 0 \tag{17}$$

$$[G_C] = \begin{bmatrix} 0 & 0 & -Y_C \\ 0 & 0 & 0 \\ Y_C & 0 & 0 \end{bmatrix}; \quad [R_C] = [I] = \begin{bmatrix} 1 & 0 & 0 \\ 0 & 1 & 0 \\ 0 & 0 & 1 \end{bmatrix}; \quad [T_C] = \begin{bmatrix} [R_C] & [0] \\ [G_C][R_C] & [R_C] \end{bmatrix} \tag{18}$$

$$\{\Delta_C\} = [T_C][\Delta_C^1] \tag{19}$$

The calculation of $\{\Delta_{CD}\}$. (see Fig.7)

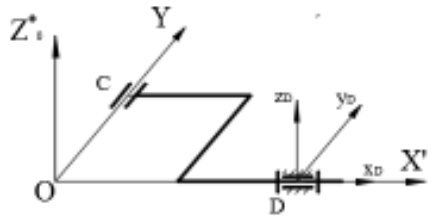

Fig.7. Exit fork

The deviation from D, in local reference system $Dx_D y_D z_D$ is writed under the form

$$\{\Delta_D^1\} = [\theta_{Dx}^1, \theta_{Dy}^1, \theta_{Dz}^1, \delta_{Dx}^1, \delta_{Dy}^1, \delta_{Dz}^1]^T \tag{20}$$

$$X_D = OD, \; Y_D = 0, \quad Z_D = 0 \tag{21}$$

$$[G_D]=\begin{bmatrix}0 & 0 & 0\\ 0 & 0 & -X_D\\ 0 & X_D & 0\end{bmatrix};\ [R_D]=[I]=\begin{bmatrix}1 & 0 & 0\\ 0 & 1 & 0\\ 0 & 0 & 1\end{bmatrix};\ [T_D]=\begin{bmatrix}[R_D] & [0]\\ [G_D][R_D] & [R_D]\end{bmatrix}$$

$$(22)\ \{\Delta_D\}=[T_D][\Delta_D^1] \tag{23}$$

5. THE GEOMETRICAL DEVIATIONS IN GENERAL SYSTEM OF REFERENCE $OX_0Y_0Z_0$

The calculation of $\{\tilde{\Delta}_{AB}\}$

$$\{\tilde{\Delta}_A\}=[T_{AB}]\{\Delta_A\} \tag{24}$$

$$[T_{AB}]=\begin{bmatrix}[R_{AB}] & [0]\\ [0] & [R_{AB}]\end{bmatrix};\ [R_{AB}]=\begin{bmatrix}1 & 0 & 0\\ 0 & c\theta_1 & -s\theta_1\\ 0 & s\theta_1 & c\theta_1\end{bmatrix} \tag{25}$$

$$\{\tilde{\Delta}_B\}=[T_{AB}]\{\Delta_B\};\ \{\tilde{\Delta}_{AB}\}=\{\tilde{\Delta}_A\}-\{\tilde{\Delta}_B\}; \tag{26}$$

The calculation of $\{\tilde{\Delta}_{BC}\}$

$$\{\tilde{\Delta}_C\}=[T_{BC}]\{\Delta_C\};\ \{\tilde{\Delta}_{BC}\}=-\{\tilde{\Delta}_C\} \tag{27}$$

$$[T_{BC}]=\begin{bmatrix}[R_{BC}] & [0]\\ [0] & [R_{BC}]\end{bmatrix};\ [R_{BC}]=\begin{bmatrix}c\theta_1c\theta_2+s\theta_1s\theta_2c\alpha & s\alpha s\theta_2 & 0\\ -c\theta_1s\theta_2s\alpha & c\theta_2 & -s\theta_1\\ -s\theta_1s\theta_2s\alpha & c\alpha s\theta_2 & c\theta_1\end{bmatrix} \tag{28}$$

The calculation of $\{\tilde{\Delta}_{CD}\}$

$$\{\tilde{\Delta}_D\}=[T_{CD}]\{\Delta_D\};\ \{\tilde{\Delta}_{CD}\}=-\{\tilde{\Delta}_D\} \tag{29}$$

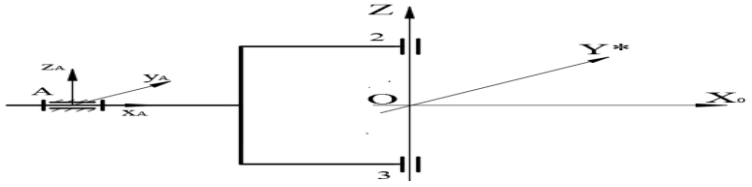

(30)

The angle θ_2 is are calculed with the expressions of the form [4]:

$$\theta_2 = \begin{cases} \operatorname{arctg}\left(\frac{1}{c\alpha}\operatorname{tg}\theta_1\right); 0 \le \theta_1 < \frac{\pi}{2} \\ \frac{\pi}{2}; \theta_1 = \frac{\pi}{2} \\ \pi + \operatorname{arctg}\left(\frac{1}{c\alpha}\operatorname{tg}\theta_1\right); \frac{\pi}{2} \le \theta_1 < \frac{3\pi}{2} \\ \frac{3\pi}{2}; \theta_1 = \frac{3\pi}{2} \\ 2\pi + \operatorname{arctg}\left(\frac{1}{c\alpha}\operatorname{tg}\theta_1\right); \frac{3\pi}{2} < \theta_1 \le 2\pi \end{cases} \quad (31)$$

6. CONCLUSIONS

By using the plücker coordinates and the method of relative displacements [5]. it is possible to obtain final analytical results for calculating the influence of technical deviations over the efforts from the 4R asymmetrical spherical quadrilateral mechanism, multiple statically undetermined. Using this mathematical model, make possible the elaboration an calculation algorithm that by numerical simulation can highlight the influence of different technical deviations that appear in the mechanism elements.

REFERENCES

1. **DUDIŢĂ, FL**., Cardan shafting, Technical Publishing House, Bucharest, 1966.
2. **DUDIŢĂ, FL., FL., DIACONESCU, D., BOHN, CR., NEAGOE, M., SĂULESCU, R**., Cardan shafting, Transilvania Expres Publishing House, Braşov, 2003 .
3. **BULAC, I,.** The numerical study of efforts from 4r spherical quadrilateral mechanism , Annals of the Oradea University, vol. XII, nr.1, 2014.
4. **BULAC, I., PANDREA, N.,** The influence of technical deviations over efforts from a 4r spherical quadrilateral mechanism, 6th Symposium , ,,Durability and Reliability of Mechanical
5. **PANDREA, N**., Solid mechanics plucheriane coordinates, Romanian Academy Publishing House, Bucharest, 2000.

DETERMINATION OF THE TECHNICAL (GEOMATRICAL) DEVIATIONS EXPRESING IN PLÜCKER COORDINATES FOR 4R SYMMETRICAL SPHERICAL QUADRILATERAL MECHANISM

Ion BULAC
Doctor, University of Pitești, email: ionbulac57@yahoo.com

Abstract-The technological (geometrical) deviations determine in the intermediate couples of the mechanism supplementary efforts due to restrained movement. The 4R asymmetrical spherical quadrilateral mechanism is multiple statically indeterminate, and for calculating the reactions from the kinematic pairs it is applied the elastic linear calculation using the relative displacements method. The equations of elastic balanced are written in the general system of reference.For this is necessary the knowledge the forms of the technical (geometrical) deviations in the general system of reference.This paper presents the calculation modality these deviations .

Keywords: cardan joint, kinematic pair, quadrilateral mechanism, cardan transmission .

1. INTRODUCTION

The technical (geometrical) deviations lead to changing of kinematic parameters and to the supplementary efforts from kinematic pairs of the mechanism.The technical (geometrical) deviations are defined in the local systems of reference of the elements .In mechanism, the elements are found in different systems of reference [1,2]. The equations of elastic balanced are written in the chosen general system of reference.In this paper is presented the mathematic model and the necessary relations for passing the geometrical deviations from the local systems of reference in the general system of reference of the mechanism.

2. THE TECHNOLOGICAL (GEOMETRICAL) DEVIATIONS AT THE 4R SYMMETRICAL SPHERICAL QUADRILATERAL MECHANISM

It is considered the 4R symmetrical spatial spherical mechanism (see Figure 1), and the reference systems [3]:

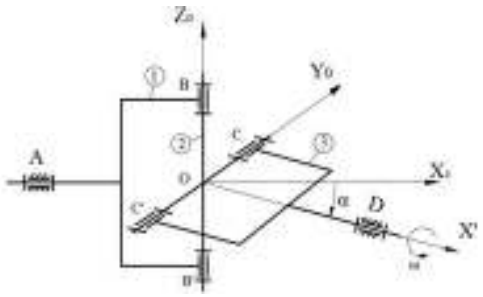

Figure 1. The 4R symmetrical spherical quadrilateral mechanism

- $OX_0Y_0Z_0$, fixed system;
- $OX'Y_0Z_0'$, obtained by rotating the reference system $OX_0Y_0Z_0$,around the axis OY_0 with

the angle α (see Figure 2,a);

- OX_0Y^*Z, obtained by rotating the system $OX_0Y_0Z_0$ around the axis OX_0 with the angle θ_1 (see Figure 2, b);
- $OX'YZ_0^{\bullet}$, obtained by rotating the system $OX'Y_0Z_0'$ around the axis OX' with the angle θ_2 (see Figure 3,c);

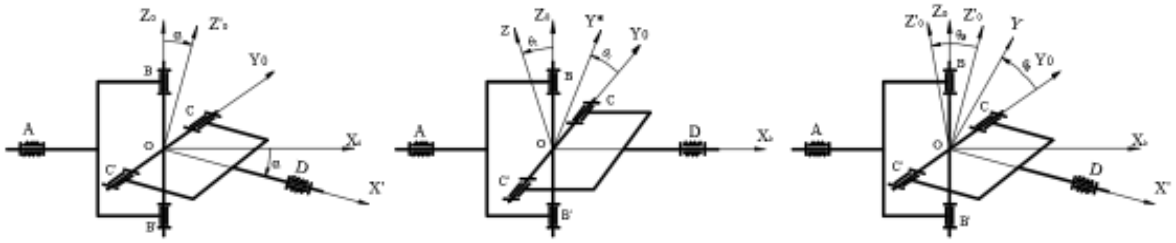

a b c

Figure 2. The mobile reference systems (a – $OX'Y_0Z_0'$; b – OX_0Y^*Z; c – $OX'YZ_0^{\bullet}$)

Notating next with $\{\Delta_i^1\},\{\Delta_i\},\{\tilde{\Delta}_i\}, i = A,2s,3s,2d,3d,5s,6s,5d,6d,8s$ the technological (geometrical) deviations expressed in plücker coordinates [4,5] in the local systems of reference, the mobile systems of reference OX_0Y^*Z, $OX'Y_0Z_0'$, $OX'YZ_0^{\bullet}$, and in the general system of reference

- $i = A,2s,3s$, for the entry fork at joint A, 1 and 2 ;
- $i = 2d,3d,5s,6s$, for the cardan cross at joint 2, 3, 5 and 6;
- $i = 5d,6d,8s$ for the exit fork at joint 5, 6 and D;

3. CALCULATION OF THE TEHNICAL (GEOMETRICAL) DEVIATIONS IN THE MOBILE REFERENCE SYSTEMS OX_0Y^*Z, $OX'Y_0Z_0'$, $OX'YZ_0^{\bullet}$

Notating with:

- $[X_i],[Y_i],[Z_i]$ - the coordinates of the origins of the local systems of reference where deviations are defined;
- $[R_i],[G_i],[T_i]$, $i = A,2s,3s,2d,3d,5s,6s,5d,6d,8s$, the rotation, translation, position matrixes of the local reference systems towards the systems OX_0Y^*Z ($i = A,2s,3s$), $OX'Y_0Z_0'$ ($i = 2d,3d,5s,6s$), $OX'YZ_0^{\bullet}$ ($i = 5d,6d,8s$);

Then [4,5]

$$[G_i]=\begin{bmatrix} 0 & -Z_i & Y_i \\ Z_i & 0 & -X_i \\ -Y_i & X_i & 0 \end{bmatrix};[T_i]=\begin{bmatrix} [R_i] & [0] \\ [G_i][R_i] & [R_i] \end{bmatrix};\{\Delta_i\}=[T_i]\{\Delta_i^1\} \quad (1)$$

4. CALCULATION OF THE TEHNICAL (GEOMETRICAL) DEVIATIONS IN THE GENERAL SYSTEM OF REFERENCE $OX_0Y_0Z_0$

Notating with:

- $[R_j],[G_j],[T_j]$, $j = AB, BC, CD$,the rotation, translation, position matrixes of the systems OX_0Y^*Z ($j = AB$), $OX''Y_0Z_0'$ ($j = BC$), $OX''YZ_0^{\bullet}$ ($j = CD$) towards the system $OX_0Y_0Z_0$;
- $[G_j]=[0]$, (the origin of the mobile systems of reference coincides with the origin of the general system of reference) ;

Then [4,5]

$$[T_j]=\begin{bmatrix} [R_j] & [0] \\ [0] & [R_j] \end{bmatrix} \quad ; \quad \{\tilde{\Delta}_i\}=[T_j]\{\Delta_i\} \quad (2)$$

$i = A,2s,3s$; $j = AB$, for the entry fork ; $i = 2d,3d,5s,6s$; $j = BC$, for the cardan cross,
$i = 5d,6d,8s$; $j = CD$ for the exit fork ;

The relations for calculating the geometrical deviations expressed in plucker coordinates are presented in TABLE 1 for each element of mechanism.

TABLE 1

$\{\tilde{\Delta}_A\}$ the displacement of the bearing from A and the displacement of crosses tail 1	$\{\Delta^l_A\}=[\theta^l_{Ax},\theta^l_{Ay},\theta^l_{Az},\delta^l_{Ax},\delta^l_{Ay},\delta^l_{Az}]^T$
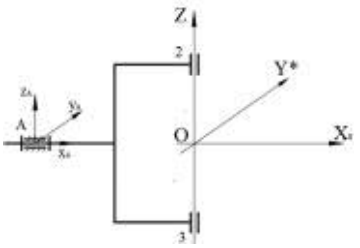	$X_1=-(l_1+l_3)\ ;\ Y_1=0\ ;\ Z_1=0$ $[G_A]=\begin{bmatrix}0 & 0 & 0\\ 0 & 0 & l_1+l_3\\ 0 & -(l_1+l_3) & 0\end{bmatrix}\ ;\ [R_A]=[I]$ $\{\Delta_A\}=\begin{bmatrix}[I] & [0]\\ [G_A] & [I]\end{bmatrix}[\Delta^l_A]\ ;\ \{\tilde{\Delta}_A\}=[T_{AB}]\{\Delta_A\}$
$\{\tilde{\Delta}^S_2\}$ the fork displacement 1 at the joint 2	$\{\Delta^l_{2s}\}=[\theta^l_{2sx},\theta^l_{2sy},\theta^l_{2sz},\delta^l_{2sx},\delta^l_{2sy},\delta^l_{2sz}]^T$
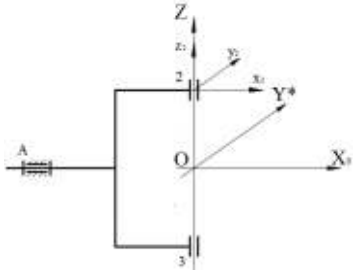	$X_{2s}=0\ ;\ Y_{2s}=0\ ;\ Z_{2s}=l_6$ $[G_{2s}]=\begin{bmatrix}0 & -l_6 & 0\\ l_6 & 0 & 0\\ 0 & 0 & 0\end{bmatrix}\ ;\ [R_{2s}]=[I]$ $\{\Delta_{2s}\}=\begin{bmatrix}[I] & [0]\\ [G_{2s}] & [I]\end{bmatrix}[\Delta^l_{2s}]\ ;\ \{\tilde{\Delta}_{2s}\}=[T_{AB}]\{\Delta_{2s}\}$
$\{\tilde{\Delta}^d_2\}$ the cross displacement at the joint 2	$\{\Delta^l_{2d}\}=[\theta^l_{2dx},\theta^l_{2dy},\theta^l_{2dz},\delta^l_{2dx},\delta^l_{2dy},\delta^l_{2dz}]^T$

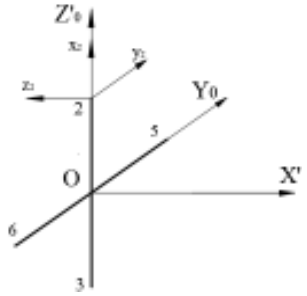	$X_{2d}=0\ ;\ Y_{2d}=0\ ;\ Z_{2d}=l_6$ $[G_{2d}]=\begin{bmatrix}0 & -l_6 & 0\\ l_6 & 0 & 0\\ 0 & 0 & 0\end{bmatrix}\ ;\ [R_{2d}]=\begin{bmatrix}0 & 0 & -1\\ 0 & 1 & 0\\ 1 & 0 & 0\end{bmatrix}$ $\{\Delta_{2d}\}=\begin{bmatrix}[R_{2d}] & [0]\\ [G_{2d}][R_{2d}] & [R_{2d}]\end{bmatrix}[\Delta^l_{2d}]\ ;\ \{\tilde{\Delta}_{2d}\}=[T_{BC}]\{\Delta_{2d}\}$
$\{\tilde{\Delta}^s_3\}$ the cross displacement 1 at the joint 3	$\{\Delta^l_{3s}\}=[\theta^l_{3sx},\theta^l_{3sy},\theta^l_{3sz},\delta^l_{3sx},\delta^l_{3sy},\delta^l_{3sz}]^T$
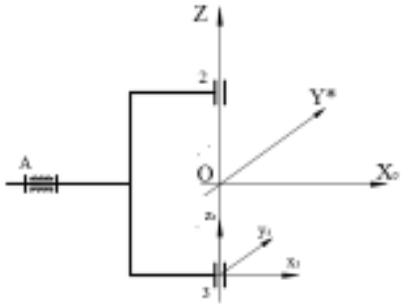	$X_{3s}=0\ ;\ Y_{3s}=0\ ;\ Z_{3s}=-l_7$ $[G_{3s}]=\begin{bmatrix}0 & l_7 & 0\\ -l_7 & 0 & 0\\ 0 & 0 & 0\end{bmatrix}\ ;\ [R_{3s}]=[I]$ $\{\Delta_{3s}\}=\begin{bmatrix}[I] & [0]\\ [G_{3s}] & [I]\end{bmatrix}[\Delta^l_{3s}]\ ;\ \{\tilde{\Delta}_{3s}\}=[T_{AB}]\{\Delta_{3s}\}$
$\{\tilde{\Delta}^d_3\}$ the cross displacement at the joint 3	$\{\Delta^l_{3d}\}=[\theta^l_{3dx},\theta^l_{3dy},\theta^l_{3dz},\delta^l_{3dx},\delta^l_{3dy},\delta^l_{3dz}]^T$
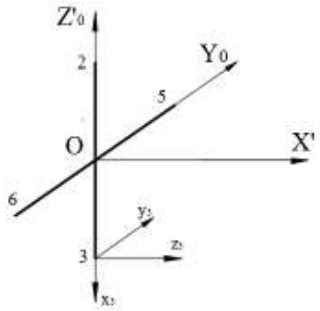	$X_{3d}=0\ ;\ Y_{3d}=0\ ;\ Z_{3d}=-l_7$ $[G_{3d}]=\begin{bmatrix}0 & l_7 & 0\\ -l_7 & 0 & 0\\ 0 & 0 & 0\end{bmatrix}\ ;\ [R_{3d}]=\begin{bmatrix}0 & 0 & 1\\ 0 & 1 & 0\\ -1 & 0 & 0\end{bmatrix}$ $\{\Delta_{3d}\}=\begin{bmatrix}[R_{3d}] & [0]\\ [G_{3d}][R_{3d}] & [R_{3d}]\end{bmatrix}[\Delta^l_{3d}]\ ;\ \{\tilde{\Delta}_{3d}\}=[T_{BC}]\{\Delta_{3d}\}$
$\{\tilde{\Delta}^s_5\}$ the cross displacement at the joint 5	$\{\Delta^l_{5s}\}=[\theta^l_{5sx},\theta^l_{5sy},\theta^l_{5sz},\delta^l_{5sx},\delta^l_{5sy},\delta^l_{5sz}]^T$

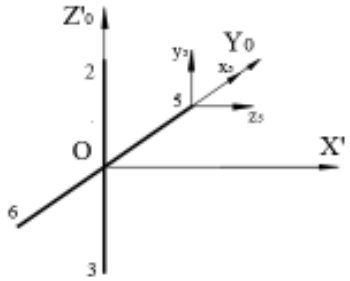	$$X_{5s}=0\ ;\ Y_{5s}=l_9\ ;\ Z_{5s}=0$$ $$[G_{5s}]=\begin{bmatrix}0 & 0 & l_9\\ 0 & 0 & 0\\ -l_9 & 0 & 0\end{bmatrix}\ ;\ [R_{5s}]=\begin{bmatrix}0 & 0 & 1\\ 1 & 0 & 0\\ 0 & 1 & 0\end{bmatrix}$$ $$\{\Delta_{5s}\}=\begin{bmatrix}[R_{5s}] & [0]\\ [G_{5s}][R_{5s}] & [R_{5s}]\end{bmatrix}\{\Delta^l_{5s}\}\ ;\ \{\tilde{\Delta}_{5s}\}=[T_{BC}]\{\Delta_{5s}\}$$
$\{\tilde{\Delta}^d_5\}$ the fork displacement 2 at the joint 5	$$\{\Delta^l_{5d}\}=[\theta^l_{5dx},\theta^l_{5dy},\theta^l_{5dz},\delta^l_{5dx},\delta^l_{5dy},\delta^l_{5dz}]^T$$
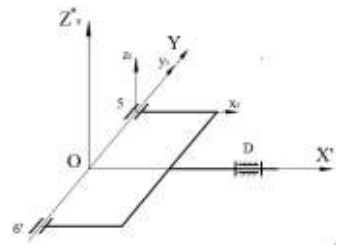	$$X_{5d}=0\ ;\ Y_{5d}=l_9\ ;\ Z_{5d}=0$$ $$[G_{5d}]=\begin{bmatrix}0 & 0 & l_9\\ 0 & 0 & 0\\ -l_9 & 0 & 0\end{bmatrix}\ ;\ [R_{5d}]=[I]$$ $$\{\Delta_{5s}\}=\begin{bmatrix}[I] & [0]\\ [G_{5d}] & [I]\end{bmatrix}\{\Delta^l_{5d}\}\ ;\ \{\tilde{\Delta}_{5d}\}=[T_{CD}]\{\Delta_{5d}\}$$
$\{\tilde{\Delta}^s_6\}$ the cross displacement at the joint 6	$$\{\Delta^l_{6s}\}=[\theta^l_{6sx},\theta^l_{6sy},\theta^l_{6sz},\delta^l_{6sx},\delta^l_{6sy},\delta^l_{6sz}]^T$$
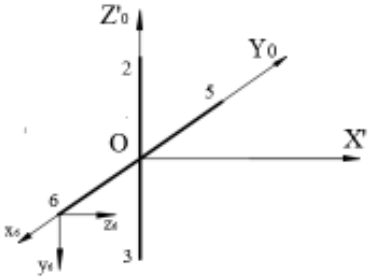	$$X_{6s}=0\ ;\ Y_{6s}=-l_8\ ;\ Z_{6s}=0$$ $$[G_{6s}]=\begin{bmatrix}0 & 0 & -l_8\\ 0 & 0 & 0\\ l_8 & 0 & 0\end{bmatrix}\ ;\ [R_{6s}]=\begin{bmatrix}0 & 0 & 1\\ -1 & 0 & 0\\ 0 & -1 & 0\end{bmatrix}$$ $$\{\Delta_{6s}\}=\begin{bmatrix}[R_{6s}] & [0]\\ [G_{6s}][R_{6s}] & [R_{6s}]\end{bmatrix}\{\Delta^l_{6s}\}\ ;\ \{\tilde{\Delta}_{6s}\}=[T_{BC}]\{\Delta_{6s}\}$$
$\{\tilde{\Delta}^d_6\}$ the fotk displacement 2 at the joint 6	$$\{\Delta^l_{6d}\}=[\theta^l_{6dx},\theta^l_{6dy},\theta^l_{6dz},\delta^l_{6dx},\delta^l_{6dy},\delta^l_{6dz}]^T$$

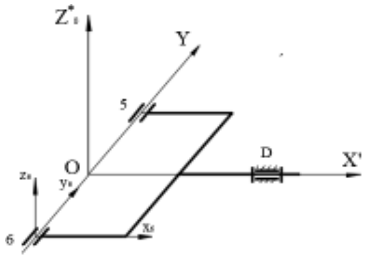	$X_{6d}=0\ ;\ Y_{6d}=-l_8\ ;\ Z_{6d}=0$ $[G_{6d}]=\begin{bmatrix}0 & 0 & -l_8\\ 0 & 0 & 0\\ l_8 & 0 & 0\end{bmatrix}\ ;\ [R_{6d}]=[I]$ $\{\Delta_{6d}\}=\begin{bmatrix}[I] & [0]\\ [G_{6d}] & [I]\end{bmatrix}\{\Delta^1_{6d}\}\ ;\ \{\tilde{\Delta}_{6d}\}=[T_{CD}]\{\Delta_{6d}\}$
$\{\tilde{\Delta}^s_8\}$ the displacement of the fork axle 2	$\{\Delta^1_{8s}\}=[\theta^1_{8sx},\theta^1_{8sy},\theta^1_{8sz},\delta^1_{8sx},\delta^1_{8sy},\delta^1_{8sz}]^T$
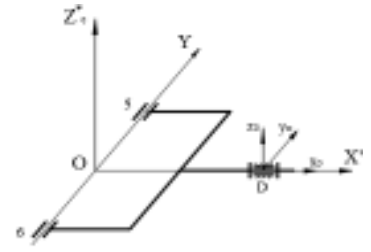	$X_{8s}=l_{10}+l_{14}\ ;\ Y_{8s}=0\ ;\ Z_{8s}=0$ $[G_{8s}]=\begin{bmatrix}0 & 0 & 0\\ 0 & 0 & -(l_{10}+l_{14})\\ l_8 & (l_{10}+l_{14}) & 0\end{bmatrix}\ ;\ [R_{8s}]=[I]$ $\{\Delta_{8s}\}=\begin{bmatrix}[I] & [0]\\ [G_{8s}] & [I]\end{bmatrix}\{\Delta^1_{8s}\}\ ;\ \{\tilde{\Delta}_{8s}\}=[T_{CD}]\{\Delta_{8s}\}$

6. CONCLUSIONS

The mathematic model for calculating the geometrical deviations in general system of reference, presentet in this paper, make possible writing the equation of elastic balanced and determination of the reaction from kinematic pairs of the mechanism which is multiple statically indeterminate.

REFERENCES

1. **DUDIŢĂ, FL**., Cardan shafting, Technical Publishing House, Bucharest, 1966.
2. **DUDIŢĂ, FL., FL., DIACONESCU, D., BOHN, CR., NEAGOE, M., SĂULESCU, R**., Cardan shafting, Transilvania Expres Publishing House, Braşov, 2003 .
3. **BULAC, I,.** The numerical study of efforts from 4r spherical quadrilateral mechanism , Annals of the Oradea University, vol. XII, nr.1, 2014.
4. **BULAC, I., PANDREA, N.,** The influence of technical deviations over efforts from a 4r spherical quadrilateral mechanism, 6th Symposium , ,,Durability and Reliability of Mechanical
5. **PANDREA, N**., Solid mechanics plucheriane coordinates, Romanian Academy Publishing House, Bucharest, 2000.

BLOCK DIAGRAM MODELS FOR CORRELATED STRUCTURES

Dr.ing. **Adrian Stere PARIS,** Univ. Politehnica Bucharest, email: adrian.paris@upb.ro
Dr. Constantin TÂRCOLEA, Univ. Politehnica Bucharest, email: constantin_tarcolea@yahoo.com

Motto; The Gaussian copula had 'killed Wall Street' and 'devastated the global economy'. Felix Salmon, Recipe for Disaster: The Formula That Killed Wall Street, WIRED, 2009

Abstract The copula function offers new opportunities for advanced engineering design and can model correlated structures between random variables in reliability; in other words the dependence can describe time varying and nonlinear features of statistical links of marginal distributions. The paper proposes the study of reliability block diagrams by the analysis of the bridge model with links like serial-parallel, parallel-serial, based on total probability formula. The proposed reliability model built by copula functions is a new possible variant for statistical approach in the quality practice.

K**eywords**: quality, reliability, dependence, block model

1. Introduction

Reliability is an important and challenging subject, which involves the disciplines of science and engineering. Researchers in both these fields have been working on reliability problems for several decades, to summarize various ageing and dependence concepts of the lifetimes that have been widely studied in the field of reliability [9].

The study of the system's reliability considers usually the components as independent, particularly in the case of reliability block diagrams.

In reality there are the mathematical usages "dependent variable" and "independent variable".These have been extremely effective in producing confusion when dealing with data. An event is dependent when the probability of its happening is altered by the happening of some other.

The dependence function enables the study of interdependences of different characteristics in the reliability engineering too, which includes link between components, materials, environment, etc. The probability of failure of a structural component with given marginal distributions and correlation coefficient of two variables cannot be determined uniquely.

A possibility to describe the implicit and explicit dependencies between random variables is the concept of copula (the name comes from the Latin for "link" or "tie", similar but unrelated to grammatical copulas in linguistics).

Copulas are popular in the high-dimensional statistical applications as they allow easily modelling and estimating the distribution of random vectors by estimating marginals and copulae separately. The concept of ‘‘copulae,’’ is a tool for understanding relationships among multivariate outcomes. A copula is a function that links univariate marginals to their full multivariate distribution. Copulas were introduced in 1959 in the context of probabilistic metric spaces [3].

In this paper, the goal is limited to the dependence functions (copulae) that are relevant to reliability analysis and particularly for the block diagrams.

Copula is a device that fully quantifies the dependence among random variables.The multivariate normal distribution has been studied since the 19th century. The normal (Gaussian) copula has even come to the attention of the general public due to its use in the valuation of structured products and the decline of these products during the financial crisis of 2007 and 2008 [6].

The Gaussian copula C of bivariate normal distribution with linear correlation coefficient R is:

$$C(u,v) = \Phi_2(\Phi^{-1}(u), \Phi^{-1}(v), R), 0 \le u, v \le 1; \ -1 \le R \le 1, \quad (1)$$

where Φ_2 is the joint distribution function of the bivariate standard normal distribution function and Φ^{-1}denotes the inverse of the distribution function of the univariate standard normal distribution [5]. In the bivariate case the copula expression can be written as [2]:

$$C_R^{Ga}(u,v) = \int_{-\infty}^{\Phi^{-1}(u)} \int_{-\infty}^{\Phi^{-1}(v)} \frac{1}{2\pi\sqrt{(1-R^2)}} \exp\{-\frac{s^2-2Rst+t^2)}{2(1-R^2)}\} dsdt \quad (2)$$

2. Copula models and software

There are many parametric copulae families available, which usually have parameters that control the strength of dependence [3, 10].

Even the simplest computer aided processing data for reliability models becomes difficult without specialized applications. An extended presentation of the statistical software was presented in [8]. More accessible software solutions are suggested in [7]; such a solution for the calculus of the bivariate standard normal distribution is illustrated in fig.1a and b.

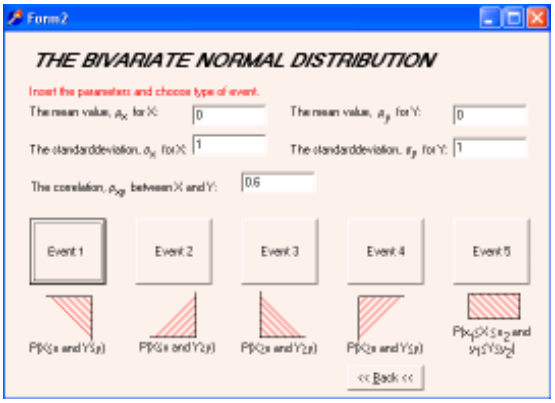

Fig.1a The Bathtub Curve

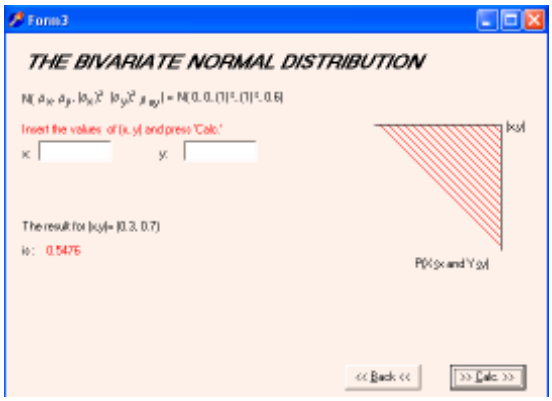

Fig.1b A Polynomial hazard-rate function:

A possible illustration of the numerical results herein above is presented in fig. 2a for the cloud of experimental data and in fig.2b for the bivariate normal function.

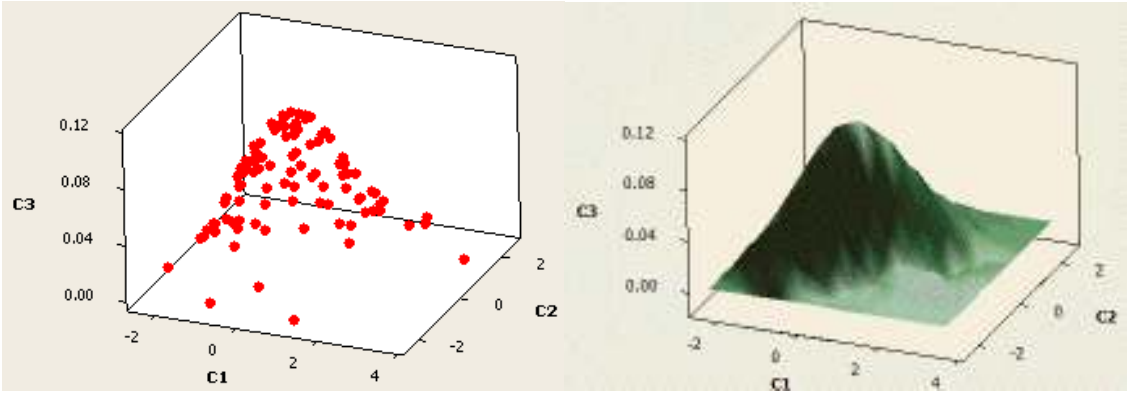

Fig.2a 3D scatterplot of C3 vs C2 and C1 Fig.2b Response surface plot of C3 vs C2 and C1

3. Case study

A structure is considered complex, when the reliability block diagram either cannot be reduced to a series-parallel structure with independent elements or does not exists. For instance, a reliability block diagram does not exists if more than two states (good/failed) or one failure mode (e.g. short/open) must be considered for an element of the system.

Moreover, the reduction of a reliability block diagram to a series-parallel structure with independent elements is in general not possible with distributed structures or when elements appear in the diagram more than once [1].

As an example it was investigated a few different (classical) reliability block diagrams [9] with dependences and copulae functions (Fig.3a, 3b, 3s). The working variant used fix values for the time t. Standard notations are: P= Probability; R=Reliability; F=Failure function (Cumulative distribution function); C=Copula.

Parallel-serial system (fig.3a)

$R_{1;2}(t)=1-F_{1;2}(t)=1-P_{1;2}(T_1\leq t \cup T_2\leq t)=1-P(T_1\leq t)-P(T_2\leq t)+P_{1;2}(T_1\leq t \cap T_2\leq t)=$

$=1-F_1(t)-F_2(t)+C(F_1(t),F_2(t))$ (3)

$R_{3;4}(t)=1-F_3(t)-F_4(t)+C(F_3(t),F_4(t))$ (4)

$R_a(t)=1-(1-R_{1;2}(t))*(1-R_{3;4}(t))=1-(F_1(t)+F_2(t)-C(F_1(t),F_2(t)))*(F_3(t)+F_4(t)-C(F_3(t),F_4(t)))$ (5)

Serial-parallel system(fig.3b)

$R_b(t)=R_{1;3}(t)*R_{2;4}(t)=(1-F_{1;3}(t))*(1-F_{2;4}(t))=(1-P(T_1\leq t\cap T_3\leq t)\cup(T_2\leq t\cap T_4\leq t))=$

$=1-C(F_1(t),F_3(t))-C(F_2(t),F_4(t))+C(F_1(t),F_3(t),F_2(t),F_4(t))$ (6)

Bridge network(fig.3s)

$R_s(t)=R_5(t)(1-C(F_1(t),F_3(t))-C(F_2(t),F_4(t))+C(F_1(t),F_3(t),F_2(t),F_4(t)))+$

$(1-R_5(t))(1-(F_1(t)+F_2(t)-C(F_1(t),F_2(t)))*(F_3(t)+F_4(t)-C(F_3(t),F_4(t))))$ (7)

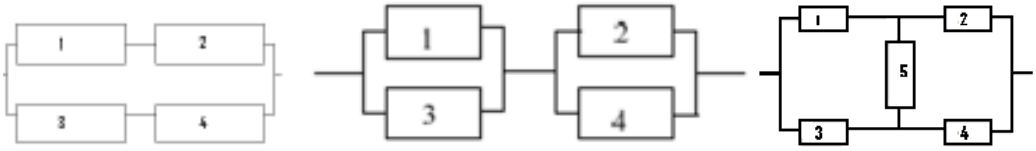

Fig.3a Diagram of parallel-serial system Fig.3b Diagram of serial-parallel system Fig.3s The five unit bridge network system

4. Conclusions

Copulae have been applied to construct bivariate cumulative distributions for the reliability analysis. The joint probability distribution of multiple random variables with given marginal distributions and correlation coefficients were achieved using copulae. The effect of copulae on reliability for modelling dependence structures between variables with the joint probability distribution of multiple variables is developed considering practical reliability structures. The copula approach embraces the reliability methods that use for example the Nataf transformation.

The paper investigated a few different reliability block diagrams using dependences and copulae functions. It was detailed the bridge network reliability: serial-parallel and parallel-serial systems were first analysed and finally the proposed case.

The efficient application of specialized statistical software was illustrated for the calculus of the bivariate standard normal distribution and the plot of the cloud of experimental data and for the bivariate normal function.

5.References

1. Birolini, A. (2007), Reliability Engineering: Theory and Practice, Engineering online library, Ed. Springer Science & Business Media,

2. Embrechts P., Lindskog F., McNeil A., (2003), Modelling Dependence with Copulas and Applications to Risk Management, Chapter 8, Handbook of Heavy Tailed Distributions in Finance: Handbooks in Finance Volumul 1 din Handbooks in Finance, Editor S.T Rachev, Ed. Elsevier,

3. Frees W. E., Valdez, E. A., (1998), Understanding Relationships Using Copulas, North American Actuarial Journal, January, vol.2, no.1, pp1-25

4. Lai, C., D., Xie, M., (2006), Stochastic Ageing and Dependence for Reliability, Springer Science+Business Media, New York,

5. Li, D. X., (2000), On Default Correlation: A Copula Function Approach, Journal of Fixed Income 9/4:pp. 43-54.

6. Meyer C., (2013), The Bivariate Normal Copula, Communications in Statistics - Theory and Methods, **Volume 42**, **Issue 13**, pp 42-66.

7. Paris A.S., (2012)Statistik Anwendungen in Ingenieurwissenschaften- eine starke Innovationsunterstützung, , "Interdisciplinary approach of innovation as a progress factor" Proceedings of the 1th International Scientific Conference Bucharest, Romania, 7th December, FILS, UPB, ed Printech ISBN 978-606-521-987-8 pp. 15-20
8. Paris, A. S., **(**2011), Software applications for field reliability data, 4th Symposyum *„Durability and reliability of mechanical sistems"* Univ C. Brancusi, mai 2011, Fiability and Durability, no. 1(7)/, Ed.Acad., Tg. Jiu, pp.75-80
9. Qin H. W., Yu Z. J., (2014), Reliability Analysis of Components Life Based on Copula Model, TELKOMNIKA, Vol.12, No.1, March, pp. 219 ~ 226
10. Villa-Diharce E. R., Monjardin P. E., (2011), Análisis bivariado de confiabilidad basado en copulas (Reliability Bivariate Analysis Based on Copulas), Revista Colombiana de Estadística, Junio, volumen 34, no. 2, pp. 267-285

SOME STATISTICAL SOFTWARE APPLICATIONS FOR TAGUCHI METHODS

Dr.ing. **Adrian Stere PARIS,** Univ. Politehnica Bucharest, email: adrian.paris@upb.ro

Abstract The paper details the variety of Taguchi methods, as important contribution to the quality improvement. The extended use of these methods imposes more and more complex calculi for the practical application and optimization. It should be necessary to benefit by the new software developments, assisted by the advanced statistical methods. The paper presents a few particular applications of some statistical software for the Taguchi methods as a quality enhancement insisting on the quality loss functions, the design of experiments and the new developments of statistical process control.

K**ey words**: Taguchi methods, software applications

1. Introduction

The Taguchi philosophy is a guide and reference source, with the principal goal of improving the quality of products in the industrial practice. From the practical point of view, the goal of Taguchi methods is to find a trade-off between quality loss and product price [8, 14]. The paper presents a few applications for Taguchi methods with software support, starting with the new quality loss laws, which have symmetrical and asymmetrical distributions and therefore more adequate models in the real world [17]. Many software applications approach the Taguchi's design of experiments. New trends try to apply effectively Taguchi's methods to the traditional statistical process control (SPC).

The methods developed by Genichi Taguchi are applied mainly to engineering, but also to many others fields like marketing and advertising. Helpful to companies in both manufacturing and service industries, Taguchi's applications provide accessible material on such topics as:

- Quality loss function
- On-line quality engineering
- Signal-to-noise ratio
- Robust engineering
- Design of experiments (known as the "Taguchi method")
- Mahalanobis–Taguchi Systems (MTS), and more [2].

Nevertheless, many entrepreneurs pay insufficient attention to the introduction of those methods. One reason is that comprehensive data are often seen as expensive to obtain; another may be a lack of familiarity with methods for response-selective observational schemes and for combining information from different sources. There are several means of acquiring nonconformity cost data for a system such as and the like.

2. Processing Taguchi data and software packages

The use of mathematical software to modelling, mainly to analyze or numeric calculation is more and more popular with the new hardware developments. An important step forward was the explosion of mobile devices, like tablets and smart phones, making more accessible and rapid manipulation of data. More important, the new mobile operating system, Android (Google), based on the Linux kernel and designed primarily for touch screen mobile devices, has the largest deployment for those ones. The big advantage is the majority of free applications (including the mathematical and the statistical ones). MathAlly Graphing Calculator is quickly becoming the most comprehensive free Graphing, Symbolic, and Scientific Calculator for Android: it can solve equations, make a lot of graphs and even some frequent statistics like regression. For the experienced people with spreadsheets applications (MSExcel) there are similar software, like Polaris Office, a free office application to view, edit & share Microsoft Office compatible documents on the mobile device or PC. There is even a Romanian language spreadsheet (Foi de calcul, Google) with the same possibilities, making possible the cheapest solution (off line).

Of course, more complex statistical calculations need additional software offers, with the on line access: more and more universities and specialists present Free Online Statistics Calculators or more complete sites (http://stattrek.com/; http://shodor.org/, etc.). In the end there are a lot of expensive complex statistical packages (SPSS, MINITAB, OriginLab, etc.) R, a programming language and software environment for statistical computing and graphics, written primarily in C, Fortran, and R, and freely available becomes very popular in the last years.

3. Regression and curve fitting for Taguchi's loss function

Regression is a conceptually simple technique for investigating functional relationship between output and input decision variables [10].

All the important statistical packages offer a regression module [7], but there are also low cost solutions, suggested in [6].

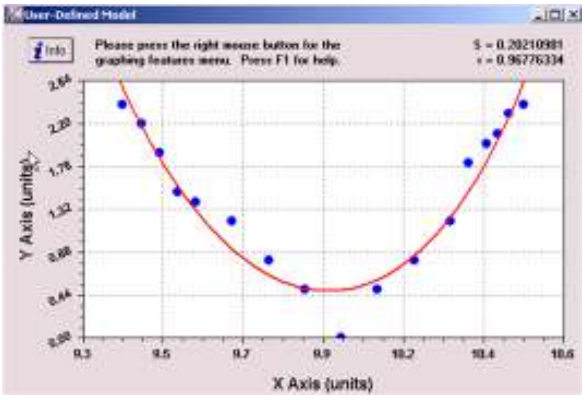

Fig.1a adapted hyperbolic cosine plot [17]

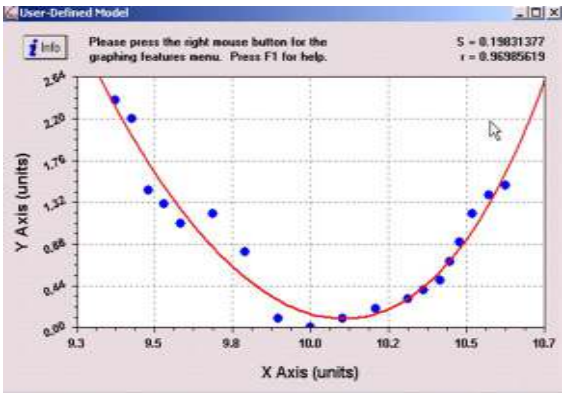

Fig.1b shifted generalized gamma plot [17]

The use of computer aided processing of experimental data opened new opportunities to develop the basic simple three forms of loss functions. The start-up was achieved with the asymmetric loss functions, using Pareto, generalized Pareto, and beta pattern [3, 12], adapted hyperbolic cosine model (Fig.1a), shifted generalized gamma (Fig.1b), etc. [17].
The next step was the introduction of response surface methodology and the multivariate loss functions [3, 12, 16, 18, 19]: the applications in quality control is illustrated by an example to improve the overall quality of a printing machine in applying coloring inks on package labels [4, 19]. The primary data from [4] are represented in Figure 2.
A computer aided regression for the fitted hyper plane of the bivariate loss function $L(y_1, y_2)$, results as the positive definite quadratic form with interactions (Fig. 3) [19]:
$L(y_1^2, y_2^2, y_1y_2)=0{,}0256y_1^2+55{,}8\ y_2^2+0{,}60y_1y_2$

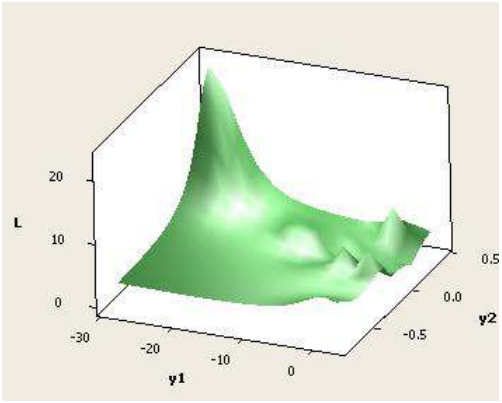

Fig. 2 The response surface with the initial data

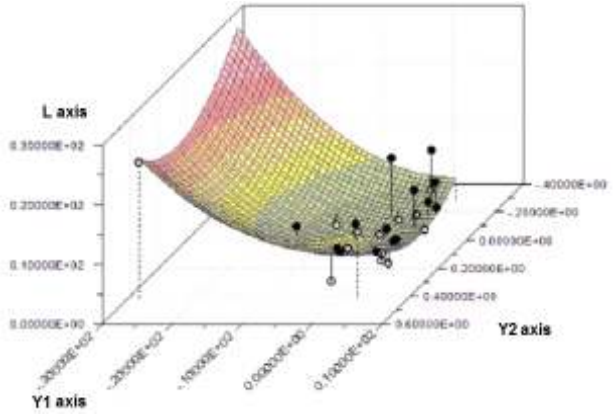

Fig.3 A quadratic loss function [19]

4. Software solutions for Taguchi's design of experiments
Maybe the most frequent application of the Taguchi's methods is the design of experiments (DOE). Since the introduction of DOE by Fisher in the 1920s, and the 1940s, when Taguchi started to research with it, there was much development with this statistical technique. Taguchi first proposed that DOE could be used not only to improve quality, but also to quantify the improvements made in terms of savings [13]. Taguchi has developed some simple methods of constructing fractional factorial designs using orthogonal arrays and linear graphs and some methods of analyzing the resulting data [25].The extended use of adapted software makes the application of Taguchi's DOE more accessible (Fig.4 a, b, c, d).

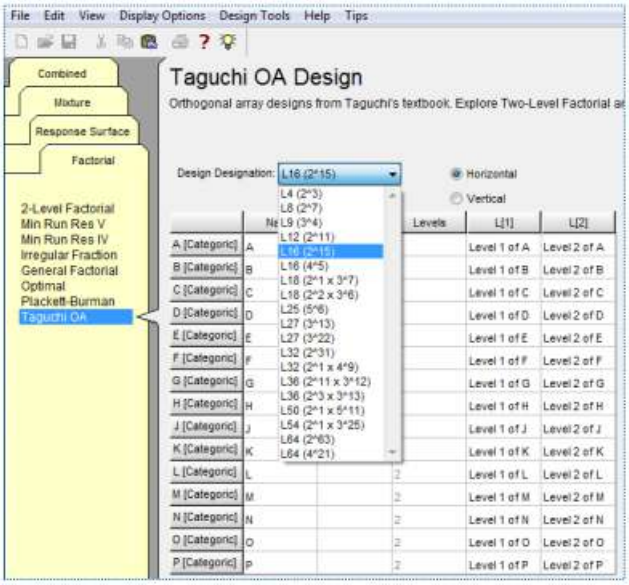

Fig.4a Taguchi's DOE with Stat-Ease

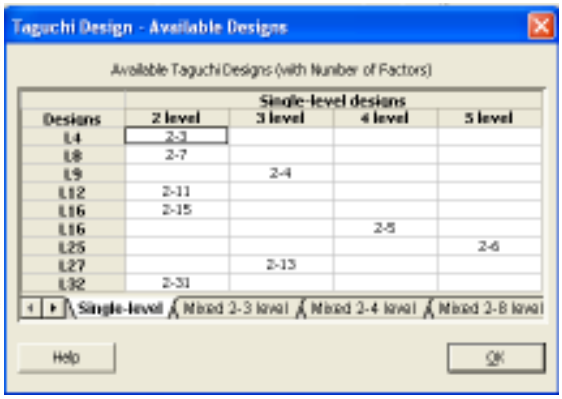

Fig.4b Taguchi's DOE with Minitab

The application of Taguchi method for optimizing turning process by the effects of machining parameters is presented in fig. 4d for the cutting of EN24steel [15].

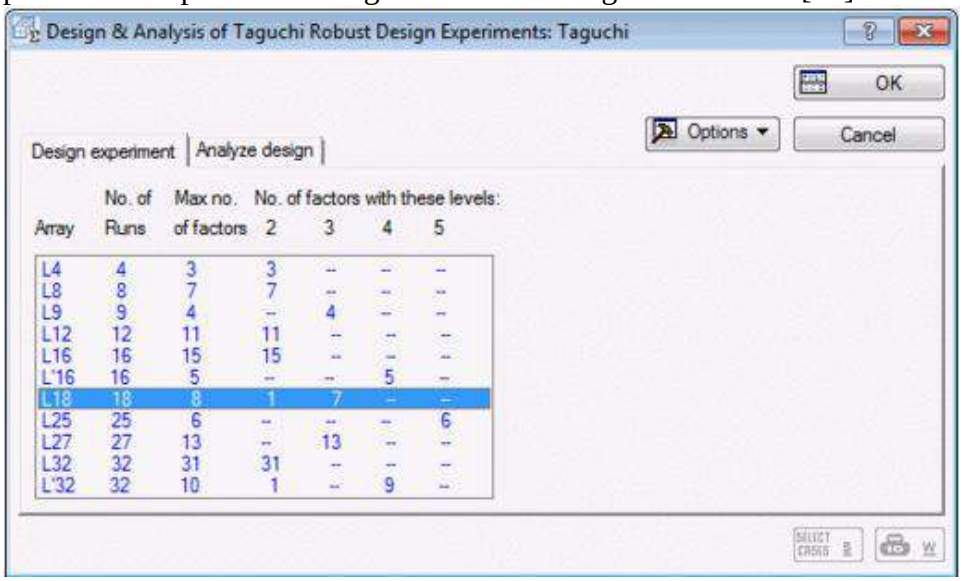

Fig. 4c Taguchi's DOE with Statistica

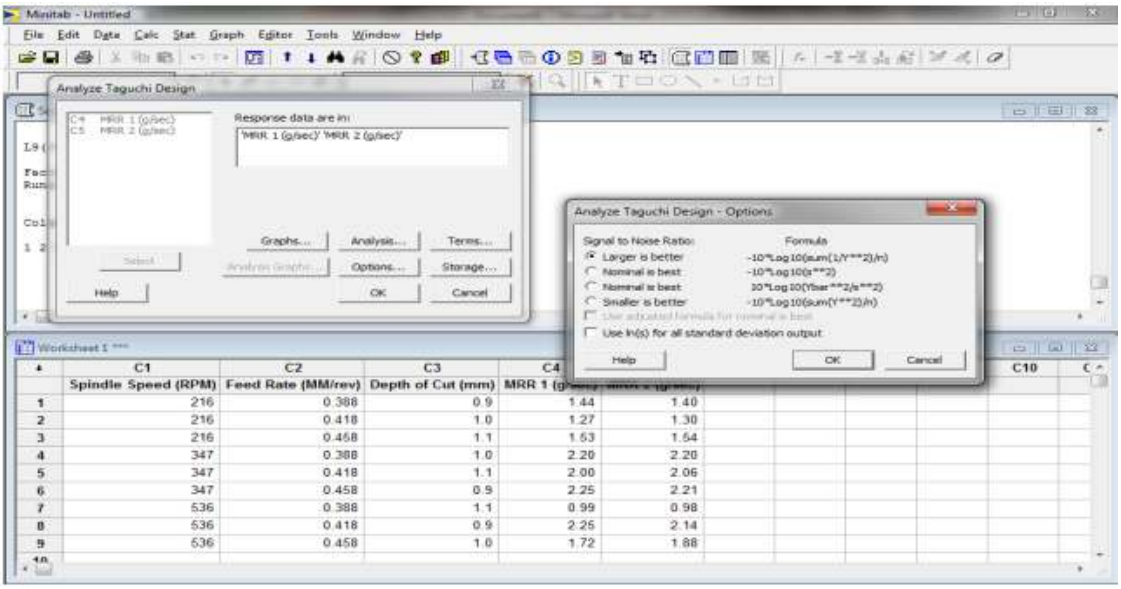

Fig.4d Analyses Taguchi Design-Option [15]

5. Taguchi's loss function and SPC

If should be used Taguchi`s quality loss function nominal-the-best, overlapping the control chart for mean, respectively the monetary value of loss, this is far more suggestive as the dimensional deviations for controlling process variability. [9].

An algorithm was developed for the optimization design of control charts based on the probability distribution of the random process shifts (e.g. mean shift). The design objective was to minimize the overall mean of Taguchi's loss function per out-of-control case (denoted as ML) by adjusting the sample size, sampling interval and control limits of the chart. The comparison studies show that the ML chart is significantly superior to the Shewhart control chart in view of overall performance [20].

The in-control and out-of-control costs can be easily found after examining the figure 5 (the loss function as dotted line). It can be seen that any deviation from the target value will incur a cost even if it was within the control limits [1].

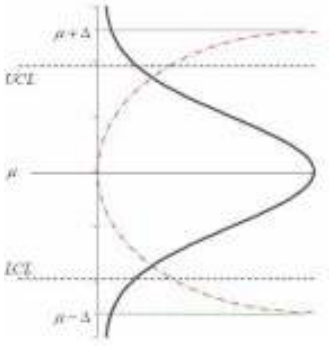

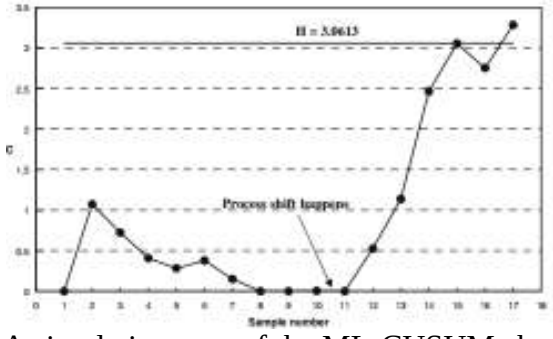

Fig.5 A diagram for the new model [1] Fig.6 A simulation runs of the ML-CUSUM chart [5]

A CUSUM control chart detecting process shifts in the mean value through minimizing the overall mean value (ML) of a Taguchi's loss function over the probability distribution of the random process mean shift (fig.6) is described in [5].

6. Conclusions

A concise overview of Taguchi's methods and statistical software is presented in this paper with extension to specialized software solutions. A final choice for adequate software for quality data processing should consider the customer conditions for experience, data volume and necessary investment, starting with spreadsheets to the complex statistical software, with the new developments for smart phones, based on the new mobile operating system, Android. For small data samples and less details it is cheap to use low cost or freeware/shareware software packages. New trends try to apply effectively Taguchi's methods to the traditional statistical process control (SPC).

5.References

1.Al-Ghazi A., Al-Shareef K., Duffuaa S. O., (2007), Integration of Taguchi's Loss Function in the Economic Design of x Control Charts with Increasing Failure Rate and Early Replacement, Proceedings of IEEE International Conference on Industrial Engineering and Engineering Management, Dec., ed. Curran Associates, Inc., Singapore, pp.1209-1215.

2. Dehnad, K., (1989) Quality Control, Robust Design, and Taguchi Method, Ed. Springer

3.Demetrescu, M., Paris, A.S. , Tarcolea, C., (2008),- Loss Functions with Interactions and Practical Application Proceedings of the 10th WSEAS Int. Conference on MATHEMATICAL and COMPUTATIONAL METHODS in SCIENCE and ENGINEERING (MACMESE'08) Bucharest, Romania, November 7-9, Mathematics and Computers in Science and Engineering, Published by WSEAS, pp. 296-299

4. Demetrescu, M., Paris A.S. , Tarcolea C., (2010),Uni-and multivariate loss functions and the Taguchi theory, BSG PROCEEDINGS 17, (DGDS-2009) Oct. 2009, Bucharest, Geometry Balkan Press, pp. 79-83

5. Jiao R. J., Helo P. J., (2008), Optimization design of a CUSUM control chart based on Taguchi's loss function, The International Journal of Advanced Manufacturing Technology, Springer Verlag, Berlin, February, Volume 35, Issue 11, pp 1234-1243

6. Paris A.S., (2012), Statistik Anwendungen in Ingenieurwissenschaften- eine starke Innovationsunterstützung, "Interdisciplinary approach of innovation as a progress factor" Proc. 1th Intl. Sc. Conf. Buc., Ro., 7th Dec., FILS, UPB, Ed. Printech pp. 15-20

7. Paris, A., S. – (2011), Software applications for field reliability data, 4th Symposyum *„DURABILITY AND RELIABILITY OF MECHANICAL SISTEMS"* Univ C. Brancusi, mai 2011, Fiability and Durability, no. 1(7), Ed.Acad., Tg. Jiu, p.75-80

8. Paris, A.S., Metode Taguchi (2005), In: Enciclopedia calitatii – coordonatori Ion Hohan si Ulrich Wiener; 476 pag. Editura OIDICM, Bucuresti p.301-302

9. Paris, A. S. – (2012), An overlap proposal between statistical process control and *Taguchi's quality loss function*, Proceedings of the 12th International Conference on Technology and Quality for Sustained development TQSD Ed. Printech, Buc, pp 86-89
10. Paris, A, . S., Târcolea, C. , Regression models applied to manufacturing systems, (2010), Proceedings in Manufacturing Systems, Editura Academiei Române, vol.5, nr.4, pp. 249-253.

11. Paris, A.S., Târcolea, C. (2004), Taguchi Applications on Manufacturing Systems; Editura Academiei Romane International Conference on Manufacturing Systems - **ICMaS** 2004 08-09.10.2004 UPB, Romanian Journal of Technical Sciences APPLIED MECHANICS, Proceedings of the International Conference on Manufacturing Systems, ICMAS'2004, vol. 49, n° Special, pp.459-462.

12. Paris, A.S., Târcolea, C. (2010) Loss functions used in the quality theory 3rd Symposyum *„Durability and reliability ofmechanical sistems"* Univ C Brancusi Tg. Jiu
13. Roy R. K., (2001), Design of Experiments Using the Taguchi Approach: 16 Steps to Product and Process Improvement, A Wiley-Interscience publication, Editor John Wiley & Sons,

14. **Taguchi** G., **Chowdhury** S., **Wu** Y., (2004), Taguchi's Quality Engineering Handbook, John Wiley,

15.Taneja K.J., Bector M., Kumar R. (2012) Application of Taguchi Method for Optimizing Turning Process by the effects of Machining Parameters, International Journal of Engineering and Advanced Technology (IJEAT) Volume-2, Issue-1, October 2012, pp. 263-274
16. Târcolea, C., Paris, A. S., **(**1995), Modele bidimensionale de tip Taguchi. In: Managementul Industrial, an 3, nr.1-2,.pp.58-62
17. Târcolea, C., Paris, A. S., (2011), Loss functions used in the quality theory, U.P.B. Sci. Bull. Series A, Vol. 73, Iss. 1, , ISSN 1223-7027, pp 45-54
18.Târcolea, C., Paris, A.S., Drăgoi, G. (1997), Etude de la qualite dans la phase de conception -modele de type Taguchi multidimensionel. In vol.: Les cahiers des enseignement francophones en Roumanie: Module d'enseignment francophone "Conception integree des systemes mecatroniques intelligentes" -UPB oct., pp.124-130.
19.Târcolea, C., Paris, A.S., Sylvan, D., (2014), Loss Functions and Taguchi Theory, The 7-th International Conference of Differential Geometry and Dynamical Systems, (DGDS-2013), BSG Proceedings 21, Geometry Balkan Press, pp. 175-180, http://www.mathem.pub.ro/proc/bsgp-21/K21-ta-846.pdf
20. WU Z., SHAMSUZZAMAN M., PAN E. S., (2004), Optimization design of control *charts based on Taguchi's loss function and random process shifts*, Int. J. Prod. Res., vol.42, no.2, pp. 379–390

THE COEFFICIENT OF FRICȚION IN THE FRETTING PHENOMENON

Prof.dr.eng. Stefan GHIMIŞI, Constantin Brâncuşi University of Târgu Jiu,Romania, ssghimisi@gmail.com

Abstract: Fretting is now fully identified as a small amplitude oscillatory motion which induces a harmonic tangential force between two surfaces in contact. The present paper argues that adhesion forces and elastic deformation in the contact zone may contribute significantly to the relative displacement during fretting of metals A tangential force whose magnitude is less equal on greater than the force of limiting friction will not give rise to a sliding motion. It is determined the energy loss dissipated per fretting cycle

Keywords: Fretting, adhesion, friction coefficient.

1. Introduction

To study the phenomenon of fretting it is necessary to determine appropriate working arrangements with the establishment of borders between different regions as accurate. You can establish criteria for transition between partial slip and slide, all these criteria depending on normal force and tangential displacement brought on the contact.

Experimental research aimed to determine the size of different existing regions within a sphere-plan contact subjected to tangential displacement of small amplitude [1,2,3].

Following the experimental investigations there was determined the size of the wear resulting from fretting tests. Thus, there were determined the rays of gluing circles obtained in the central regions of the traces of wear, for variable normal pressure forces and for different durations, respectively the size of the ring area of microslip, that surrounds the seams.

In a theoretical approach to the phenomenon of fretting the size of the areas specific to the phenomenon (stick and partial slip) was considered depending on various factors that influence the phenomenon [4].

Also, the fretting phenomenon can be approached by two directions: a direction in which the friction coefficient between surfaces in contact is considered constant (the most common approach) and another approach to the phenomenon, involving variation of the friction coefficient in the fretting contact, variation due to the existence of adhesion between surfaces in contact.

This paper aims to address the phenomenon of fretting in terms of a variable coefficient of friction between the contact area.

For the experimental investigation of the phenomenon of fretting we used an experimental stand that allowed the investigation of four point contact under fretting.

There were thus determined the sizes of different fretting zones depending on the parameters of dependence, in this way being possible to determine the extent of these areas for a given configuration of the fretting contact.

2.Experimental means

Given the experimental stands on which it was tried to approach experimentally the phenomenon of fretting it was taken into account a point contact of I-st class ball / plane contact type. This contact was chosen because the actual contact area is approximately equal to the apparent contact area and for this type of contact there is a fairly comprehensive theory concerning the local tensions in contact and the size of contact area (Hertz, Mindlin, Johnson).

Also the sphere / plan contact highlights (experimental research) the fretting mechanism characterized by three regimes: I-adhesive, II- partial sliding, III total sliding.

For the study of the fretting phenomenon in case of elastics assemblages spring slides with multiple sheets, I used the experimental stall from fig.1[5].

The stall can be used for the testing at fretting of some couples by different materials. This stall can be adapted for study of the lamellar springs with many sheets.

The lamellas used in experiments have the dimensions 560x56x2 mm and are realized by spring steel having hardness 55 HRC.

The balls are spring balls and have 19 mm in diameter. The lamella is supported in inferior side on 4 balls in superior side the charge of the contact is made through the agency of 4 balls. The rod-crank mechanism permits a displace at the end (extremity) of the 20 mm lamella and can modify this displace by changing of the system eccentricity. The system is auctioned through the agency of electrical engine having revolution of 750 rot/min.

Helping with this experimental stall we can made fretting tries for normalness and different forces for different numbers of solicitation cycles.

After conducting various experiments there were obtained different traces of wear that correspond to a fretting wear. Thus, it could be determined the fretting wear dependence on the number of cycles and normal load force, and could be compared different traces of fretting by comparing the size of various areas of contact fretting for some conditions.

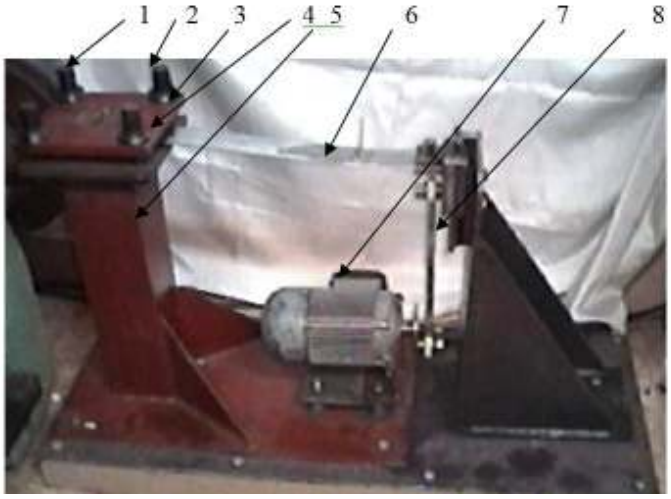

Fig. 1. Experimental stand for the study of fretting. [5]

Traces of wear obtained (Fig. 2) were taken with a video camera, subsequently being processed on the computer. The movement at the contact level was measured by video camera and computer. Measurement of the movement was for the two rows of balls. On these experimental traces obtained it can be observed a central area corresponding to the a central area of adhesion between balls and lamella, and a ring zone surrounding the central area, corresponding to a partial sliding area.

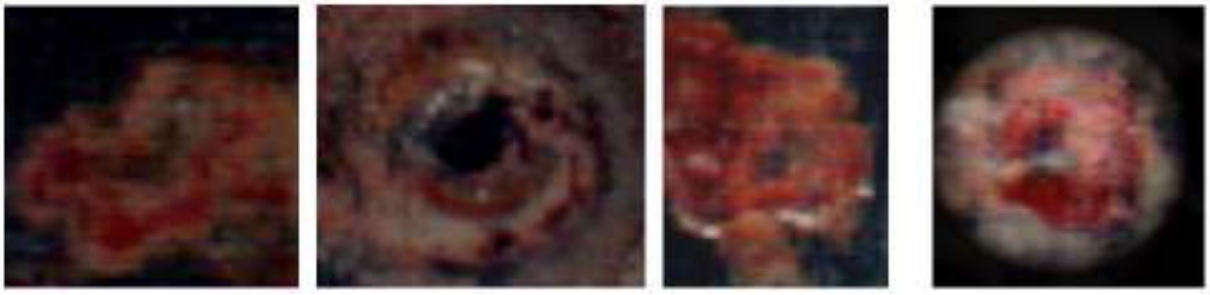

Fig. 2 The wear traces of fretting

The results are obtained with sufficient precision, being thus possible a proper experimental investigation of the fretting phenomenon and being possible to experimentally confirm this theoretical results obtained from investigating of a sphere-plan contact subjected to an oscillatory movement of small amplitude.

3. The dependence of friction coefficient

After experimental tests, the size ratio between the radius of adhesion and the whole radius of the wear trace is shown in Table 1 and Table 2 for a normal pressing force of 250 N. The fretting coefficient between surfaces in contact is not constant but varies according to a law of the form[2]:

$$\mu_{ad} = \frac{\tau_0}{p_{ad}} + \beta \qquad (1)$$

with the normal pressure at adhesion given by a law of the form[6]:

$$p_{ad} = \left(1 - r_a^2\right)^{1/2} - \frac{2}{3}\frac{k_{ad}^{1/2}}{\left(1 - r_a^2\right)^{1/2}} \qquad (2)$$

thus:

$$\mu_{ad} = \frac{\tau_0}{\left(1 - r_a^2\right)^{1/2} - \frac{2}{3}\frac{k_{ad}^{1/2}}{\left(1 - r_a^2\right)^{1/2}}} + \beta \qquad (3)$$

Based on the theoretical diagrams of dependence of the central radius of adhesion the results obtained from experimental investigation of fretting contact can be checked.

So, in Fig.3 there are presented the radius of circles obtained following the fretting test with a normal force of 250N.

The radius of the adhesion circle is represented by load factor "k". It is noted that the adhesion area corresponds to a loading factor approximately equal to 0.24[6].

Table 1.Traces of wear (F = 250N, front)

Nr. crt.	Loading [N]	Number of cycles	Radius central [mm]	Radius ext. [mm]	c_a=c/a	p_{ad}	⌴
1	250	20000	0.21621	0.5029	0.4299	0.87953	0.21370
2	250	30000	0.22514	0.6518	0.3454	0.91599	0.20917
3	250	40000	0.27878	0.6974	0.3997	0.89365	0.21190
4	250	50000	0.29076	0.7640	0.3805	0.90198	0.21087
5	250	60000	0.30679	0.8329	0.3683	0.90703	0.21025

Table 2. Traces of wear (F = 250N, back)

Nr. crt.	Loading [N]	Number of cycles	Radius central [mm]	Radius ext. [mm]	c_a=c/a	p_{ad}	⌴
1	250	20000	0.25508	0.4980	0.41048	0.88875	0.21252
2	250	30000	0.26596	0.6285	0.42316	0.88279	0.21328
3	250	40000	0.28529	0.6840	0.41709	0.88567	0.21291
4	250	50000	0.37127	0.7634	0.48633	0.84965	0.21770
5	250	60000	0.41306	0.7970	0.51826	0.83057	0.22040

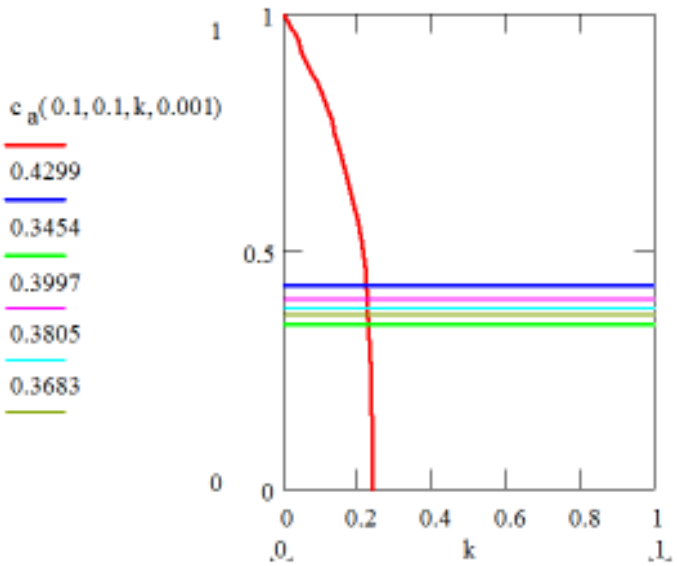

Fig. 3 Radius of the adhesion circle:

$$c_a(\tau_0, \bar{\beta}, k, k_{ad})$$

In Fig.4. and fig.5 are the dependence of friction coefficient of adhesion normal pressure for two cases investigated (normal force of 250N and two ball positions: front and back)

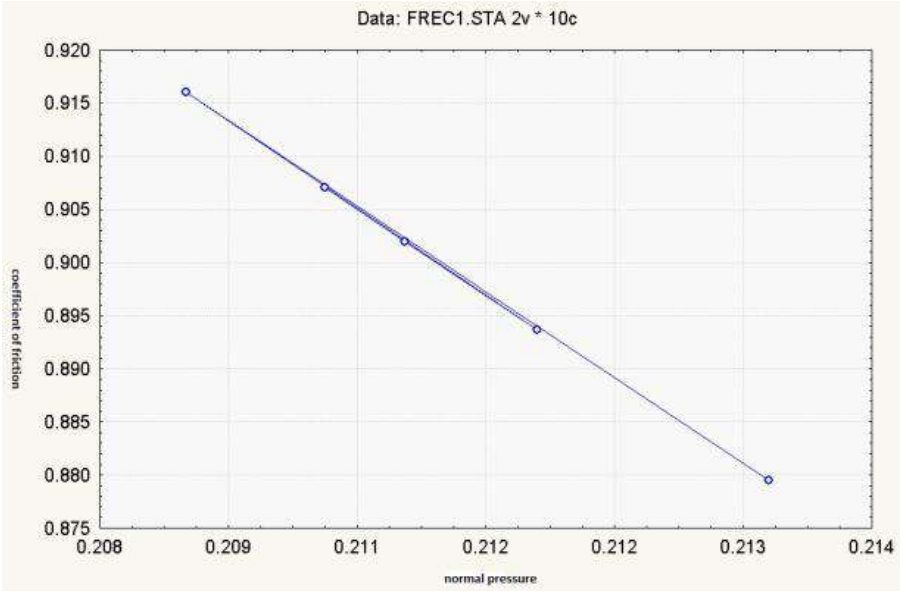

Fig. 4. The coefficient of friction ($\mu=\mu(p_{ad})$-front

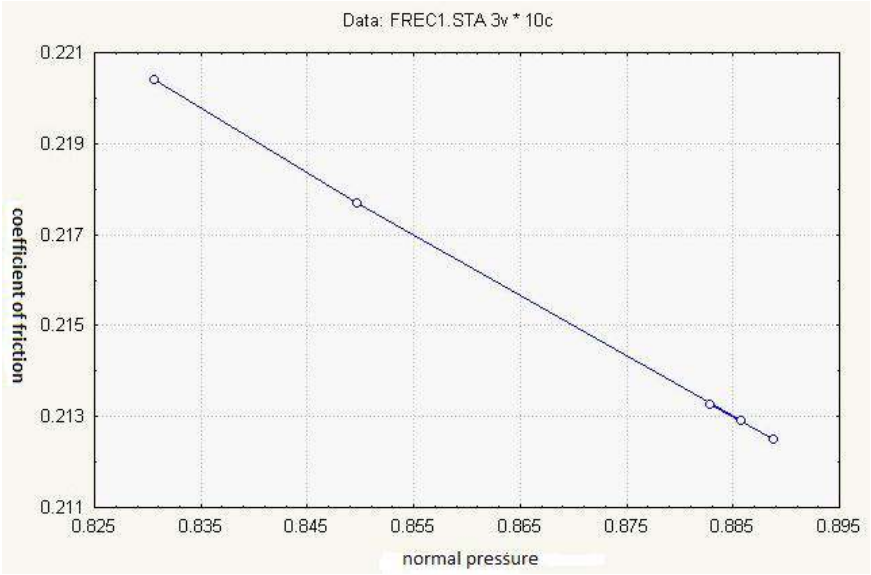

Fig. 5. The coefficient of friction ($\mu=\mu(p_{ad})$-back

3.Conclusion

Experimental tests have confirmed that the coefficient of friction between surfaces is not constant but variable. Variation is explained by the phenomena of adhesion that appear between the surfaces in contact. Thus, the assumption of a variable coefficient of friction between the surfaces was confirmed by experiments, theoretical results obtained in the study of fretting by considering a variable fretting coefficient receiving the confirmation of the experiment.

REFERENCES

[1] **Ghimisi Stefan**, Study of the transition in the fretting phenomenon, Baltrib'09, V International Scientific Conference, Lithuanian University of Agriculture, Kaunas, Lithuania, 19-21 decembrie 2009, PROCEEDINGS, ISSN 1822-8801, pag.230-236

[2] **Ghimisi Stefan**, Transition in the fretting phenomenon based on the variabile coefficient of fretting, Fiability& Durability, nr 2/2010, pag.89-92, Editura Academica Brancuşi, Târgu Jiu, ISSN 1844ICMERA 2010, 2-4 december Bucharest, Romania, Publisher Institute of Electrical and Electronics Engineers(IEEE), China, ISBN 978-1-4244-8867-4,pag.308-312

[3] **Ghimisi Stefan, Luca Liliana, Popescu Gheorghe**, Transition in the fretting phenomenon based on the variabile coefficient of friction, International Conference on Mechanical Engineering, Robotics and Aerospace ICMERA 2010, 2-4 december Bucharest, Romania, Publisher Institute of Electrical and Electronics Engineers(IEEE), China, ISBN 978-1-4244-8867-4,pag.308-312

[4] **Vingsbo O. and Soderberg M**.,On fretting maps,Wear, 126 (1988) 131-147

[5] **Ghimisi Stefan,** Experimental investigation of the fretting phenomenon-dependence of number cycles, Baltrib'09, V International Scientific Conference, Lithuanian University of Agriculture, Kaunas, Lithuania, 19-21 decembrie 2009, PROCEEDINGS, ISSN 1822-8801, pag.226-230,

[6] **Ghimisi Stefan**, Fenomenul de fretting. Editura Sitech, Craiova, 2001

METHODS OF CALCULATION FOR STRESS CONCENTRATORS IN CASE OF FILLET WELDS

Claudiu BABIS; Oana CHIVU, Zoia APOSTOLESCU, Dan NITOI, Anamaria FEIER
Material and Welding Technology, University POLITECHNICA from Bucharest, Splaiul Independenţei no. 313, Bucharest, Romania
claudiubbs@gmail.com; virlan_oana@yahoo.co.uk; zoia@camis.pub.ro; nitoidan@yahoo.com

Abstract: The existence of stress concentrators at the intersection between base and filler material in case of fillet welds, drastically reduces the fatigue life of these structures. For this reason, appreciation of the values of these concentrators tensions is useful for predicting fatigue life time. The paper aims to present some elements of calculation of stress concentrator is of great use in practical applications.

Key-words: weld, stress concentrator, structure;

1. Introduction

Both welding and seam welding are based on a series of stress concentrators that worsen the fatigue life of the welded structures. This is due to the fact that these stress concentrators, known as peak stress, induce local small cracks that expand when dynamically stressed and cease the running of the respective welded structure. [1].

The studies carried out before nowadays have proved that the decrease of the fatigue strength of parts when being welded, occurs even if there is a high quality welding which does not change the flow of the power lines of that part [2].

Regarding the behavior to fatigue of the welded joints, different methods of assessing the fatigue strength are presented, depending on the type of welded structure (vehicles, naval structures) [3].

Figure 1 illustrates three classes of stress concentrators: for example, a welded structure made of a plate with width s and a connection plate with length L and height H, welded to this plate [4].

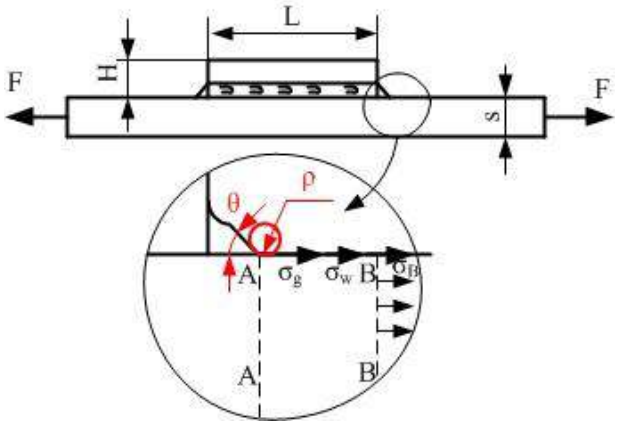

Fig. 1 Stress definition for a welded joint [1]

The tensile force of the plate F has the same direction with the connection plate. The local geometry of the weld bead is given by the angle θ and the groove radius ρ.
It is a fact that the spot likely to crack in this case is the upper part of the weld bead at the end of the connection plate. The potential crack line is shown by the dotted line A-A in Figure 1.

As shown in Figure 1, there are three types of stresses such as:

-$\sigma_B = \sigma_n$, nominal stress of the horizontal plate located at a certain distance from the weld bead (line B-B);

-σ_g , stress given by the geometry of the potential initial crack spot (upper part of section A-A);

- σ_W , stress given by the crack in the weld bead at the potential initial crack spot (upper part of section A-A);

In fact, only the nominal stress σ_B and weld bead crack stress σ_W are illustrated whereas the stress induced by the geometry effect σ_g is only theoretically defined.

The ratios between nominal stress $\sigma_B = \sigma_n$ and the other two are expressed as follows:

$$\sigma_g = K_g \sigma_B \quad (1)$$

and

$$\sigma_w = K_w \sigma_g \quad (2)$$

As a consequence:

$$\sigma_k = K_g K_W \sigma_B = K_t \sigma_B \quad (3)$$

where: K_g is the geometrical stress concentrator; K_W- is the welding crack stress concentrator; K_t- stress concentrating factor including K_g and K_w.

All these equations govern a linear elastic behaviour of the material. In fact, this is not the case of the crack stress of the weld bead σ_W .

The geometrical stress concentrator K_g is given by the connection plate. This connection plate represents a geometrical irregularity whose stress value ranges from nominal stress value σ_B to σ_g at the top of the weld bead. This stress fluctuation also takes place when the weld bead is inexistent and the connection plate is attached to the horizontal plate. In this case, the resulted stress σ_g can be calculated based on the geometrical effect, using strain gauges instead of weld beads. The geometrical stress concentrating factor K_g can be easily highlighted, applying the Finite Elements Analysis (FEA) to our welded joint. This analysis is based on special requirements regarding the quality of the model such as the element type as well as the selected network. This K_g depends on the height H of the connection plate and even more on its corresponding length L. Usually, K_g ranges between 1.2 and 1.5.

The greater the length L of the connection plate, the higher the stress concentration. Since K_g is given by the total geometry of the joint (s, H and L), it becomes known as the geometrical stress concentration factor.

If the weld bead is considered to be situated on the plate, then, the stress on top of the weld bead will grow as a result of the discontinuity produced by the weld bead itself [5]. Hence, the factor determining stress concentration is K_W and is called the welding crack stress. This stress concentration factor is given by the bending angle θ of the weld bead and by the ratio ρ/T between the groove radius of the weld bead and the material and the thickness of the respective part. The values of the θ must be low and the values of the ratio ρ/T must be high. Stress can be approximately determined by means of small strain gauges on the weld bead.

The remaining stress which inevitably appear in the welding process also contribute to the decrease of the fatigue strength [6].

2. Methods of calculation of stress concentrators

In the case of fillet welding, the theoretically thickness of the welded row is equal with the high of the isoscel triangle inscribed in the weld transversal section (figure 1).

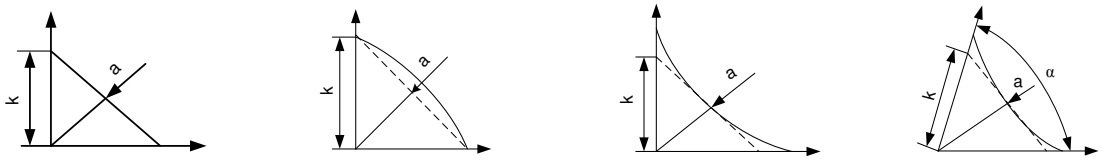

a b c d

Fig. 2 Possible shapes of the welded corner rows
a-plane; b – convex, c – concave, d – sharp concav

According to the figure 2, depending of the fraction k/a, the welded rows could be:

-plane, when $k/a \approx \sqrt{2}$ (figure 2.a), convex, when $k/a > \sqrt{2}$ (figure 2.b), concave, when $k/a < \sqrt{2}$ (figure 2 c and d). Because the weld convex shape, favorize concentration of the stresses in the deposed metal it is recomended to used the concave shape mostly to structures that works in oscillating conditions. It has to be mentioned that in the case of concave rows an optimally angle has to be define because when the concavity increases the residual stresses also increases. Some norms provides the α angle to be larger than 70^o.

The global factor that describes the influence of the welded geometry is the theoretic coefficient of the concetrating stres α_k defined by:

$$\alpha_k = \frac{\sigma_{max}}{\sigma_n} \tag{4}$$

where σ_{max} represents the maximal stress value near the stress concentrator and σ_n – represents the nominal stress. Any change of the shape that determines a stress concentration has a result in lower strngth caracteristics and durability. The degree of fatigue limit decrease is represent by the coefficient of efective concentration k, calculated by the formula:

$$k = \frac{\sigma_R}{\sigma_{RK}} \tag{5}$$

where: σ_R - represents the fatigue limit that corresponds to a simetry degree R determined with a probe without stress concentrator, and σ_{RK} - represents the fatigue limit determined with a probe with stress concentrator.

The value for the coefficient of efective concentration k (k_σ, k_τ) is different by the theoretic coefficient α_k, because it depends, on a side, to the material properties, chemical properties and on the other side, depends by the technological properties and length factor. At the corner welding in convex shape that has tensile solicitations, the formula for the theoretical coefficient of concentration based on fotoelastic analyses is [1]:

$$\alpha_k = 1 + 0{,}2 * \left(\frac{s(2c2 - c1)}{c2 * r}\right)^{1/2} \tag{6}$$

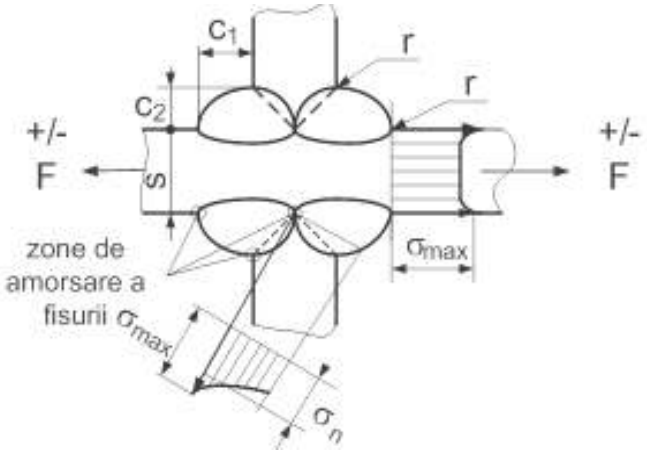

Fig. 2 Stress distribution in danger sections of the corner weld

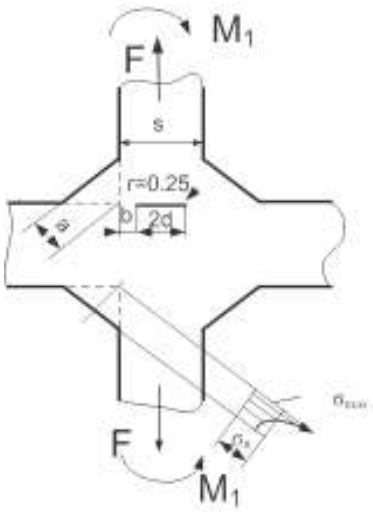

Fig. 3 Stress distribution in bisector plane of the corner weld in the case of unpenetrated weld

At the complete merge weldings in isoscel triangle shape ($c_1 = c_2 = c$), at the calculation of theoretical coefficient of concentration it is used the relation:

$$\alpha_k = 1 + 0{,}2 * \left(\frac{2s - c}{r}\right)^{1/2} \tag{7}$$

The normal values of α_k are $\alpha_k = 2{,}0 - 2{,}6$

A favorable situation are represented by the complete merge concave shape weldigs where [2], where the theoretical coefficient of concentration is based on the relation:

$$\alpha_k = 1 + 0{,}4 * \left(\frac{2s - c}{R}\right)^{1/2} \tag{8}$$

Because, usually, in practice, R>>r, the values of α_k are lower than in previouse cases, the concave shape is prefred in welding technology.The usual values of concentration coefficient value are : $\alpha_k = 2 - 5$ in the case of tensile testing and $\alpha_k = 2 - 2{,}5$ in the case of bending testing.

3. Conclusion

The more radius between the base metal and filler material is higher when welding with both concentrators tensions decrease and increase fatigue life.

4. REFERENCES

1. Tom Lassen, Fatigue life analyses of welded structures, ISTE Ltd, 2006
2.. Ratiu, M. D.; Hau,G.;Bek, W.-Suitability for steady state vibrations of piping fillet welds-a fracture mechanics aproach; Impell Corporation Wainut Creek, California
3. Solomon, G.;Marina, G.;Iacobescu, G.-Constructii sudate; Editura Bren
4. Ratiu, M. D.;Mateiu, H.-Rezistenta la oboseala gigaciclica a imbinarilor cu suduri in colt (2009); Sudura XIX, 2-20
5. A. Almar Næss, Fatigue Handbook, Trondheim, Tapir, 1985
6. A. Almar Næss, Fatigue Handbook, Trondheim, Tapir, 1985
7. Claudiu **Babis,** Gheorghe Solomon, Dan Nitoi, Dumitru Titi Cicic - Cercetări privind rezistenta la oboseală a sudurilor de colt (Researches regarding Fatigue Strength of Fillet Welds) - ASR International Conference, 13- 14 octombrie 2011, Chisinău, Republic of Moldova
8.*** EUROCODE 3: Design of steel structures, 1993. Part 1–9: Fatigue strength of steel structures, European Norm EN 1993-1–9.
9. *** - AWS D1.1. Structural welding code

MODELING OF AN ULTRASONIC ENGINE WITH THREE DEGREES OF FREEDOM

Sl. Dr.ing. Oana Roxana CHIVU, Prof. Dr. AMZA Catalin, Sl. Dr.ing. APOSTOLESCU Zoia, Sl. Dr.ing. BABIS Claudiu, Conf. NITOI Dan Florin, Dr.ing. Andrei DIMITRESCU

Material and Welding Technology, University POLITECHNICA from Bucharest, Splaiul Independenţei no. 313, Bucharest, Romania

Abstract: In the work is presented the modeling of ultrasonic motor with three degrees of freedom. The basic and operating diagram of ultrasonic motor with piezoceramic active elements. The presentation of all vibration modes discovered by computer is make it and the possibility of being accomplished from practical viewpoint. From viewpoint all vibration modes presented are briefly described and as for the features of the useful are exhibited more to length.

Key words: ultrasonic motor; vibration modes

1. Theoretical considerations

The modeling of motor with three degrees of freedom represents a very important step in the advanced study and design of one ultrasonic motor.

The stage of modeling using the method of finite element is very useful because reduces a lot the necessary time of experimentations.

This thing is owned to the fact that the practical scan range of frequencies is not anymore necessary in ultrasonic domain starting with the frequency of f=18000 Hz

The method of finite element designate the frequency in which there are produced the oscillations of traveling necessary for transformation and delivery from piezoceramic active element to active element.

2. Description of the operational way to an engine with three degrees of freedom

In this work will be studied, design and achieve one ultrasonic engine with three degrees of freedom who can realize two translational motions and a motion of rotation.

The ones three degrees of freedom consist in the translational motion along the OX si OY axis and in the motion of rotation around OZ axis of whole system.

For the realization of translational motions are used two piezoceramic active elements and from lamella shape and as for the rotation motion is used an piezo-ceramic element which acts the whole system.

According as what was presented , the piezoceramic active femelements that serve this system are lamella and ring type.In this chapter will be presented the modelling of the two types of piezoceramic elements , in first part the piezoceramic active element of lamella type and in the second part of the chapter the active element of disk type.

In this way shall be defined the frequencies of useful vibrations which there are able to produce through their shapes of ‘’traveling’’type the desirable movements.

3. Modelling of the piezo-ceramic active element from lamella type

Foget the liniar displacement on two directions of ultrasonic engine is used two piezo-ceramic plates having the lenght L= 45 mm, width l=15mm and thickness h=2.5mm. For the realization of modal analyses that involve the introduction of a piezoceramic material properties was choose right as an element of digitization a structure of Scalar Brick 5 type which has a parallelepiped form.

Bellow it is presentet ones of the several modes of vibration which belong to piezoceramic plates.

Another mode of vibration which can't be used-up in the ultrasonic engine operation is produced to frequency f=54246 Hz and is presented in figure 1.

The oscillations of ''traveling'' type searched in sight of realization the movement are produced to frequency f=45105 Hz and there are presented in figure 2.

Around this frequency the experiments were concentrated and where the movement of activated element with constant values in time was obtained . The motion of mobile element is continuous and produce the movement of mass driven by motor in both directions of plan.

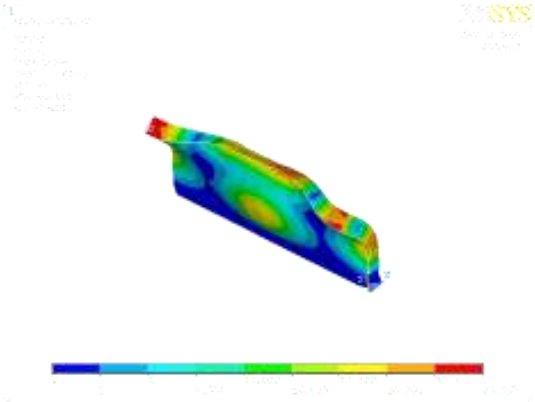

Figure 1. The mode of vibration to a frequency f = 54246 Hz.

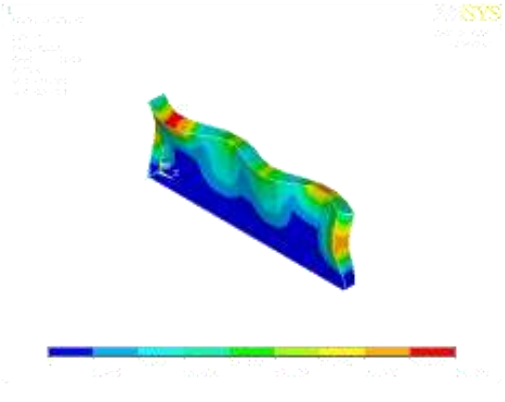

Figure2. The vibration mode of'' traveling'' type to frequency f = 45105 Hz.

In figure 3 is presented another one interesting mode of vibration which is produced to frequency f=90477 Hz in which the oscillation are from ''traveling type''but there are produced in two plans XOY and XOZ.In this situation the utilization of vibrations in the ultrasonic engine actuation is very difficult.. the continuation of the study for this kind of vibration is very interesting, only that is not represent a part from the activity of this work.

There are presents the vibration ways of piezoceramic element from ring type , element that achive the rotation motion of the engines. The second one piezoceramic active element is from ring type and has the inside diameter d= 40mm, outside diameter D=46 mm and the thickness h=7 mm. For obtain the desirable vibration modes was achieved a modal analyses from which are presented the main vibration modes from the domain of ultrasonic frequencies. In figure 6 is presented the first mode of vibration to frequency =38857 Hz, which practically don't presents any kind of interest.

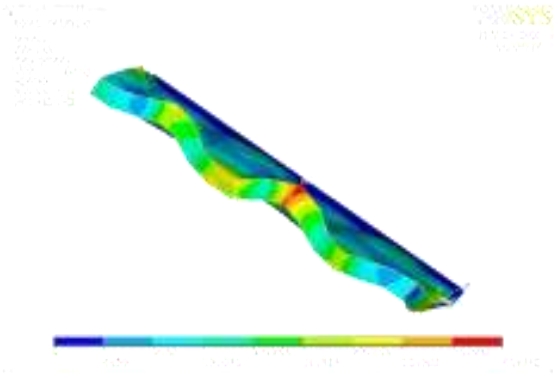

Figure 3. The vibration mode of'' traveling'' type to at frequency f = 90477 Hz.

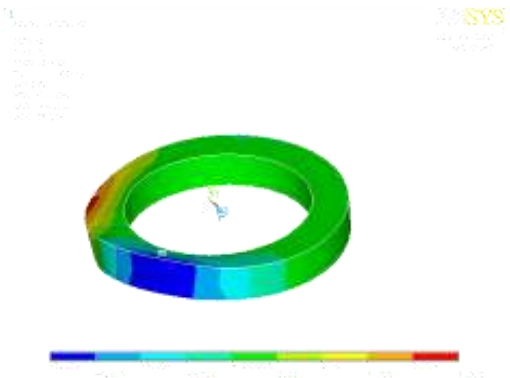

Figure 4. The mode of vibration at frequency
f=38857 Hz.

In the figures below are presented a mode of oscillations which isn't a ''traveling type''.

After the procurance of periodic desirable oscillations to frequency f=45057Hz, these disappear in a such way as it can see it in figure5, these become unsymmetrical and can't be useful from practical viewpoint.

This kind of rotation motion with same features is also obtained to a frequency f=65628 Hz .The researches were concentrated around frequency f=65000Hz which is the most used in the operation of this ultrasonic motor.

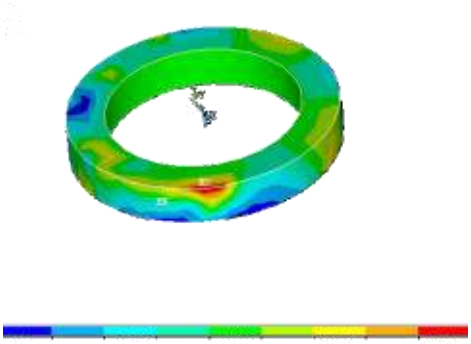

Figure 5. The mode of vibration from ''traveling'' type at frequency
f = 45057 Hz.

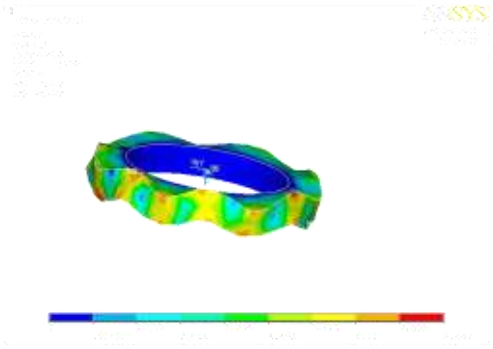

Figure 6. The mode of vibration from ''traveling'' type to frequency
f = 65628 Hz.

4. Conclusions

The modeling stage using the method of finite element is very useful because reduces a lot the necessary time of experimentations and give the possibility of understanding what phenomena are produced to under-microscopically level.

In this way can be created an image for vibration modes of piezo-ceramic active elements therefore these must be useful for the production of activated element movements. The reduction of working time is owed the fact that is not anymore necessary the scanning of frequency ranges from the ultrasonic domain starting with a frequency f=18000Hz. The method of finite element denotes with higher precision the frequency where the oscillations of traveling type necessary transformation and transmission from piezoceramic active elements to the activated ones are produced.

According as what was presented the points situated on the surface of piezo-ceramic element due to vibration form of travelling type, they will execute trajectories of elliptical shapes which will drive through the friction force among the two elements to the ‘’step–by-step’’ movements of the mobile activated elements

In the same time the method of the finite element helps to understand this kind of oscillation and builds mentally one model of operation the ultrasonic engines.In a certain way in the article is presented the vibration modes of piezo-ceramic active elements from lamella and disk type used in the construction of the engines with three degrees of freedom.

REFERENCES

[1] AMZA, Gh., ş.a Modelarea matematica a unui motor ultrasonic cu mai multe grade de libertate- Construcţia de maşini nr.8-9, XLIX, Bucureşti 1997.

[5] AMZA, Gh., ş.a Theoretical modeling and characterization of multidegrees of freedom ultrasonic motors for microrobots and micromachine applications, pag. 167-175, TCMM 40, Editura Tehnică, Bucureşti, 2000.

[2] *AMZA, Gh., Niţoi, D., Elements for designes and modeling of an ultrasonic motor, Timişoara, 2001.*

[3]A.LANGELLA, Crivelly Visconti, Technological Characteristics of a New Optical Sensor for Smart Composites, Advanced Composite Materials, Detroit Michigan, 1991.

[4]ABRAHAM SALEHI, Andrew Tay, Strain Concentrations Arouund Embedded Optical Fibers by FEM and Moire Interferometry, Advanced Composite Materials, Detroit Michigan, 1991.

[5] ACHENBACH, J., Fang, S., Asymtotic analysis of the modes ofwave propagation is solid cylinder, j. Acoust. Soc. Am. 1970.

[6]ADACHI, M., Shiosaki, T., Temperature compensated piezoelectric lithiuim tetraborate cristal for hight frecvency surface acoustic wave and bulk wave device application, in Proc. 1985.

[7] BALTRUKONIS, J., Gottenberg, W., Thickness shear Vibrations of circular bars, J. Acoust. Soc. A., 1959.

[8]CHENG, M., Finite element analysis of finite axisymmetric cylinders, M.S. Thesis, Tennesse Tech., Univ., Cookeville, 1998.

[9]DANCOV, I., Tokarev, E., Elastic, piezoelectric and dielectric properties of monocristalline lithium niobiate between 78 and 800 K, Inorganic Materials, 1983.

[10]A. LANGELLA, Crivelly Visconti, Technological Characteristics of a New Optical Sensor for Smart Composites, Advanced Composite Materials, Detroit Michigan, 1991.

CONSERVATION OF THE HISTORICAL BRIDGES IMPORTANT HISTORICAL SIGHTS

Researcher PhD eng. Anamaria FEIER, Researcher PhD eng. Monica BUZBUGAN, Assoc. prof. Oana CHIVU
INCD URBAN INCERC, Traian Lalescu 2, Timisoara, Romania, Asociatia de Sudura din Romania
National R&D Institute for Weldind and Material Testing, Mihai Viteazul 30, Timisoara, Romania
IMST Bucuresti

e-mail:anamaria_butisca@yahoo.com.au, mdobra@isim.ro, virlan_oana@yahoo.co.uk

Abstract: Lack of information about the history, the necessary data about the material characteristics and the presence of structural defects, leads to the need for detailed studies that have as a result more accurate determinations of the safety. The aim of this paper is to highlight the importance of a historic steel cantilever bridge in historical area from the city who host the structure.

Keywords: historical bridges, historical sights, Rehabilitation

1. INTRODUCTION

Bridges appeared at the crossing rivers, deep valleys, etc., and have evolved from tree trunks placed over the obstacle to complex solutions. Some natural bridges were formed by erosion of rocks, while some are still in operation today. An example of natural bridge is the so called "Bridge of God" from Ponoarele village.

After 1850 when the industry has developed a lot, the question of using mild steel in structure of bridges appeared. In Romania the first bridge of mild steel was built in 1895, it was named King Carol I bridge and it was built by Saligny. After 1900, more precisely in 1914, Traian bridge was erected in Arad.

Fig. no. 1: King Carol I and bridge Traian

2. DESCRIPTION OF THE TWO HISTORICAL BRIDGES FROM ROMANIA

Description of " King Carol I" bridge

Bridge "King Carol I" has 5 openings 4x140m +1 x190m consoles of 50 m

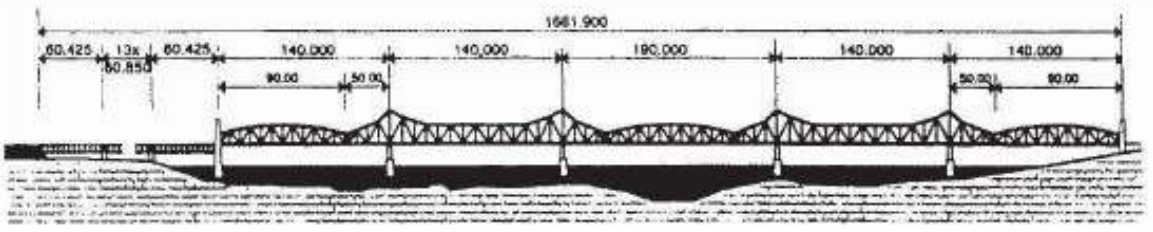

Fig. no. 2: Elevation of bridge King Carol I

It was inaugurated in 1895, it was the first steel bridge built in Romania. Saligny made a documentary visit on the site of the Firth of Forth bridge, in order get same answers for the design and construction of the bridge " King Carol I". An attempt to start the project was in 1887 when it was the first design contest, but only after the second design contest the company that provides delivery of the deck was established. The name of the company was Fives-Lille from Paris. The material used was mild .

The most important structural rehabilitation was in 1963. Consolidation was achieved in continuous circulation since the bridge had a significant importance in the communication paths so that breaks in service for consolidation were short of about 90-180 minutes a day.

Description of " Traian" bridge ofrom Arad,bridge over Mures River

Traian Bridge from Arad has 3openings, carriageway width is 8.05 m and the width of the bridge is 9.6 m There are walkways that are suspended circulating width 1.5 m each of them. Traian Bridge was carried out between 1912-1914, deck frame was machined in Resita in The Bridge Factory. Now it is one of the iconic structures of Arad, part of the city's architectural heritage.

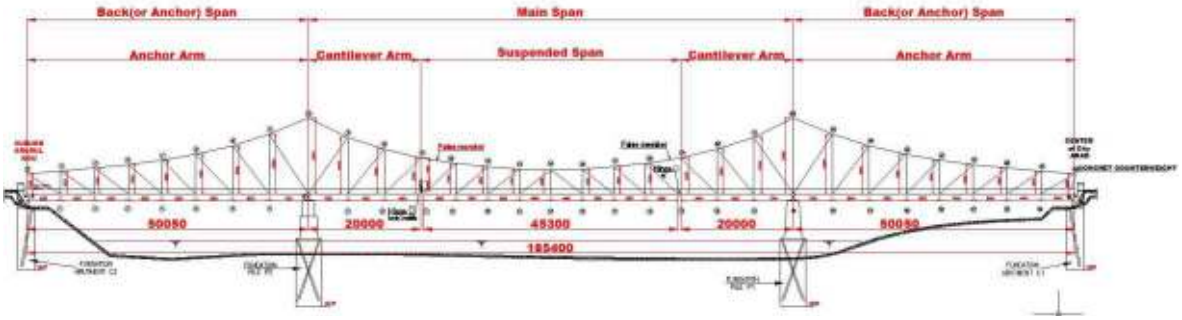

Fig. no. 3: Elevation of bridge Traian from Arad City

Bridge's curves form gives the impression of a suspension bridge, but in reality it is the classical system of trusses with Gerber type joints. The bridge has three spans and a total length of 185 m:

-central -span 85.30 m

-marginal openings 50.05 m

The cross sections of the main truss girders are composed of angle sections interlocked and riveted strap conductors with the following sections:

-lower chord sections riveted with two vertical walls in the form of Π

Both briges are Structural systems Decks with Gerber beams, cantilevers. A cantilever bridge is a structure using cantilevers, which are horizontal structures supported only on one end. Cantilevers must be anchored (or counterweighted) on one side in order to hold up the necessary weight on the free standing side.

Structural systems Decks with Gerber beams have the following characteristics:

Advantages:

· Best balancing of moments between spans and supports

· No settlements stresses

· Esthetic appearance

Disadvantages:

· Less rigidity

· Serious danger of deck fall during earthquakes due to narrow supports

· Special connecting systems, required to reduce possibility of fall

Structural verification of historical steel bridges is done by specific rules of the administration who have them in heritage.

It is important and necessary to maintain the operation of old metal road bridges.

Most of the steel bridges are built in the early twentieth century, with some great historical and artistic value as true monuments of the art construction. Their appearance is exquisite integrate harmoniously into the landscape. The current international trend is to keep operating safely the existing structures. For this purpose, information about the life and history of the bridge is necessary. In the western part of the country there are currently a large number of road bridges, built in the late nineteenth and early twentieth century, particularly bridges aesthetically capturing the elegance and slenderness. Structures still in good condition lasts, although in many cases poor maintenance is recorded numerous defects, collisions, broken parts, damaged and corroded some of them characterized by the total lack of documentation.

Rehabilitation of bridges is done by means of two methods:

-direct rehabilitation

-indirect rehabilitation

Direct rehabilitation

- Adding new material to the old riveted elements. This gives a higher load capacity. In general for old deck, the new parts are not welded, only in exceptional cases.

Indirect rehabilitation

- Introduced additional material by independent structural parts, works with existing structure as a whole becomes operative structures and especially for mobile tasks.
- Rehabilitation is usually indirect curved elements by introducing a prestressed tie the feet stretched.

CONCLUSIONS

The safety of structures, including many important aspects of vulnerability, is an issue of general importance for a society. When structure fails, the subsequent consequences can be severe, resulting in loss of life, damage to environmental quality and economic losses to society. A large number of bridges are located in cities as the flagship for the area. Once rehabilitated can be also integrated into the city's heritage.

REFERENCES

[1] I. SSF-RO: Technical project for the rehabilitation of the Traian Bridge in Arad, Timisoara, August 2007

[2] PETZEK, E.: Safety in Operation and Rehabilitation of Steel Bridges, Doctorat Thesis, UPT Timisoara 2004

[3] EN 1993-1-8: Eurocode 3: Design of steel structures. Part 1-8: Design of joints CEN- European Committee for Standardization, 2005

[4] EN 1993-1-1: Eurocode 3: Design of steel structures. Part 1-1: General Rules and Rules for Buildings CEN - European Committee for Standardization, 2005 Environmental Economics

[5] EN 1990 : Eurocode 0: Basis of structural Design CEN - European Committee for Standardization, 2005

[6] Petzek Edward; Bancila Radu, Evaluation of service security of steel structures, NATO Science for Peace and Security Series C - Environmental Security, 2009, pp: 301-323

[7] Bancila, R.; Petzek, E.; Boldus, D., Extended life for old highway bridges from the western part of Romania, International Conference on Metal Structures Location: Poiana Brasov, ROMANIA, SEP 20-22, 2006, pp 583-593

[8] Anghel Saligny „ Project du pont le Danube a Cernavoda. Note de calcul" Direction Generale des Chemins de fer Roumains. Service por la construction de la ligne Fetesti-Cernavoda.

[9]. . Butişca (cas. Feier) A., Petzek E, "Behavior of hinges elements in cantilever historical bridges"., Metalurgia International Editura Stiintifica F.M.R. 2013, Nr.7 ISSN 1582-2214 ISSN 1582-2214 pp.191-194

[10]. Butişca A.; Bancila R. Petzek E. Rominu S.,"Importance of rehabilitation of historical steel bridge Traian of Arad", Proceedings of 12th International Multidisciplinary Scientific Geoconference 17-23 iunie 2012 ISSN 1314-2704 pp.1011-1016;

[11]. Rominu S., Butişca A.,"Rehabilitation versus reconstruction of a new steel bridge". Proceedings of 12th International Multidisciplinary Scientific Geoconference 17-23 iunie 2012 ISSN 1314-2704 pp.1083-1090

[12]. Butişca(cas. Feier) Anamaria, Petzek E., Bancila R. Hernea S. " Economical importance of eye-bar in the rehabilitation of cantilever steel bridge Traian". Proceedings of 13th International Multidisciplinary Scientific Geoconference 16-23 iunie 2013 ISSN 1314-2704, pp 97-102

[13]. Hernea S. Butişca(cas. Feier) Anamaria, "ROBUSTNESS OF STRUCTURES-A NEW APPROACH OF VULNERABILITY AND STRUCTURAL RELIABILITY", Proceedings of 13th International Multidisciplinary Scientific Geoconference 16-23 iunie 2013 ISSN 1314-2704, pp. 263-270;

[14]. Petzek E., Butişca A., Toma L., "Eye Bars.-Pins Connections", Advanced Materials Research, Structural Integrity of Welded Structures, Volume 814, pp 222-229, 2013

[15]. Butişca A.;Rominu S., „"Bridge King Carol I at 116 years" Scientific Bulletin of the Politehnica University of Timisoara. Transactions on Hydrotechnics, ISSN 1224-6042, ISSUE 56(70) No. 2 2011, pp.75-79

LOADS TRANSMITED TO THE METALLIC TOWERS OF THE EXTRACTING INSTALLATIONS IN THE CASE OF THE APPLICATION OF THE SAFETY BRAKE

PhD, Eng., Assoc. Lecturer, Răzvan Bogdan Itu, Department of Industrial Mechanical Engineering and Transport, University of Petroșani, raz.van4u@yahoo.com
PhD Student, Eng, Alexandru Ioan Pop, Department of Industrial Mechanical Engineering and Transport, University of Petroşani, ionutpop6@yahoo.com

Abstract: In the paper there are presented certain aspects concerning the determination of loads transmitted through the bearings of the extracting pulleys of the structure of the metallic towers of the extracting installations In the case of the application of the safety brake The exemplification of the determination of the loads transmitted to the metallic tower in the case of the application of the emergency brake has been done by taking into study the extracting installation „ Auxiliary well No.12", from Lupeni Mining Plant. The extracting installation is unbalanced. The wrapping organ of the installation machine is a double wheel with the wrapping of the extracting cable in one layer. The extracting vessels are untipping cages with two levels, with two trolleys per level. The drive of the installation's machine is asynchronous, the machine' s reducer having two drives.

Keywords: analytical calcul, force

Introduction

The normal development of the schedule of the movement of the extracting vessels or the stopping of the machine in a certain position of the vessels (maneuver braking) and the automated stopping of the machine (safety brake), independent of the will of the operator in one of the cases considered perturbations or distress, is insured by a braking device supplied with every extracting machine. Cases considered perturbations or distress are: lack of tension, a decrease in fluid pressure required for acting the brake, over-height of the extracting vessels, passing the max. speed limit overweight etc.

In the paper there are presented certain aspects concerning the determination of loads transmitted through the bearings of the extracting pulleys of the structure of the metallic towers of the extracting installations in the case when the emergency brake is applied due to an overcome of the max speed allowed.

In order to study the loads from the extracting cables transmitted to the structure of the metallic towers of the extracting installations through the extracting pulleys in the case when the emergency brake is applied it has been taken into study the tower of the extracting installation Auxiliary well No.12 Lupeni Mining Plant. The general and exploitation data of the installation taken into study are presented as follow.

The extracting installation taken into study

The extracting installation which works on auxiliary well no.12, from E.M. Lupeni, which is destined for the underground supply with materials and tools as well as for transporting personal. The personal and materials transport is done to and among levels 300, 400, 480, 650 and 690. The extracting installation that supplies the well (Fig.1) is unbalanced (without a balance cable) and has an extracting machine type 2T-3,5 1,8 (Fig.2) equipped with two asynchronous motors type AKH2-16-39-12YXP4, of 500 kW power and a nominal rpm of 490 rot/min(fig.3).

Figure 1. Extracting installation

Figure 2. Extracting machine

Figure 3. Extracting pulleys

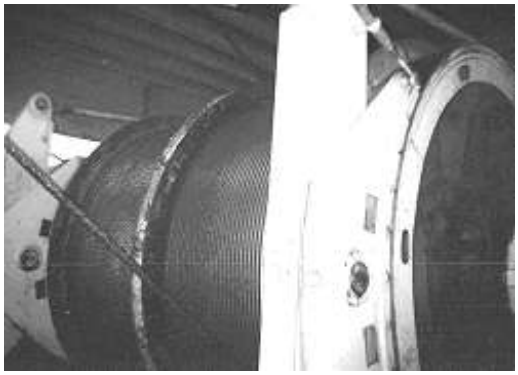

Figure 4. Wrapping organ

The reducer of the machine is of type 2U 1600 having the transmittance ratio of 11, 5 The extracting cables with diameters of Φ 44 mm and a mass (on a linear meter) of 7,05 kg/m on the left branch (from the extracting machine to the well) and Φ 44 mm and a mass 7,03 kg/m on the right branch are wrapped around the two extracting pulleys of Φ 4000 mm with a mass (the pulley, the axel of the pulley and the bearing of the axel) of 1850 kg (Fig.3), laying on the tower at a height of 22,95 m (pulley axel).

The cables are wrapped in a single layer (row) on each of the two wheels (wrapping organ (Fig.4)) of the machine, from which one is fixed and one is mobile and which are hooked at one end by the exterior end (side margin) of them. The other end of the cables going through the extracting pulleys is hooked to the extracting vessel through the cable tie device (D.L.C.). The extracting vessels are untipping cages with two levels, with two trolleys each level having a mass (own mass plus D.L.C.) of 4924 kg.
The mass of a trolley is of 650 kg, and the effective load is 1800 kg/trolley. Another main compo-nent of the extracting installation is the metallic tower (Fig.5) with a height until the pulley axel of 22,95 m. The structure of the tower is composed of the extracting pulley platform sustained by the leading component and the two abutments set up as a frustum pyramid The extracting machine lies on the ground (at a height of 3.695 m to the 0 level of the well (well collar), sideways from the tower (well tower), at a distance (of the wheel axel), towards the vertical portion of the extracting cables which enter the well of 32m. The length of the cable chord (the distance between the tangent points of the cable to the deviating pulley from the tower and the wheel of the extracting machine, in the central position of the chord (perpendicular on the wheel axel)), is for the left branch L_{cs}=35,450m, and L_{cd}=35,646m for the right branch. The incline angles of the cables chords are $\beta_s = 38^0\ 43'\ 55''$ for the left branch and $\beta_d = 33^0\ 05'\ 43''$, for the right branch, and the deviating angles (which are formed in the limit positions of the cable chord towards the interior side(interior angle) or exterior (exterior angle) of the wheel, over the central position of the chord) are: $\alpha_{e\ st} = 1^0 38' 53''$ şi $\alpha_{i\ st} = 0^0 42' 11''$ For the left branch and $\alpha_{e\ dr} = 1^0 40' 33''$ şi $\alpha_{i\ dr} = 0^0 39' 43''$ for the right branch.

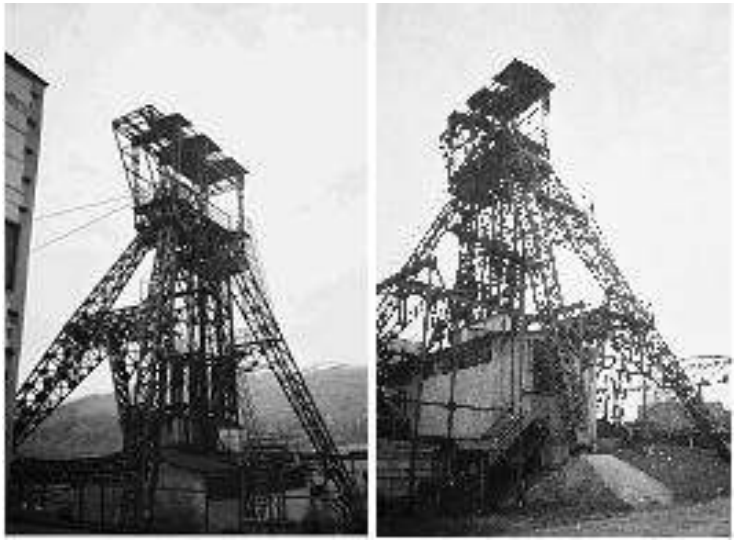

a) b)

Fig.5. Metallic tower
a)North –West view; b) South-West view

Determination of loads

For the determination of the loads(efforts) which act upon the installation taken into consideration it has been taken into study the case when one of the vessels loaded with materials is descending on one of the branches.

On the calculation of loads it has been considered the fact that their variation is determined not only by the kinematics of the installation (kinematical parameters) but also by certain geometrical elements which define the position of the extracting machine towards the well geometrical elements regarding only the installations where the extracting machine lies on the ground.([1],[3],[4]).

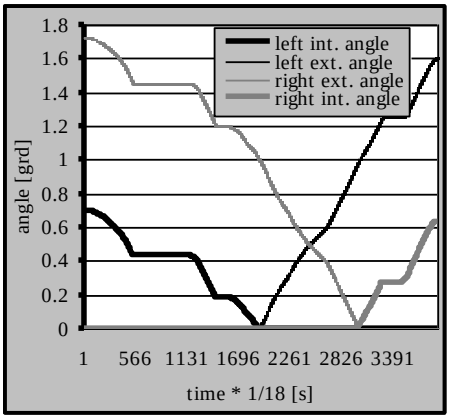

Figure 6. Deviating angles case 1

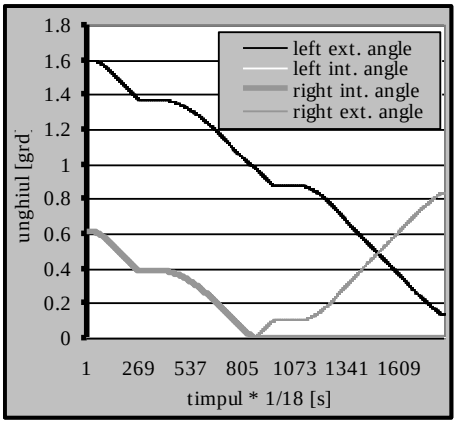

Figure 7. Deviating angles case 2

In Fig 6 and Fig 7 is presented the variation diagram for the deviation interior and exterior angles on the two extracting branches and for the two wheels of the wrapping organ of the extracting cable in the two considered cases.

For this purpose it has been taken into analysis the case when the full vessel(filled to max load) is descending on the left branch (case 1, the right case is climbing and the left one is descending) and the case the vessel is descending on the right branch (case 2, left vessel is climbing and the right one is descending).

The diagrams for the space, speed, and acceleration for the two cases taken into analysis are presented into Fig 8 case 1 and in Fig 9 case 2.

The variations of acceleration and space have been used for the calculation of the loads applied to the tower.

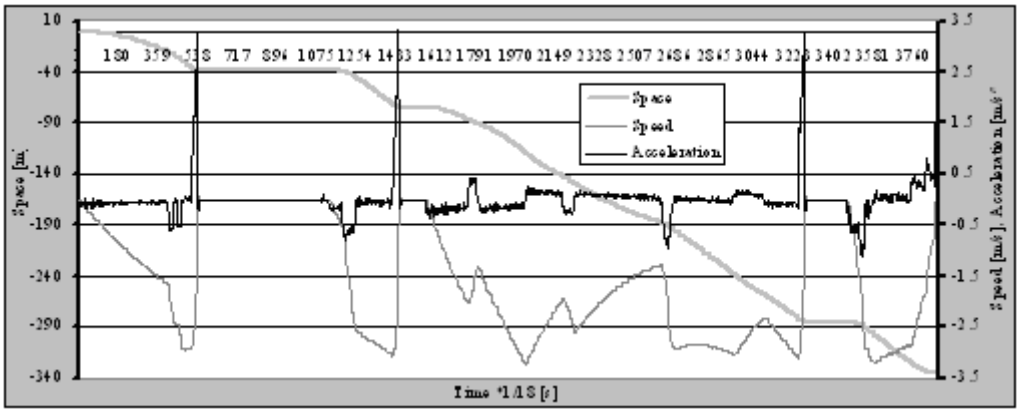

Figure 8. Speed acceleration and space for case 1

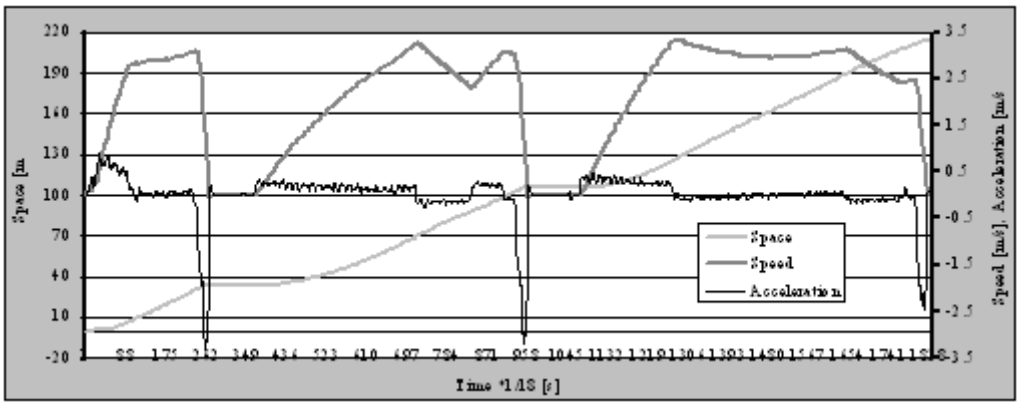

Figure 9. Speed acceleration and space for case 2

The determination of the loads acting upon the tower through the deviating pulleys has been done using the d'Alembert principle (the kinetics-static method [2]) taking into consideration the static forces (the weight of the extracting cable, the cage the trolley the pulley and the load), the friction forces (multiple friction and aero-dynamic resistances which for installations with cages is approximated with a coefficient of k'=0,2 from the useful load [1]) and the dynamic forces (which intervene only in the acceleration and deceleration periods, Fig. 8 and Fig. 9)).

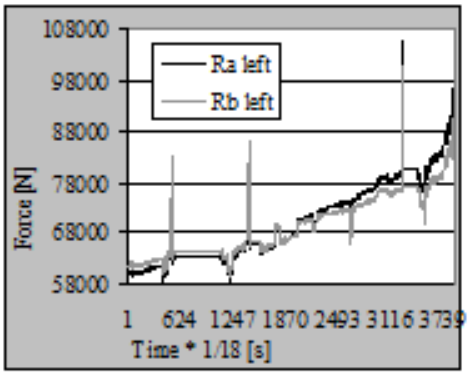

Figure 10. Reactions from the bearing of the left pulley when the left cage descends and the right one climbs,

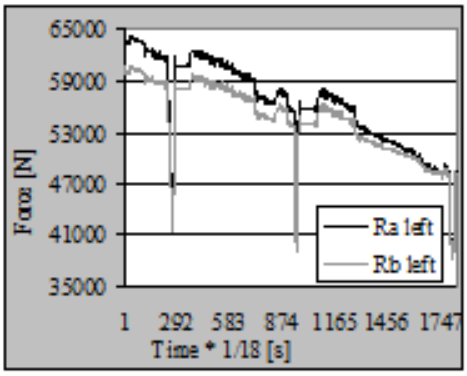

Figure 11. Reactions from the bearing of the left pulley when the left cage climbs and the right one descends.

The variation of the resultant forces from the bearings of the extracting pulleys for the two considered cases in the case of the application of the safety brake on the surpassing the max admitted speed is presented in fig 10 and fig 12, for case 1, for the left and right pulley and fig 11 and fig 13, for case 2, also for the left and right pulley.

The variation of the total resultants (reactions) the forces from the extracting pulleys for the two cases taken into consideration in the case of the appliance of the safety brake on the surpassing of the max speed is presented in fig 14 case 1 and fig 15, case 2, for both pulleys.

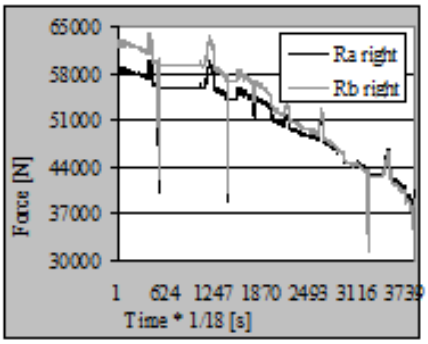

Figure 12. Reactions from the bearing of the right pulley when the left cage descends and the right one climbs,

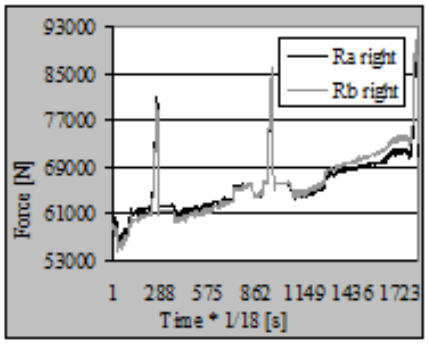

Figure 13. Reactions from the bearing of the right pulley when the left cage climbs and the right one descends.

In fig 16 and fig 17, there are presented the variations of the total loads on the tower for the two cases.

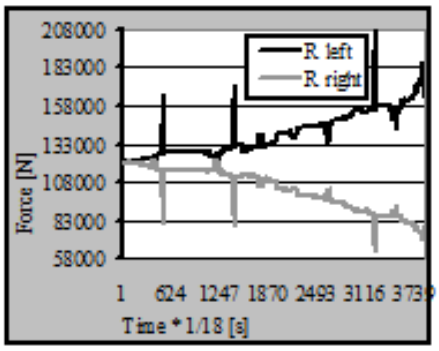

Figure 14. Reactions from the bearing of the left and right pulley when the left cage descends and the right one climbs, Case 1

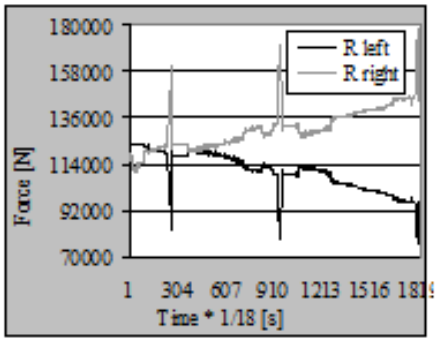

Figure15. Reactions from the bearing of the left and right pulley when the left cage climbs and the right one descends, Case 2

Conclusions

The calculation the structure of the mining extracting towers is done taking into consideration all the unfavorable combinations practically possible of the different loads called groups of loads. Following the classification and grouping of the loads transmitted to the extracting mining towers in the paper there are presented certain aspects concerning the establishing of the exceptional short term loads due to the extracting cycle in the case of the appliance of the safety brake which are transmitted to the structure of the metallic tower of an extracting unbalanced installation with extracting vessels untipping cages and an extracting machine with two wheels and the wrapping of the extracting cable on one layer and acting asynchronous. The loads transmitted to the tower through the bearings of the extracting pulleys from the tower due to the efforts from the extracting cables have been considered for an extracting cycle when the empty cages are climbing and descending on one of the two extracting branches. The variation of loads is due both for the cinematic parameters as well as for the geometric parameters of the extracting installation. As noticed from the variation of the total loads which act upon the tower during an extracting cycle in the case of the appliance of the safety brake the maximum values are in case 1 towards the end of the cycle and in case 2 at the beginning of the cycle (Fig 16 and Fig 17, and not at it's end like in case 1. The maximum values of the loads determined are further used to determine the values of mechanical stress and strain from the elements of the structure of the metallic tower of the installation in order to verify its resistance.

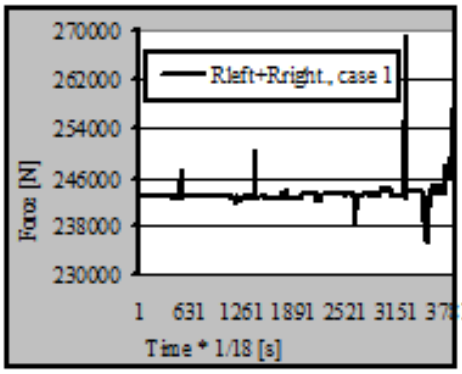

Figure 16. Total loads when the left cage descends and the right one climbs
Case 1

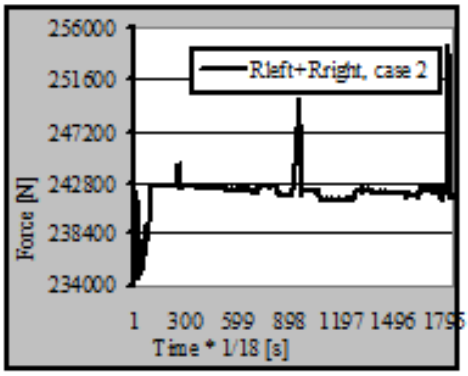

Figure 17. Total loads when the left cage climbs and the right one descends
Case 2

References

[1]. Magyari A., *Instalaţii mecanice miniere*, Editura tehnică, Bucureşti, 1990;
[2]. Ripianu A., ş.a. *Mecanică* tehnică, Editura Didactică şi Pedagogică, Bucureşti, 1982;
[3]. Dumitrescu I., Ridzi M. C., Itu V., - Stress and displacements in the structure of the extracting towers/*Tensiuni şi deplasări din structura turnurilor instalaţiilor de extracţie*, New aspects of Engineering Mechanics, Structures end Engineering Geology, Proceedings of the WSEAS International Conference on ENGINEERING MECHANICS, STRUCTURES END ENGINEERING GEOLOGY (EMESEG '08), Mathematics and Computers in Science Engineering, A. Series of Reference Books and Textbooks, HERAKLION, Crete Island, Grece, July 22-24, 2008, Published by Wseas Press, Page 358-363, ISBN: 978-960-6766-88-6, ISSN: 1790-2769
[4]. Itu V., Ridzi M. C., Dumitrescu I., - On diagnosis of brake mechanism of hoisting machines / Despre *diagnosticarea mecanismului de frânare a maşinilor de extracţie*, New aspects of Engineering Mechanics, Structures end Engineering Geology, Proceedings of the WSEAS International Conference on ENGINEERING MECHANICS, STRUCTURES END ENGINEERING GEOLOGY (EMESEG '08), Mathematics and Computers in Science Engineering, A. Series of Reference Books and Textbooks, HERAKLION, Crete Island, Grece, July 22-24 2008, , Published by Wseas Press, Page 352-357, ISBN: 978-960-6766-88-6, ISSN: 1790-2769;
[5]. * * * Docum*entaţie tehnică*, E. M. Lupeni.

STRAINS AND DISPLACEMENTS FROM THE STRUCTURE OF THE TOWER OF THE EXTRACTING INSTALLATION

PhD, Eng., Assoc. Lecturer, Răzvan Bogdan Itu, Department of Industrial Mechanical Engineering and Transport, University of Petroșani, raz.van4u@yahoo.com
PhD Student, Eng, Alexandru Ioan Pop, Department of Industrial Mechanical Engineering and Transport, University of Petroşani, ionutpop6@yahoo.com

Abstract: The development in safe conditions of the extracting process continuously imposes the need of optimal functioning of the extracting installations as important links in the transport flow of the mineral substance and of the sterile for the transportation between the underground and the surface of personal, machines and different mining tools. In the paper there is presented an analysis of the behavior of the towers of the extracting installation with regards to strains and displacements of the resistance structure during the functioning of the extracting installations with pulleys as a wrapping organ for the cables.

Keywords: tower, extracting installation, strains, displacements.

Introduction

The calculation the structure of the mining extracting towers is done taking into consideration all the unfavorable combinations practically possible of the different loads called groups of loads and are established taking into account in their form the compatibility of their acting simultaneously.

The loads are classified into: permanent, short term - temporary, long term - temporary, and exceptional. The groups of loads with loads that can be introduced into groups of loads are the fundamental group of loads which contains permanent loads, long term loads, one or more short term loads and the special loads grouped from the fundamental group and one of the exceptional loads.

In order to establish the state of strain and displacements from the structure of the tower due to the short term functioning loads transmitted through the extracting cables during an extracting cycle, it has been taken into study the tower of the extracting installation ,,Auxiliary well Jieţ“ Lonea Mining Plant, which has the general and working data presented as follows.

The installation taken into study

The extracting installation which works on auxiliary well Jieţ, from Lonea mining plant, which is devoted [4] for the underground supply with materials and tools as well as for transporting personal among levels 400 and 715 (the surface level being 715).

The extracting installation that supplies the well (fig.1) is unbalanced and has a hoistingmachine type BAMERT 3000 900 equipped with two asynchronous motors type MAF, (fig.2) of 125 kW power and a nominal rpm of 585 rpm.

The gear reducer of the machine is of type TD-170 having the gear ratio of 11,5.

The extracting ropes with diameters of Φ 27,5 mm and a mass (on a linear meter) of 3,2 kg/m on the left branch (from the extracting machine to the well) and Φ 27,5 mm and a mass 3,2 kg/m on the right branch are wrapped around the two extracting pulleys the superior and the inferior one, of Φ 2000 mm with a mass (the pulley, the axle of the pulley and the bearing of the axle) of 2050 kg (fig.3), laying on the tower at heights of 34,4 m respectively 31,4 m (pulley axle).

Figure 1.Extracting installation ,, Auxiliary well Jieţ "

Figure 2.Extracting machine type BAMERT 3×0,9

Figure 3. Installation tower ,, Auxiliary well Jieţ "

The ropes are wrapped in two layers on each of the two drums of the machine, from which one is fixed and one is mobile and which are hooked at one end by the exterior end (side) of them. The other end of the ropes going through the extracting pulleys is hooked to the extracting vessel through the rope tie device DLC.

The extracting vessels are untipping cages with one level, with two trolleys per level having a mass (own mass plus D.L.C.) of 3355 kg. The mass of a trolley is of 650 kg, and the effective load is 1600 kg/trolley.

Figure 4. Pulley platform

Figure 5. Leading component

Figure 6. Abutment

The concrete made tower (fig.3) with a height until the pulley axle of 34.4 m. The structure of the tower is composed of the extracting pulley platform (fig.4) sustained by the leading component(fig 5) and the abutment (fig 6) The extracting machine lies on the ground (at a height of 2,8 m to the 0 level of the well (well collar), sideways from the tower (well tower), at a distance (of the wheel axle), towards the vertical portion of the extracting ropes which enter the well of 27,32 m.

The length of the rope chord (the distance between the tangent points of the rope to the deviating pulley from the tower and the wheel of the extracting machine, in the central position of the chord (perpendicular on the wheel axle)), is for the left branch L_{cs}=37,62 m, and L_{cd}=44,89 m for the right branch.

The slope angles of the ropes chords are β_s = 530 47' 04" for the left branch and β_d = 490 39' 36", for the right branch, and the deviating angles (which are formed in the limit positions of the rope chord towards the interior side(interior angle) or exterior (exterior angle) of the wheel, over the central position of the chord) are: αe st =19'29'' and αi st=0 for the left branch and $\alpha_{e\ d}$r=31'53'' and $\alpha_{i\ dr}$=0 for the right branch [4].

Loads transmitted to the tower

Considering the elevator leaving the horizon 580 until it reaches the surface ramp (783 horizon) it has been taken into study the case of personal transport entering the underground when the left elevator full of personal is descending on the right wing (case 1), the right elevator is descending on the right wing (case.2) and in the case of the application of the safety brake (case 3 and case 4).

The kinematics elements for the cases taken into analysis are presented in figure 7, 8, 11 and 12.

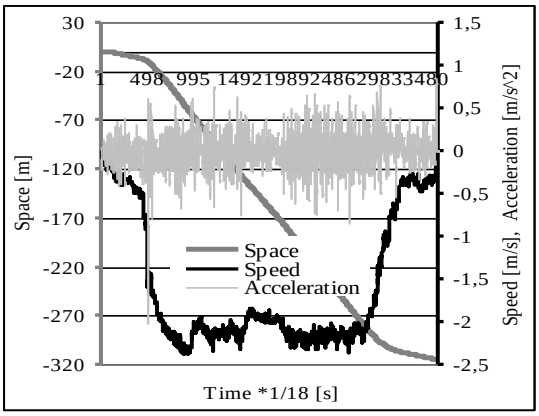

Figure 7. Kinematic elements on the elevator left climbing personal entrance, case1

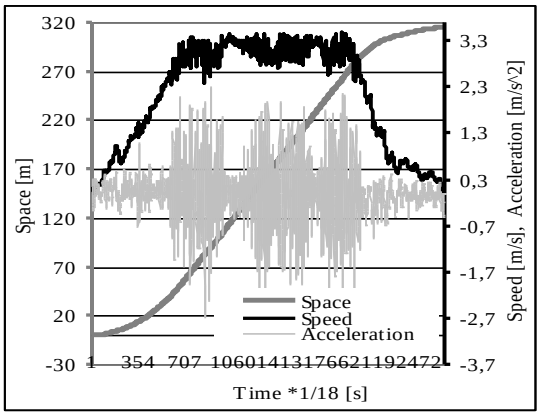

Figure 8. Kinematic elements on the elevator left descending personal entrance , case 2

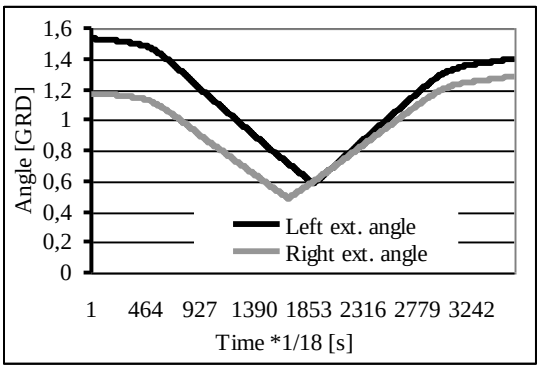

Figure 9. Deviating angles for case 1 from Figure 7

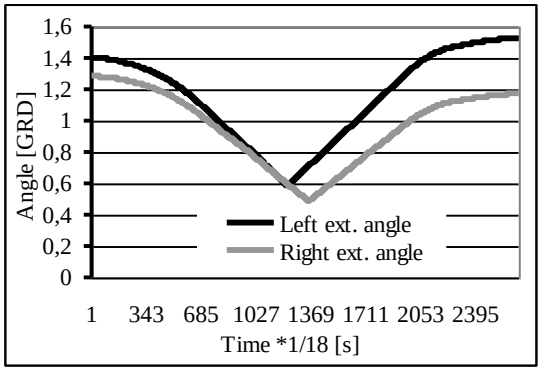

Figure 10. Deviating angles for case 2 from Figure 8

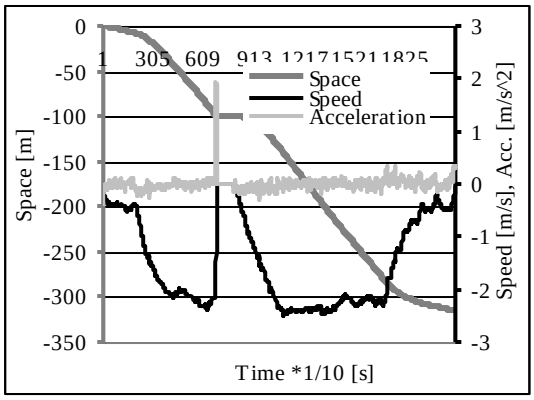

Figure 11. Kinematic elements for case 3

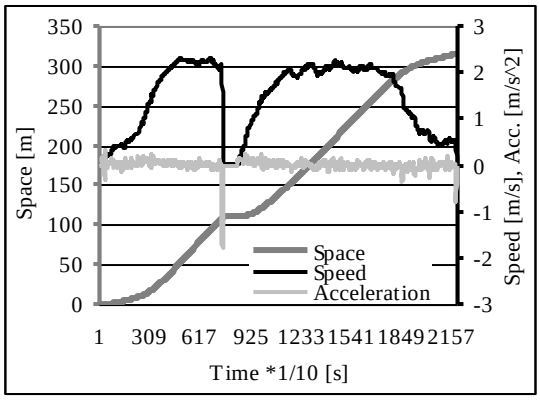

Figure 12. Kinematic elements for case 4

In the calculation of loads it has been used the d'Alembert [1], [2] principle decomposing the efforts from the cable chords, in their touch points on the pulleys into components on three perpendicular directions which correspond to the axis system chosen in the discretisation of the structure of the tower of the installation. The components of the efforts from the cable chords variate both because of the incline angles of the chords but also because of the deviation angles [3] of them (Figures 9,10, 13 and 14).

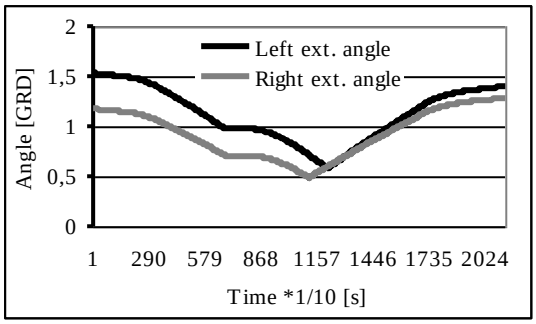

Figure 13. Deviating angles for case 3 from Figure 11

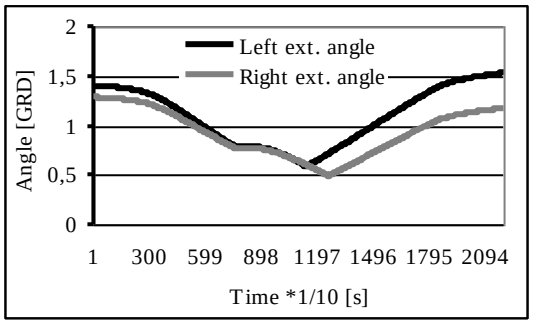

Figure 14. Deviating angles for case 4 from Figure 12

The variation the loads on the entire tower for each case taken into study is presented in figure 15, 16, 17 and 18.

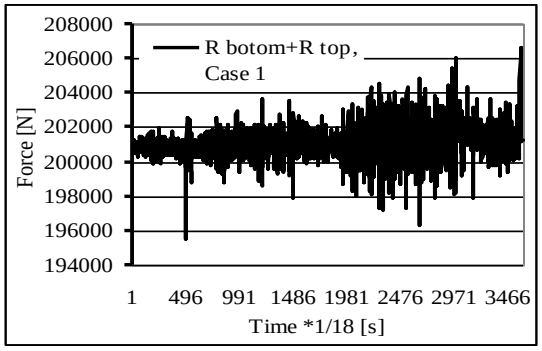

Figure 15. Total loads when the elevator left climbing , right descending case 1

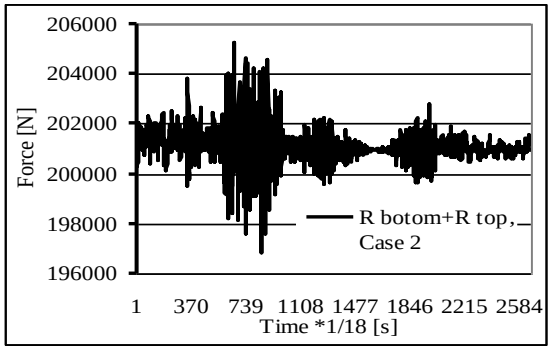

Figure 16. Total loads when the elevator left descending, right climbing, case 2

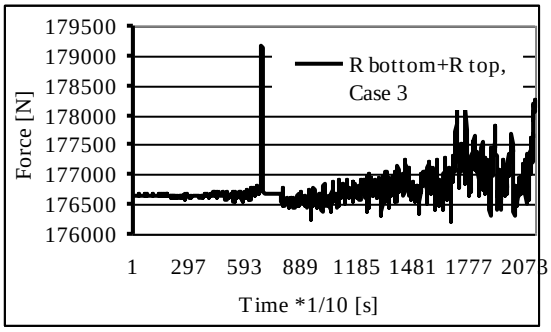

Figure 17. Total loads for case 3

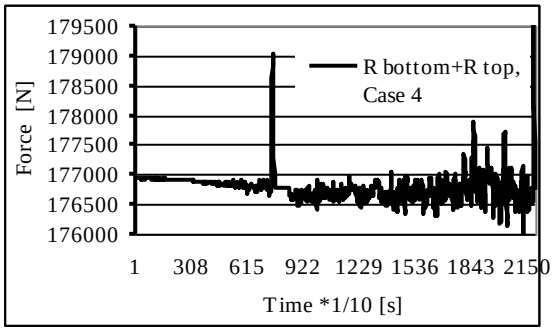

Figure 18. Total loads for case 4

Sstrain and displacements

The strein and the deplacements [1], [2] for each case taken into study is presented in figure 19, 20, 21, 22, 23, 24, 25 and 26.

Conclusions

There have been determined and localized the max values of strain and displacements from the tower structure, in order to establish the measuring points, in order to verify through experimental measurements the values obtained through numerical calculation.

Following these results there have been obtained information necessary in order to improve the maintenance of the extracting installations and to improve the existing system of repair and supply for this type of installations.

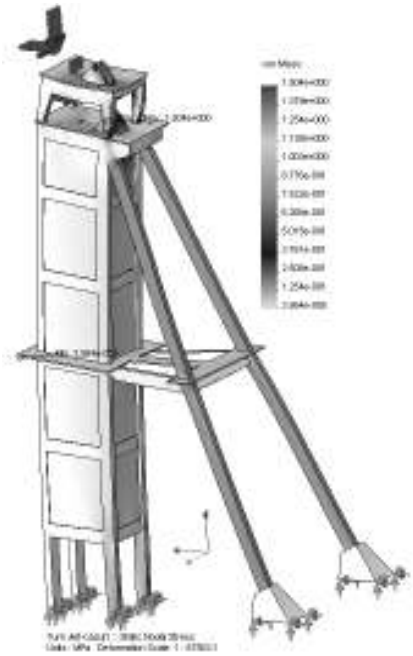

Figure 19. Strain, case 1

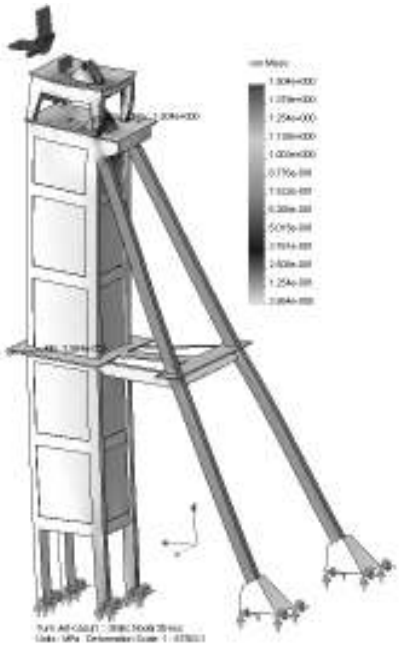

Figure 20. Displacements, case 1

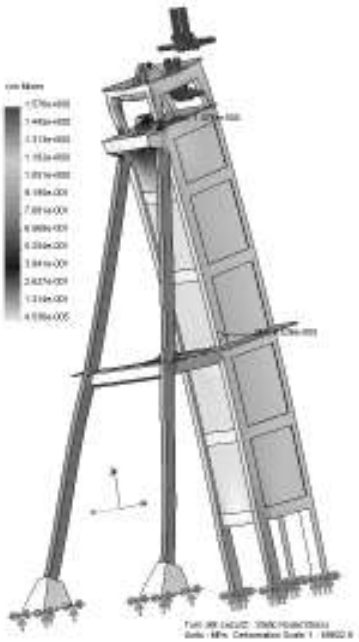

Figure 21. Strain, case 2

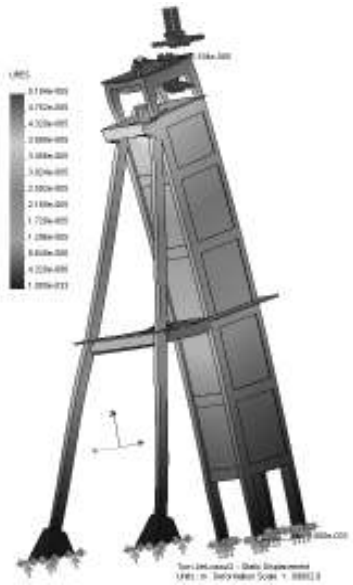

Figure 22. Displacements, case 2

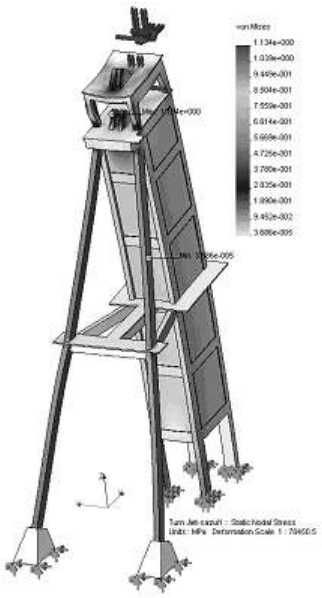

Figure 23. Strain, case 3

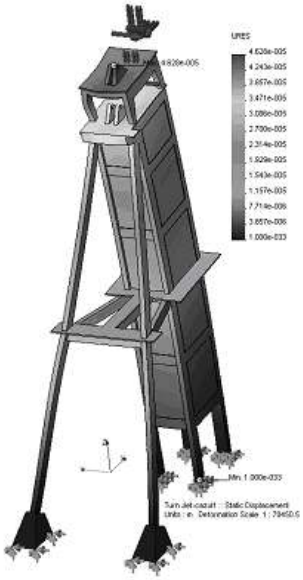

Figure 24. Displacements, case 3

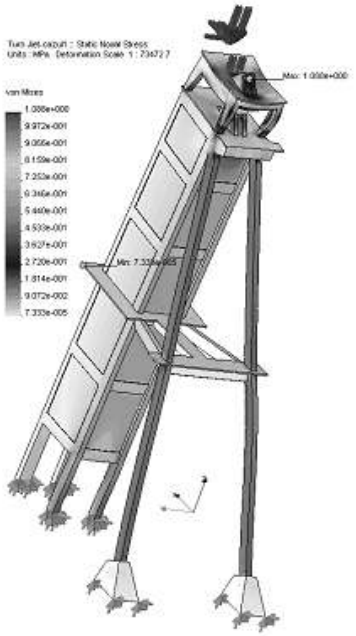

Figure 25. Strain, case 4

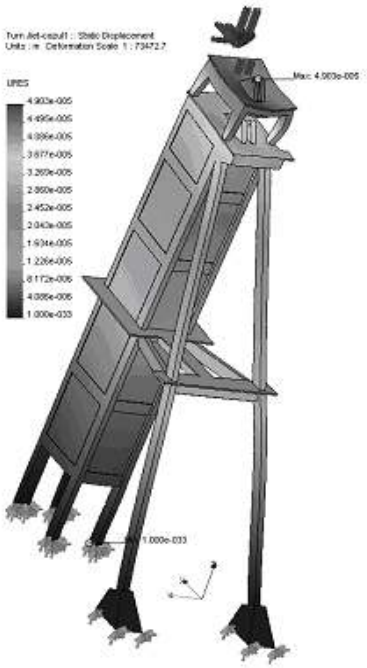

Figure 26. Displacements, case 4

References

[1] Itu, V., Ridzi, M.C., Strains and displacements in the elements of the metallic towers of *the extracting installations due to the tower's own weight*, Mines Magasine , vol 170, nr. 8/2005, pag.25-31;
[2] Itu, V., Ridzi, M. C., Dumitrescu Iosif - *Măsurarea deplasărilor şi tensiunilor mecanice la turnurile de extracţie metalice miniere*, Editura Universitas, Petroşani, 2010, ISBN 978-973-741-168-6, 136 pag.
[3] Magyari, A., Mining mechanical installations, Editura tehnică, Bucharest, 1990;
[4] * * * Technical documentation, Lonea Mining Plant.

STUDIES ON MACHINE PARTS MADE OF WELDED CONSTRUCTION

Lect.Dr.Eng. Constanța RĂDULESCU
University „ Constantin Brâncuși'' of Târgu-Jiu – **Romania,** rpc10gj@gmail.com
Prof. Dr. Eng. Marius Liviu CÎRȚÎNĂ
University „ Constantin Brâncuși'' of Târgu-Jiu – **Romania,** cirtinaliviu@gmail.com

Abstract: In this work it was analyzed a welded construction of a rollers which is part of a conveyor belt of a roll 84 inches. The roler taken under discussion is a roler that has an outer diameter of 89 mm and length of 504mm. The roller is accomplished up of a cylinder wherein spindles the axis of rotation are fixed with the help of some double disc by welds corner. Because it is known that the roller is requested by the concentrated force 5 kN, keeping account the dimensions of the elements and the material from which they are executed were determined requests that confronts the roler.

Keyword: weld, machine parts, welded construction

1. INTRODUCTION

According to the literature, the design and technological design of welded structures occupy more than 75-80% of labor making for a device, machinery or a structure made by welding [1], [2] .

The design activity and design of welded structures technological consists of several stages: determining the technical and economic conditions on the welded construction; establishing the conditions for stress and exploitation, choice of shape and size of each piece of construction, of material quality elements, choice of welding process and quality class of weldment; final determination indications and transit Technology manufacturing of welded construction.

For preparation of manufacturing sequence of a welded construction it is necessary to respect the following steps: assembly drawing and welded parts drawings; manufacturing technology preparation and implementation of operations plans.

2. STRESS DETERMINATION AND CHECKING CALCULATION OF WELDINGS OF A ROLLER

In this paper we analyze welded construction of a conveyor roller. The roll is part of a 84 inches rolling conveyor [3], [4]. The conveyor belt has two types of rolls : upper rolls and lower rolls. The upper roller is a subassembly consisting of a cylinder (shell) in which a shaft is mounted, and at the ends are fixed boxes, bearings, felt rings and bearings caps. The lower roller is made of a cylinder (shell) in which the rotation axis spindles are secured by means of double disc with welds corner (figure 1). Also it is known that the rolling conveyor is requested by the concentrated force of 5 KN.

To do the calculation and verification of welds is necessary to establish first the grade of material. Thus, for cylinder (mantle) roll it is chosen a brand S235JR EN125-2 steel.

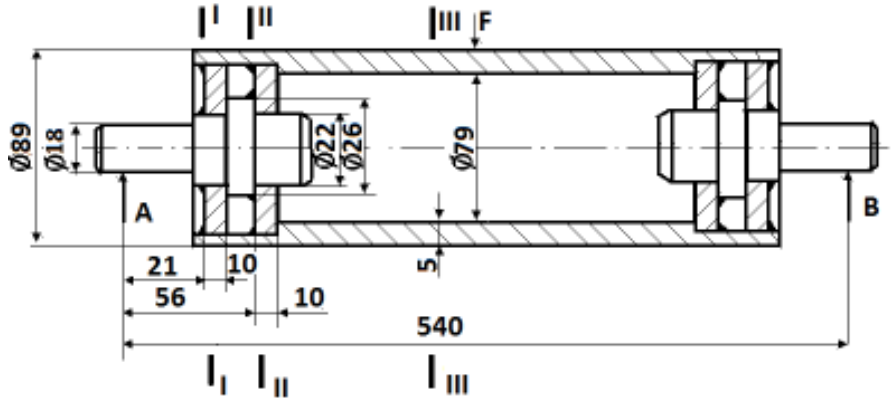

Fig.1. Rola transportorului cu bandă

Because the conveyor rollers working at temperatures of 10-15, will choose the grade of material like in the literature as follows: geometric form factor K = 1.4; functional importance factor S = 0.7 and loading factor B = 1.

In this case, the hazard ratio will be:

$$G = K \cdot S \cdot B = 1{,}0 \qquad (1.1.)$$

For the roll shell will choose a S235JR EN125-2 steel , grade 2 of quality and for the drives ring will choose a S235JR EN125-2 steel grade1 of quality. For determining the request, we will consider the sizes of elements in I-I and II-II sections.

In section III-III, it is considered the general system of rollers like a simply leaning beam, static determined (fig.2).

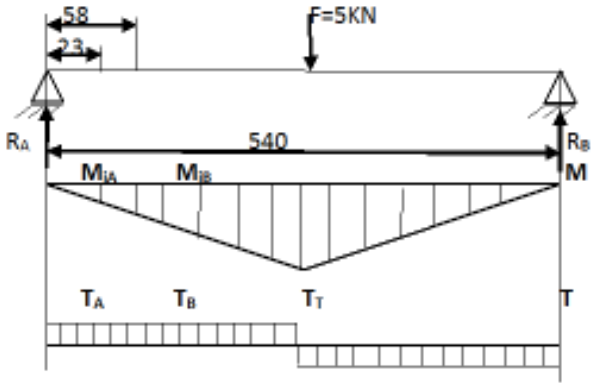

Fig. 2. Forces and reactions from sections,,III-III''

The reactions of A and B will be:

$$A = B = \frac{F}{2} = 2{,}5kN \qquad M_1 = F\frac{l}{4} = 5.\frac{0{,}540}{4} = 0{,}68kNm$$

$$M_2 = R_A \cdot 0{,}023 = 0{,}06kN \qquad M_3 = R_A \cdot 0{,}058 = 0{,}15kN \tag{1. 2}$$

$$T_1 = \frac{F}{2} = 2{,}5kN, \qquad T_2 = T_3 = T_1 = 2{,}5kN$$

When the roll has accelerated motion on the rollers acts an additional torsional stress which is:

$$M_{t\,max} = 0{,}028kNm \tag{1.3}$$

Once calculated this, you can proceed to determine the sizes of the welds in sections ,,I-I'' and ,,II-II''.

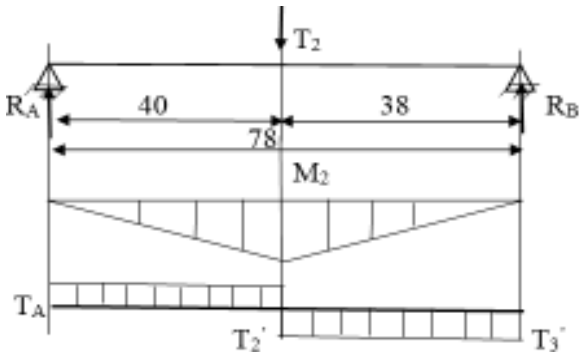

Fig.3. Forces and reactions from sections ,,I-I,, și ,,II-II,,

Because the roll axes are fixed in its shell through two welded with welding corner can consider that these claims are without bending. In this case, the forces in real plane are shown in figure 3 and determined by relations:

$$T_2' = \frac{R_A \cdot 78}{38} = \frac{2{,}5 \cdot 78}{38} = 5{,}13kN \quad si \quad T_3' = T_2' - R_A = 5{,}13 - 2{,}5 = 2{,}63kN \tag{1.4}$$

For checking of sections ,,I-I" and ,,II-II'' starts from the fact that both contain the same corner welds. In section ,,I-I'' stress elements are:

$$T_2' = 5{,}13kN \quad si \quad M_{t2} = 28 \cdot 10^3\, N \cdot mm \tag{1.5}$$

It will do the calculations to verify the weld from A-A section which is connecting shaft to the annular disc. In this case it will be considered that the shear force is taken fully of welding. The tangential stress, in these circumstances, it will be determined using relations:

$$\tau_{T_2'} = \frac{T_2'}{A_{cs}} = \frac{5{,}13\text{kN}}{424{,}12\text{mm}^2} = 12{,}1\ \text{N/mm}^2 \quad \text{si} \quad \tau_{M_2} = \frac{M_{t2}}{W_{2cs}} = \frac{28 \cdot 10^3\ \text{Nmm}}{2498{,}3\text{mm}^3} = 11{,}2\ \text{N/mm}^2$$

$$A_1 = \left(R^2 - r^2\right) \cdot \pi = (16^2 - 11^2) \cdot \pi = 424{,}12\text{mm}^2 \tag{1.6}$$

$$W_1 = \frac{\pi}{32 \cdot D}(D^4 - d^4) = \frac{\pi}{32 \cdot 32}(32^4 - 22^4) = 2498{,}3\text{mm}^3$$

The resultant tangential stress is given by:

$$\tau_{r.cs} = \tau_{T_2'} + \tau_{M_2} = 23{,}3\ \text{N/mm}^2 \tag{1.7}$$

Because we have a dynamic loading and fatigue is not a request, it follows that [5], [6]:

$$R_\sigma = 0 \quad \text{and} \quad \sigma_{acs} = 60\ \text{N/mm}^2 \tag{1.8}$$

The safety factor is:

$$c_\tau = \frac{\tau_{acs}}{\tau_{cs}} = \frac{60}{23{,}3} = 2{,}6 > c_a = 2 \tag{1.9}$$

Further calculation will be checking calculation for weld section A-A , which connects the annular disc to roll shell, so : $T_2' = 5{,}13\text{kN}$ si $M_{t2} = 28 \cdot 10^3\ \text{N} \cdot \text{mm}$.

It is calculated:

$$\tau_{T_2'} = \frac{T_2'}{A_{cs}} = \frac{5{,}13\text{kN}}{992{,}74\text{mm}^2} = 5{,}17\ \text{N/mm}^2 \quad \text{si} \quad \tau_{M_2} = \frac{M_{t2}}{W_{2cs}} = \frac{28 \cdot 10^3\ \text{Nmm}}{14555{,}3\text{mm}^3} = 1{,}92\ \text{N/mm}^2$$

$$A_1 = \left(R^2 - r^2\right) \cdot \pi = (41.5^2 - 38.5^2) \cdot \pi = 753.98\text{mm}^2 \tag{1.10}$$

$$W_1 = \frac{\pi}{32 \cdot D}(D^4 - d^4) = \frac{\pi}{32 \cdot 83}(83^4 - 77^4) = 14555{,}3\text{mm}^3$$

The resultant tangential stress resultant is given by:

$$\tau_{r.cs} = \tau_{T_2'} + \tau_{M_2} = 7{,}1\ \text{N/mm}^2 \tag{1.11}$$

Because $\sigma_{acs} = 60\ N / mm^2$, resulting safety factor:

$$c_{\tau} = \frac{\tau_{acs}}{\tau_{cs}} = \frac{60}{7,1} = 8,45 > c_a = 2 \qquad (1.12)$$

In this way are determined the welding sizes and the requests size for cross-section of the roller.

3. CONCLUSION

After all these calculation resulting the welds sizes corresponding to stresses to which the rolls are subjected for feeding tread band of the 84 inches rolling conveyor.

4. BIBLIOGRAFIE

1. Mateescu, D. – Construcții metalice: calculul si proiectarea elementelor din oțel, Ed. Tehnică,
București, 1980
2. Dumitraș, C. – Culegere de probleme pentru proiectarea mașinilor, utilajelor și construcțiilor sudate, Institutul Politehnic București, 1985
3. Ianasi, C.A. – Size calculations and checking cuopling of a conveyor belt, Annals of the ,,Constantin Brâncuşi,, University of Târgu-Jiu, Engineering Series, Issue 2/2015, pp 49-51, ISSN 1842-4856.
4. Ianasi C.A., Mihut, N. – Mechanical and geometrical characterization of the conveyors belts from mineral resources exploitation – Advanced Materials Research, vol,137, pp. 99-104, 2014.
5. Pasăre M., Ianăşi C., Rezistenţa Materialelor, teorie şi aplicaţii, Sitech, Craiova, ISBN 978-606-11- 0720-9, 194 pg., 2010
6. Pasăre M., Rezistenţa Materialelor, vol. 1., Editura Sitech, Craiova, ISBN 978-973-746-621-1, 212 pg., 2007.

TENSILE STRENGTH STUDY ON REINFORCED BEAMS

Lecturer PhD. Cătălina IANĂŞI
Constantin Brancusi University of Tg-Jiu, Romania
ianasi_c@yahoo.com

Abstract: In this paper is shown a model (together with mathematical modeling) for quantification the resistance of a wooden item, with and without composites reinforcement. As reinforcement will be used composite materials from carbon fiber (CFRP).Wooden items are from beach dry wood reinforced with special carbon fibers glued with epoxy resin so the obtained composite has a very good flexure and great stifness.

Key words:composite materials, carbon fiber, epoxy resin, flexure, stiffening

1.INTRODUCTION

In Strength of Material we work with elements of resistance as beams, pillars, floor, masonry portal and is necessary to reinforce these elements when they present wear and fatigue phenomena [4]. Consolidation and reinforcement is done with items as sheets and plates of carbon fiber. We propose to use a section, from two materials, to make the beam. In the middle, where are low tensions will have a low resistance material with E1 (wood), in the extreme (top-down) will have a material with greater resistance with E2 (carbon fiber) [8].The beam will be bending tested on a universal testing machine [3].

2. MATHEMATICAL MODELING

The experimental test were done on two samples of un-reinforced beams, three samples of reinforced beams with one composite plate and one down slide of wood and three samples with two composite plates and two up and down slides of wood. We measured the load and the displacement of each beam. The un-reinforced beams crushed at a small loads and had also small displacements. The reinforced beams crushed at bigger loads and had also bigger displacements compare with the un-reinforced beams.

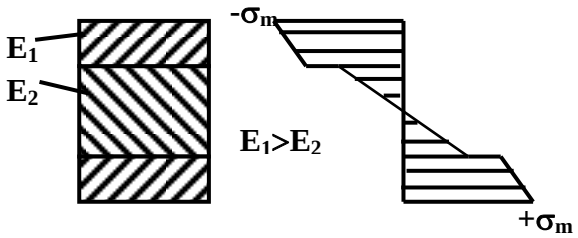

Fig.1 Normal tension σ for
bending request in the inhomogeneous beam

We calculate the maximum axial tension at breaking request as:

$$\sigma_r = \frac{F_m}{A} [MPa] \quad (1)$$

These parameters allow assessing the effectiveness of using the material, the largest of it indicating a better constructive solution. For the sample subjected to bending, located at the ends and middle driven with aforce which will increase to the maximum value F_m producing break, we calculate the maximum σ breaking tension [2]. Standard sample was a beam of dry beech, rectangular section, with approximate dimensions of 25x50 mm. Were used carbon fibers as a reinforcing material.

$$M_m = 0,25F_m \cdot l [Nmm], \quad W_t = \frac{b_0 h_0^2}{6} [mm^3], \quad \sigma_m = \frac{M_m}{W_t} [MPa] \quad (2)$$

The studied bending phenomenon studied give us conclusive results as studying 23 variants of reinforcement specimens subjected to bending test.

3. EXPERIMENTAL RESULTS

It is proposed to use a cheap and easily processed material that is a beam of dry beech. As a rigid material with good strength and relatively low cost we use a composite that can be a carbon fiber sheet and a carbon fiber plate. For the investigation leading to relevant results will be studied more constructive solutions. The results of the bending tests are shown in table number 1 from below.

Table 1 Experimental calculated parameters

Current issue	Variant	Sample	F Force [daN]	Sectional area A_o (mm^2)	Tension σ_t (MPa)	Comments
1	a	1	0,2	1218	80	reference sample
2		2	0,4	1218	135	
3	b	1	0,6	1180	198	one carbon plate
4	c	1	0,8	1410	125	
5		2	1,0	1380	122	
6	d	1	1,2	1725	136	
7	e	1	1,4	1600	125	average σ_t=133,3 MPa
8		2	1,6	1600	140	
9		3	1,8	1675	148	
10	f	1	2,0	2610	102	average σ_t=86,5 MPa; buckling
11		2	2,2	2610	82	
12	g	1	2,4	2610	168	

13	h	1	2,6	2400	156	reference sample
14	i	1	2,8	20300	89	average σ_t=94 MPa
15		2	3,0	20300	112	
16	j	1	3,2	18500	160	average σ_t=139,4 MPa, one layer sheet
17		2	3,4	19200	140	one layer sheet
18		3	3,6	19000	147	one layer sheet
19		4	3,8	19000	125	one layer sheet
20		5	4,0	19000	159	two layers sheet
21	k	1	4,2	26500	138	average σ_t=120,6 MPa
22		2	4,4	26500	140	
23		3	4,6	26500	122	

A wood beam, generally, can withstand a relatively small concentrated bending force because the maximum bending strength that can handle the material is also small [1]. If in the great strength area of the beam is added composite with greater strength than wood then the wood beam can withstand a bigger force because the maximum strength is bigger too [7]. The un-reinforced beam has rectangular section 25 x 50 x 500mm (width x height x length) and is made from dry beech with 12% humidity factor. Experimental tests were performed at 20°C, on eight beech beams, some of them un-reinforced and other reinforced with CFRP composite plates. For this tests we use an universal hydraulic machine of 20 tons force, EDZ 20where beams are tested to bending with a punctuate force placed in the middle of the beams[5,6]. One type of reinforcement is a wood beam with rectangular section $25 \times 50 \times 500$mm (width x height x length), down reinforced with one carbon fiber plate with rectangular section of 25 x 1,2 x 500 mm (width x height x length), glued by the reference sample with epoxy resin.

Fig.2 Universal hydraulic machine of 20 tons force, EDZ 20, with a beam reinforced with CFRP

By the composite plate is glued, with the same epoxy resin, another slide of beech wood of $25 \times 10 \times 500$mm (width x height x length).

Preparing the beams for bonding with epoxy resin consists of cleaning and polishing the contact surface with sandpaper. After that the resin is spread with a brush in a uniform layer over the entire contact surface of the beam. Allow the epoxy resin to dry for 23 hours then we can run the bending test. The results of the bending tests are shown in the graph from below.

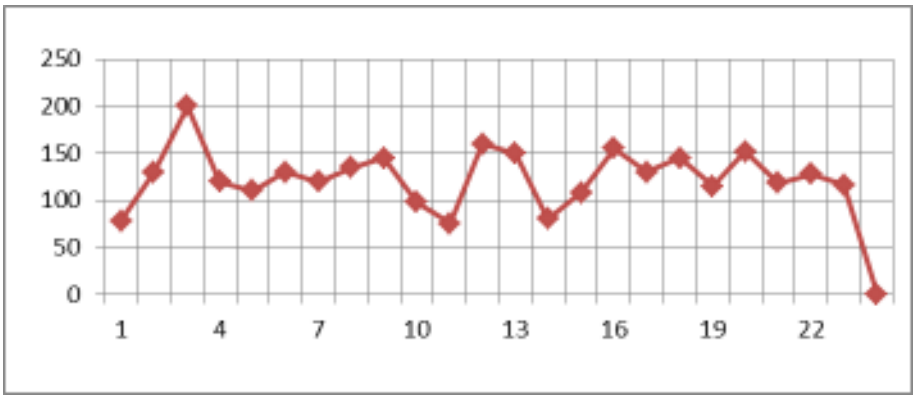

Fig. 3 Maximum σ_t variation in the samples

Compression tests gave us the following results: sample reference: σ_t=78 MPa, sample reinforced with one layer of sheet: σ_t=139,4 MPa, sample reinforced with two layers of sheet: σ_t=152 MPa, sample reinforced with carbon fiber plate: σ_t=200 MPa.

CONCLUSIONS

The greatest efficiency, in terms of rigidity, is obtained for c version followed by b version. Experiments have shown the viability of the method of increasing resistance of wood construction with composite materials. The solution is easy to implement and the costs are low. Use CFRP in composite reinforcement is still modest, imposing itself further and deeper studies.

REFERENCES

[1] Groover M.P., Fundamental of modern manufacturing, 2nd ed. 111 River Street, Hoboken (NJ), John Wiley & Sons, Inc., 2004.

[2] Malkapuram R., Kumar V., Yuvra S.N.J, Recent development in natural fibre reinforced polypropylene composites. J. Reinf. Plast. Compos. 28 (2008) 1169–1189.

[3] Borri A., Corradi M., Vignoli A., New materials for strengthening and seismic upgrading interventions. International Workshop Ariadne 10, Arcchip, April 22–28,Prague, Czech Republic, (2002),1–24, cd-rom.

[4] Triantafillou TC. Shear reinforcement of wood using FRP materials. J. Mater. Civi. Eng., ASCE 9(2), (1997), 65–69.

[5] Borri A., Corradi M., Grazini A., A method for flexural reinforcement of old wood beams with CFRP materials, Composites: Part B 36 (2005) 143–153.
[6] Li Y-F., Xie Y-M., Tsai M-J., Enhancement of the flexural performance of retrofitted wood beams using CFRP composite sheets, Construction and Building Materials 23 (2009) 411–422.
[7] Ianăşi C.**,** Research on reducing the risk of damage for the resistance elements of wooden building, 2nd WSEAS International Conference, RIMA '13, ISSN 2227-460X, Brasov, Romania, June 1-3, (2013), 161-164.
[8] Information on http://www.sika.ro

PRACTICAL STUDY ON THE CFRP REINFORCEMENT

Lecturer PhD. Cătălina IANĂŞI, "Constantin Brâncuşi" University of Tg-Jiu
ianasi_c@yahoo.com

Abstract: One of the defining goals of this paper is getting new resistant material which combine the qualities of basic materials that get into its composition but not to borrow from them their negative properties. In recent years, carbon fiber composites have been increasingly used in different ways in reinforcing structural elements. Specifically, the use of CFRP composite materials as reinforcement for wood beams under bending loads requires paying attention to several aspects of the problem which are presented in this paper.

Keywords: wood beams, CFRP composites, epoxy resin, bending test.

1. INTRODUCTION

In this paper is described an experimental study which was designed to evaluate the effect of layers number of composite material on the stiffness of the wood beams [3]. The type of reinforcement used on the beams is the carbon fiber reinforced polymer (CFRP) sheet and an epoxy resin for bonding all the elements. Structural epoxy resins remain the primary choice of adhesive to form the bond to fiber-reinforced plastics [5,7,8,9] and are the generally accepted adhesives in bonded CFRP–wood connections. Advantages of using epoxy resin in comparison to common wood-laminating adhesives are their gap-filling qualities and the low clamping pressures that are required.

Following the experimental tests we developed a numerical procedure, which can estimate the failure load of the wood beams reinforced with composite materials. The critical point of the numerical procedure consists in the selection of the most adequate characteristic values for wood limit stresses. This step was carried out using values found in other studies and from a comparison of the values obtained from the failure loads of the un-reinforced beams.

2. EXPERIMENTAL STUDY

The total number of wood specimens manufactured is 12, ten of them are reinforced and two are un-reinforced. The wood part of all beams was formed by beech dry wood which size is equal to 25 by 50 by 500 mm [3]. Three beams were reinforced using one carbon fiber sheet of thickness equal to 1.5 mm, width equal to 25 mm and the length is equal to 500 cm. The finished dimension of these beams is equal to 25 by 101.5 by 500 mm because they are two beams stick together with one carbon fiber sheet of SikaWrap 230C and Sikadur30 epoxy resin (fig.1). For carbon fiber sheet, once it is placed on the wood beam, with the epoxy resin, all what is required is to press the carbon fiber sheet with a simple roller and pull out the air [1,2,4,6]. In addition, the carbon fiber sheet has a very high tensile strength (with respect to its weight), it is available in any length, no joints are required, low thickness, easy to transport, laminate intersections are simple, economical application no heavy handling and installation equipment, available in various modules of elasticity, outstanding fatigue resistance, and it can be coated without preparation.

Moreover, the CFRP are compatible with wood with respect to its mechanical properties. The bending test results for a reinforced wood beam with one CFRP sheet are shown in table 1.

Fig. 1 Tension failure of a reinforced wood beam with one CFRP sheet

Table 1 Results for a reinforced wood beam with one CFRP sheet

Force (daN)	0,4	0,8	1,2	1,6	2,0	2,4	2,8	3,2
Deflection f_1 (mm)	1	1,5	1,9	2,1	2,3	2,6	3	4
f_2	1,5	1,7	2,2	2,4	2,6	2,9	3,2	3,8
f_3	1,1	1,8	2,00	2,5	2,7	3,1	3,4	3,7

Other four beams were reinforced using two carbon fiber sheets of thickness equal to 3 mm, width equal to 25 mm and the length is equal to 500 cm. The finished dimension of these beams is equal to 25 by 73 by 500 mm because they are two slides of wood up and down stick by the main wood beam, with two carbon fiber sheets and Sikadur 30 epoxy resin (fig.2). The bending test results for a reinforced wood beam with two CFRP sheets and two slides of wood are shown in table 2.

Fig. 2 Tension failure of a reinforced wood beam with two CFRP sheets and two slides of wood (up and down)

Table 2 Results for a reinforced wood beam with two CFRP sheets

Force (daN)	0,4	0,8	1,2	1,6	2,0	2,4	2,8	3,2
Deflection f_1 (mm)	1	2,2	3,9	4,8	6,1	7,9	8,7	10,5
f_2	1,2	2,4	3,4	4,4	6,3	7,7	8,8	10,2
f_3	1,1	2,2	3,7	4,7	6,5	7,8	8,9	10,6
f_4	1	2,5	3,8	4,9	6,4	8,2	9,1	10,8

The last three beams were reinforced using three carbon fiber sheets of thickness equal to 4.5 mm, width equal to 25 mm and the length is equal to 500 cm. The finished dimension of these beams is equal to 25 by 114.5 by 500 mm because they are two beams stick together with three carbon fiber sheets and epoxy resin (fig. 3). The bending test results for a reinforced wood beam with three CFRP sheets are shown in table 3.

Fig. 3 Tension failure of a reinforced wood beam with two CFRP sheets (in the middle of the beam) and one slide of wood

Table 3 Results for a reinforced wood beam with three CFRP sheets

Force (daN)	0,4	0,8	1,2	1,6	2,0	2,4	2,8	3,2
Deflection f_1 (mm)	1,6	2,1	3,6	4,3	5,5	6,8	8,4	10,6
f_2	1,8	2,5	3,9	4,6	5,8	6,7	8,1	10,9
f_3	1,6	2,3	4,1	5,1	6,5	7,3	8,9	11,2

The specimens tested were not subjected to lateral instability during loading. The total load on the beam was applied equally at one point equidistant from the reactions (the half length of the beam).

We use the bending device of the universal machine for mechanical tests which has the distance between the rollers l = 460 mm. Standard samples was dry beech wood beam with a rectangular section of 25x50 x500 mm (bxhxl).

After we study those examples we observe that the reinforced wood beam with two CFRP sheet in the middle of the beam (fig.3) is the most resistant and has a good elasticity breaking into a 11,2 mm deflection. Also, we can say that the number of composite material layers influences the stiffness of the wood reinforced beams.

CONCLUSIONS

It is proposed to use an inexpensive and easily processed material that is wood. As a rigid material with good strength and relatively low cost, we use a composite. A several un-reinforced and reinforced wood beams were tested in order to find their flexural capacity. The results indicate that the behavior of reinforced beams is totally different from that of un-reinforced one. The reinforcement has changed the mode of failure from brittle to ductile and has increased the load-carrying capacity of the beams.

Observations of the experimental load–displacement relationships show that vertical displacement increase for wood beams reinforced with CFRP composite plates, compared to those without CFRP plates, so we can say that the number of composite material layers influences the stiffness of the wood reinforced beams

REFERENCES

[1] Abdel-Magid B, Dagher HJ, and Kimball T. The effect of composite reinforcement on structural wood. In: Proceedings – ASCE 1994 materials engineering conference, Infrastructure: new materials and methods for repair, San Diego, CA, November 14–16; 1994.

[2] Camille A. Issa, Ziad Kmeid. Advanced wood engineering: glulam beams. Department of Civil Engineering, Lebanese American University, Byblos, Lebanon. Construction and Building Materials 19 (2005) 99–106.

[3] Ianăşi C. Research on reducing the risk of damage for the resistance elements of wooden building, 2nd WSEAS International Conference on RISK MANAGEMENT, ASSESSMENT and MITIGATION (RIMA '13) Brasov, Romania, June 1-3, 2013, pp. 161-164, ISSN 2227-460X

[4] Yeou-Fong Li, Yao-Ming Xie, Ming-Jer Tsai. Enhancement of the flexural performance of retrofitted wood beams using CFRP composite sheets. Construction and Building Materials 23 (2009) 411–422.

[5] Plevris N, Triantafillou T. Creep behavior of FRP-reinforced wood members. J Struct Eng – ASCE 1995;121(2):174–86.

[6] Plevris N, Triantafillou T. FRP-reinforced wood as structural material. J Mater Civil Eng – ASCE 1992;4(3).

[7] Tingley DA, Leichti RJ. Reinforced glulam: improved wood utilization and product performance. Paper presented at Technical Forum – Globalization of wood: supply, products, and markets. Portland (Oregon): Forest Products Society; 1993.

[8] Triantafillou T, Deskovic N. Innovative prestressing with FRP sheets: mechanics of short-term behavior. J Eng Mech – ASCE 1991; 117(7):1652–72.

[9] Triantafillou T, Deskovic N. Prestressed FRP sheets as external reinforcement of wood members. J Struct Eng – ASCE 1992; 118(5):1270–84.

Nr. crt	Name and Surname, Institution, E-mail	Pagina
1.	**AMZA Catalin** Material and Welding Technology, University POLITECHNICA from Bucharest, Splaiul Independenței no. 313, Bucharest,	**Nr.1 – pag. 86**
2.	**AMZA Gheorghe** Univ. Politechnica of Bucharest, amza@camis.pub.ro	**Supplement Nr.1 pag.28, 36, 43**
3.	**APOSTOLESCU Zoia** Material and Welding Technology, University POLITECHNICA from Bucharest, Splaiul Independenței no. 313, Bucharest, zoia@camis.pub.ro	**Nr.1 – pag. 80, 86 Supplement Nr.1. pag. 28**
4.	**BABIS Claudiu** Material and Welding Technology, University POLITECHNICA from Bucharest, Splaiul Independenței no. 313, Bucharest, claudiubbs@gmail.com;	**Nr.1 – pag. 80, 86**
5.	**BĂRBĂCIORU Iuliana Carmen** Constantin Brancusi University of Targu Jiu, Romania	**Supplement Nr.1. pag. 233, 238**
6.	**BOGDAN Constantin** Machines and Installation Departement, University of Petroşani , ROMANIA, tica1234ticabogdt@yahoo.com	**Supplement Nr.1. pag. 260, 267, 272, 279, 284, 293**
7.	**BOLCU Alexandru** University of Craiova, Faculty of Mechanics, bolcualexandru@yahoo.com	**Supplement Nr.1. pag. 122, 128**
8.	**BULAC Ion** University of Piteşti, ionbulac57@yahoo.com	**Nr.1 – pag. 48, 55**
9.	**BUNECI Mădălina Roxana** University Constantin Brâncuşi of Târgu-Jiu, ROMÂNIA mbuneci@yahoo.com	**Supplement Nr.1. pag. 244, 252**
10.	**BURADA Cristian Oliviu** University of Craiova, Faculty of Mechanics, cristian.burada@yahoo.com	**Supplement Nr.1. pag. 128**
11.	**BURLAN-ROTAR Tudor** Polytechnic University of Bucharest, tudor.burlan@yahoo.com	**Supplement Nr.1. pag. 51, 60, 134, 141**
12.	**BUZBUGAN Monica** Asociatia de Sudura din Romania National R&D Institute for Weldind and Material Testing, Mihai Viteazul 30, Timisoara, Romania mdobra@isim.ro	**Nr.1 – pag. 91**
13.	**CAINICEANU Liliana** Polytechnic University of Bucharest, lili_cainiceanu@yahoo.com	**Supplement Nr.1. pag. 51, 60**
14.	**CHISHKALA Vladimir** Ukrainian State Univ. of Railway Transport V. N. Karazin Kharkov Nat. Univ. vchishkala@ukr.net	**Supplement Nr.1. Pag. 10**

15.	**CHIVU Oana** Material and Welding Technology, University POLITECHNICA from Bucharest, Splaiul Independenţei no. 313, Bucharest, virlan_oana@yahoo.co.uk	**Nr.1 – pag. 80, 86, 91**
16.	**CIOFU Florin** Engineering Faculty, ”Constantin Brâncuşi” University, florincristian33@gmail.com	**Supplement Nr.1. pag. 84, 89, 104**
17.	**CÎRȚÎNĂ Marius Liviu** University ,, Constantin Brâncuși’’ of Târgu-Jiu cirtinaliviu@gmail.com	**Nr.1 – pag. 112**
18.	**COȘOFREȚ Doru** Military Technical Academy, Bucharest, Romania, doru.cosofret@anmb.ro	**Supplement Nr.1. pag. 67, 72**
19.	**DIMITRESCU Andrei** Material and Welding Technology, University POLITECHNICA from Bucharest, Splaiul Independenţei no. 313, Bucharest, Romania	**Nr.1 – pag. 86** **Supplement Nr.1. pag. 28**
20.	**DOBROTĂ Dan** Constantin Brancusi University of Targu Jiu, Romania, Department of Systems Engineering and Management Technology e-mail: ddan@utgjiu.ro	**Supplement Nr.1. pag. 79**
21.	**ENE (TĂRABUȚĂ) Doina** "I.N. Socolescu" Technical Architecture College, Bucharest, email: doinaene@ymail.com	**Supplement Nr.1. pag. 134, 141, 193**
22.	**FEIER Anamaria** INCD URBAN INCERC, Traian Lalescu 2, Timisoara, Romania anamaria_butisca@yahoo.com.au	**Nr.1 – pag. 80, 91**
23.	**FENECHIU Relu** Polytechnic University of Bucharest	**Supplement Nr.1. pag. 36, 43**
24.	**GEVORKYAN Edvin** Ukrainian State Univ. of Railway Transport, edsgev@gmail.com	**Supplement Nr.1. Pag. 10**
25.	**GHIMIŞI Stefan** Constantin Brâncuşi University of Târgu Jiu,Romania, ssghimisi@gmail.com	**Nr.1 – pag. 74**
26.	**GUTSALENKO Yury** Nat. Tech. Univ. “Kharkov Polytechnic Inst.” Ukrainian State Univ. of Railway Transport gutsalenko@kpi.kharkov.ua	**Supplement Nr.1. Pag. 10**
27.	**IANĂŞI Cătălina** Constantin Brancusi University of Tg-Jiu, Romania ianasi_c@yahoo.com	**Nr.1 – pag. 117, 122** **Supplement Nr.1. pag. 158, 164**
28.	**IANCU Cătălin** Engineering Faculty, ”C-tin Brâncuşi” Univ. of Tg-Jiu, ciancu@utgjiu.ro	**Supplement Nr.1. pag. 168, 174**
29.	**IONICI Cristina Felicia** University ”Constantin Brâncuşi” of Tg-Jiu, Engineering Faculty cfelix1967@yahoo.com	**Supplement Nr.1. pag. 164**

30.	**IOVAN Alina Anabela** Railway Informatics SA, Bucharest, ROMANIA, alina.iovan@infofer.ro	**Supplement Nr.1.** **pag. 206**
31.	**IOVAN Claudia Alina** University of Craiova, Faculty of Mechanics, iovanclaudiaalina@yahoo.com	**Supplement Nr.1.** **pag. 110, 116, 122, 128**
32.	**IOVAN Ştefan** West University of Timişoara, Computer Science Department, ROMANIA Railway Informatics SA, Bucharest, ROMANIA, stefan.iovan@infofer.ro	**Supplement Nr.1.** **pag. 199, 206, 213**
33.	**ITU Răzvan Bogdan** Department of Industrial Mechanical Engineering and Transport, University of Petroşani, raz.van4u@yahoo.com	**Nr.1 – pag. 96, 104**
34.	**IVANUS Cristian** Bucharest University Of Economic Studies, Romania, ivanuscristian13@stud.ase.ro	**Supplement Nr.1.** **pag. 199, 213**
35.	**KISLITSA Maxim** Ukrainian State Univ. of Railway Transport V. N. Karazin Kharkov Nat. Univ.	**Supplement Nr.1.** **Pag. 10**
36.	**LAKOV Nikolay** University of Mining and Geology"St. Ivan Rilski", Bulgaria, e-mail: nikolaylakov@mail.bg	**Supplement Nr.1 – pag.3**
37.	**LIVADARIU Adriana,** MATCHTECH Augsburg GERMANIA adriana.livadariu@gmail.com	**Nr.1 – pag. 3, 10**
38.	**LUCA Liliana** University Constantin Brancusi of Targu-Jiu, lylyanaluca@yahoo.com	**Nr.1 – pag. 17, 26**
39.	**MELNIK Olga** Ivan Kozhedub Kharkov Univ. of Air Force, Kharkov, Ukraine Ukrainian State Univ. of Railway Transport melhik@ro.ru	**Supplement Nr.1.** **Pag. 10**
40.	**MICU** Alexandra-Elza, University Politehnica Bucharest Romania salwaelza@yahoo.com	**Nr.1 – pag. 3, 10**
41.	**MIHUŢ Nicoleta- Maria** "Constantin Brâncuşi"University of Tg-Jiu nicoleta_simionescu@yahoo.com	**Supplement Nr.1.** **pag. 149, 154**
42.	**MILOSAVLJEVIĆ Milutin M.** University of Priština, Kosovska Mitrovica, Serbia	**Supplement Nr.1.** **pag. 181**
43.	**MIRIŢOIU Cosmin Mihai** University of Craiova, Faculty of Mechanics, miritoiucosmin@yahoo.com	**Supplement Nr.1.** **pag. 122, 128**
44.	**NIOAŢĂ Alin** Engineering Faculty, "Constantin Brâncuşi" University, alinnioata@yahoo.com	**Supplement Nr.1.** **pag. 84, 89, 104**

45.	**NITOI Dan** Material and Welding Technology, University POLITECHNICA from Bucharest, Splaiul Independenţei no. 313, Bucharest, nitoidan@yahoo.com	**Nr.1 – pag. 80, 86** **Supplement Nr.1.** **pag. 28**
46.	**NOVIKOV Feodor** Simon Kuznets Kharkiv National University of Economics fokusnic1@rambler.ru	**Supplement Nr.1.** **Pag. 22**
47.	**PANĂ Nicolae** Polytechnic University of Bucharest, email: npaniki@gmail.com	**Supplement Nr.1.** **pag. 134, 141**
48.	**PARIS Adrian Stere** Univ. Politehnica Bucharest, email: adrian.paris@upb.ro	**Nr.1 – pag. 62, 67**
49.	**PASĂRE Minodora** Constantin Brancusi University of Tg-Jiu, Romania minodora_pasare@yahoo.com	**Supplement Nr.1.** **pag. 158**
50.	**PECINGINĂ Irina Ramona** „Constantin Brâncuşi" University of Tg-Jiu, irinacornescu yahoo.com	**Supplement Nr.1.** **Pag. 220, 227**
51.	**PECINGINA Olimpia** "University of Constantin Brancusi", Tg-jiu ,, ROMANIA, pecinginaolimpia@yahoo.com	**Supplement Nr.1.** **pag. 260, 267, 272, 279, 284, 293**
52.	**POP Alexandru Ioan** Department of Industrial Mechanical Engineering and Transport, University of Petroşani, ionutpop6@yahoo.com	**Nr.1 – pag. 96, 104**
53.	**POPA Roxana Gabriela** „Constantin Brâncuşi" University of Tg-Jiu, roxanna_popa@yahoo.com	**Supplement Nr.1.** **Pag. 220, 227**
54.	**POPESCU Constantin** Polytechnic University of Bucharest, email: puiu_2001uss@yahoo.com	**Supplement Nr.1.** **pag. 134, 141**
55.	**POPESCU Iulian** University of Craiova rodicaipopescu@yahoo.com	**Nr.1 – pag. 17, 26, 35, 41**
56.	**RĂDULESCU Constanța** University ,, Constantin Brâncuși'' of Târgu-Jiu rpc10gj@gmail.com	**Nr.1 – pag. 112**
57.	**ROȘCA FÂRTAT Gabi** Polytechnic University of Bucharest, email: rosca_gabi@yahoo.com	**Supplement Nr.1.** **pag. 134, 141**
58.	**SAMOILESCU Gheorghe** "Mircea cel Bătrân" Naval Academy, Constanta, Romania.	**Supplement Nr.1.** **pag. 67, 72**
59.	**SASS Ludmila** University of Craiova, Faculty of Mechanics, ludmila_sass@yahoo.com	**Nr.1 – pag. 35, 41**
60.	**SCUTELNICU (PĂUN)Elena** Polytechnic University of Bucharest; e-mail: ellenapaun@yahoo.com	**Supplement Nr.1.** **pag. 188, 193**
61.	**SCUTELNICU (VANE)Madalina** Polytechnic University of Bucharest; e-mail: madalina.scutelnicu@yahoo.com	**Supplement Nr.1.** **pag. 188, 193**

62.	**STĂNCIOIU Alin** Engineering Faculty, "Constantin Brâncuşi" University stancioiualin09@gmail.com	**Supplement Nr.1.** **pag. 94, 99**
63.	**STANESCU Constantin** Polytechnic University of Bucharest, prof_cstanescu@yahoo.com	**Supplement Nr.1.** **pag. 51, 60, 134, 141, 188, 193**
64.	**STĂNESCU Marius Marinel** University of Craiova, Faculty of Mechanics, mamas1967@gmail.com	**Supplement Nr.1.** **pag. 128**
65.	**STOIAN Ovidiu** University of Craiova, Faculty of Mechanics, george_ovidiu_boss@yahoo.com	**Supplement Nr.1.** **pag. 122**
66.	**TĂRĂBUȚĂ Octavian** "Mircea cel Bătrân" Naval Academy, Constanta, Romania.	**Supplement Nr.1.** **pag. 67, 72**
67.	**TĂRÂȚĂ Daniela Florentina** University of Craiova, Faculty of Mechanics, danielatarata@yahoo.com	**Supplement Nr.1.** **pag. 116, 122**
68.	**TÂRCOLEA Constantin** Univ. Politehnica Bucharest, email: constantin_tarcolea@yahoo.com	**Nr.1 – pag. 62**
69.	**TAŞCĂ Gabriel Dan** Univ. Politechnica of Bucharest	**Supplement Nr.1** **pag.28**
70.	**TEMPEA Iosif** University Politehnica Bucharest Romania iosiftempea@yahoo.com	**Nr.1 – pag. 3, 10**
71.	**TEODORESCU Marius Cornel** Univ. Politechnica of Bucharest	**Supplement Nr.1.** **pag. 28**
72.	**UNGUREANU Viorica Mariela** Constantin Brancusi University of Targu Jiu, Romania lvungureanu@yahoo.com	**Supplement Nr.1.** **pag. 238, 244**
73.	**VANE Daniel** Polytechnic University of Bucharest; e-mail: vane.daniel@yahoo.com	**Supplement Nr.1.** **pag. 188, 193**
74.	**VÎGA Dragos Vasile** Departament of machines and installations, University of Petrosani, ROMANIA e-mail: dragosviga71@gmail.com	**Supplement Nr.1.** **pag. 260, 267, 272, 279, 284, 293**
75.	**ŽIVKOVIĆ Milutin** High Technical Mechanical School Trstenik, Serbia, milutinzivkovicts@gmail.com	**Supplement Nr.1.** **pag. 181**
76.	**ŽIŽOVIĆ Mališa** University Singidunum, Belgrade, Faculty of business, Valjevo, Serbia	**Supplement Nr.1.** **pag. 181**

INDEX KEYWORDS	
A	
ADHESION	ANALYTICAL CALCUL
B	
BLOCK MODEL	BENDING TEST
C	
CATIA SOFTWARE	CARDAN JOINT
CARDAN TRANSMISSION	CHEBYSHEV'S PARADOX
CHEBYSHEV DYAD	CRANK-ROD
CFRP COMPOSITES	COMPOSITE MATERIALS
CARBON FIBER	
D	
DOUBLE SCARA ROBOT	DEPENDENCE
DISPLACEMENTS	
E	
EXTRACTING INSTALLATION	EPOXY RESIN
F	
FIVE-BAR MECHANISM	FRETTING
FRICTION COEFFICIENT	FORCE
FLEXURE	
H	
HYPPOCRATES'S LUNULES	HISTORICAL BRIDGES
HISTORICAL SIGHTS	
K	
KINEMATIC PAIR	
M	
MODELLING	MECHANICAL ANALYSIS
MECHANISM TO PLOT LUNULES	MACHINE PARTS
MECHANISM DEAD POINT	
N	
NASTRAN/PATRAN	
P	
PENTAGON.	
R	
RELIABILITY	REHABILITATION
Q	
QUADRILATERAL MECHANISM	QUALITY
S	
SCARA ROBOT	SOFTWARE APPLICATIONS
STRESS CONCENTRATOR	STRUCTURE
STRAINS	STIFFENING
T	
TAGUCHI METHODS	TOWER
TRAJECTORIES, QUADRANGLE	
U	
ULTRASONIC MOTOR	
V	
VIBRATION MODES	
W	
WELD	WELDED CONSTRUCTION
WOOD BEAMS	